NTNU – Trondheim
Norwegian University of
Science and Technology

Power Plant with CO2 Capture based on PSA Cycle

Ole Marius Moen
Henrik Sørskår Stene

Master of Science in Mechanical Engineering
Submission date: June 2014
Supervisor: Olav Bolland, EPT
Co-supervisor: Luca Riboldi, EPT

Norwegian University of Science and Technology
Department of Energy and Process Engineering

NTNU
Norwegian University
of Science and Technology

Department of Energy
and Process Engineering

EPT-M-2014-73

MASTER THESIS

for

Students
Ole Marius Moen and Henrik Sørskår Stene

Spring 2014

Power plant with CO_2 capture based on PSA cycle
Kraftverk med CO_2-fangst ved bruk av PSA-prosess

Background and objective

The main objective of this master thesis is to develop a dynamic process flowsheet model to study the performance of a coal-fired power plant when integrated with CO_2 capture, either as a post-combustion method or pre-combustion method. The CO_2 capture technology considered in this work is based on a Pressure Swing Adsorption (PSA) process, which operates in a cyclic manner. In this process CO_2 is removed from an exhaust gas or from a synthesis gas by adsorption.

When it comes to an integration of a process island adopting the adsorption technology and a power production island, either a conventional Pulverized Coal-fired (PC) plant or an Integrated Gasification Combined Cycle (IGCC), it is greatly important to study the performance of the units operating within the process island and investigate how they impact the efficiency penalty and power production rate. The goal of this project is to estimate the net power plant efficiencies for both the pre- and post-combustion cases.

The work will include the definition of a suitable dynamic model to represent the performances of a PSA cycle. A process simulation tool like gPROMS (general Process Modeling System), or similar, will be used. The power plants will be modeled using the software products GT Pro, Steam Pro and Thermoflex.

The following tasks are to be considered:

1. Review of literature related to adsorption modelling strategies and PSA processes.
2. Use of process simulation tool (i.e., gPROMS) to model a PSA cycle for carbon capture, either in a post- and pre-combustion scenario. For post-combustion CO_2 capture, the CO_2 is removed from the flue gas of an Advanced SuperCritical (ASC) pulverized fuel (PF) bituminous power plant. For pre-combustion CO_2 capture, the CO_2 is removed from the syngas of an Integrated Gasification Combined Cycle (IGCC).
3. Optimization of the PSA cycles. Given some performance targets to be met by the adsorption unit, verify the cycle configurations which better match them.
4. Overall simulations of the power islands with integrated PSA systems for CO_2 removal, both in the post- and pre-combustion approach.

5. Full-plant assessment of the performance and evaluation of the feasibility of adsorption as a technique for decarbonisation.

-- " --

Within 14 days of receiving the written text on the master thesis, the candidate shall submit a research plan for his project to the department. When the thesis is evaluated, emphasis is put on processing of the results, and that they are presented in tabular and/or graphic form in a clear manner, and that they are analysed carefully.

The thesis should be formulated as a research report with summary both in English and Norwegian, conclusion, literature references, table of contents etc. During the preparation of the text, the candidate should make an effort to produce a well-structured and easily readable report. In order to ease the evaluation of the thesis, it is important that the cross-references are correct. In the making of the report, strong emphasis should be placed on both a thorough discussion of the results and an orderly presentation.

The candidate is requested to initiate and keep close contact with his/her academic supervisor(s) throughout the working period. The candidate must follow the rules and regulations of NTNU as well as passive directions given by the Department of Energy and Process Engineering.

Risk assessment of the candidate's work shall be carried out according to the department's procedures. The risk assessment must be documented and included as part of the final report. Events related to the candidate's work adversely affecting the health, safety or security, must be documented and included as part of the final report. If the documentation on risk assessment represents a large number of pages, the full version is to be submitted electronically to the supervisor and an excerpt is included in the report.

Pursuant to "Regulations concerning the supplementary provisions to the technology study program/Master of Science" at NTNU §20, the Department reserves the permission to utilize all the results and data for teaching and research purposes as well as in future publications.

The final report is to be submitted digitally in DAIM. An executive summary of the thesis including title, student's name, supervisor's name, year, department name, and NTNU's logo and name, shall be submitted to the department as a separate pdf file. Based on an agreement with the supervisor, the final report and other material and documents may be given to the supervisor in digital format.

☐ Work to be done in lab (Water power lab, Fluids engineering lab, Thermal engineering lab)
☐ Field work

Department of Energy and Process Engineering, 14 January 2014

Olav Bolland
Academic Supervisor

Research Advisor: Luca Riboldi

Preface

This master thesis, Power Plant with CO_2 Capture Based on PSA Cycle, concludes the fifth year of a Master of Science degree. The thesis was written in Trondheim, for the Department of Energy and Process Engineering at the Norwegian University of Science and Technology.

The aim of the work is to model and simulate a pulverized coal power plant and an integrated gasification combined cycle power plant integrated with CO_2 capture by pressure swing adsorption. The goal is to evaluate the feasibility of PSA as a technology for decarbonisation. This study may be helpful as a part of the ongoing research within the field CO_2 capture and storage.

We would like to thank our main supervisor Olav Bolland and our co-supervisor Luca Riboldi at the Norwegian University of Science and Technology (NTNU) for advice and guidance throughout the thesis.

Abstract

Two coal-fired power plants with CO_2 capture by Pressure Swing Adsorption (PSA) have been modeled and simulated. The two power plants considered were Integrated Gasification Combined Cycle (IGCC) and conventional Pulverized Coal Combustion (PCC). A mathematical model of the PSA process for each of the power plants was developed and the goal was to evaluate the feasibility of PSA as a technology for decarbonisation. The performance with CO_2 capture by PSA was compared to a reference plant without CO_2 capture and to a power plant with CO_2 capture by absorption, which is considered as the benchmark technology. The size and number of the PSA columns were estimated to determine the footprint.

For the PCC power plant, the PSA model was a two-stage process consisting of a front and a tail stage. Two-stages mean that it consisted of two consecutive PSA processes. The front stage was a three-bed, five-step Skarstrom process with rinse. The tail stage was a two-bed, five-step Skarstrom process with pressure equalization. Zeolite 5A was used as adsorbent. For a specified capture rate of 90.0 %, the process achieved a purity of 96.4 % and a specific power consumption of 1.3 MJ/kg_{CO2}. The net plant efficiency dropped 16.6 percentage points from 45.3 % to 28.7 % when introducing CO_2 capture by PSA. In comparison, the PCC plant using absorption achieved a net plant efficiency of 33.4 %. The results indicate that the current state of the art PSA technology for decarbonisation as an alternative to absorption is not realistic for PCC power plants.

For the IGCC power plant, the PSA model was a seven-bed, twelve-step Skarstrom configuration with four pressure equalization steps using activated carbon as adsorbent. The process achieved a purity of 87.8 % and a capture rate of 86.3 % with negligible power consumption. The PSA process did not satisfy the performance targets of 90 % recovery and 95.5 % purity, and due to the low purity it is uncertain whether or not transport and storage of CO_2 is at all feasible. The net plant efficiency dropped 12.5 percentage points from 47.3 % to 34.8 %. In comparison the IGCC plant with absorption achieved a net plant efficiency of 36.4 %. The results showed that PSA as a capture technology for IGCC power plants could not perform quite as well as absorption. However, PSA as a capture technology could have a potential if the purity could be increased, and is therefore more promising than PSA for PCC power plants.

Sammendrag

To kullkraftverk med CO_2-fangst basert på "Pressure Swing Adsorption" (PSA) har blitt modellert og simulert. Kraftverkene som ble studert var av typen "Integrated Gasification Combined Cycle" (IGCC) og "Pulverized Coal Combustion" (PCC). En matematisk modell av PSA prosessen for hvert av kraftverkene har blitt utviklet og hensikten var å vurdere PSA som en teknologi for CO_2-rensing. Kraftverkene med CO_2-rensing basert på PSA ble sammenlignet med kraftverk uten CO_2-rensing og med CO_2-rensing basert på absorpsjon, som anses som den ledende teknologien. Størrelsen på og antallet av adsorpsjonskolonner ble estimert for å bestemme dimensjoner og plassbehovet.

PSA modellen i PCC kraftverket var en to-stegs prosess, som betyr at det var to PSA prosesser i serie. Det første steget bestod av tre kolonner og var en fem-trinns Skarstrom prosess med "rinse". Det andre steget bestod av to kolonner og var en fem-trinns Skarstrom prosess med trykkutjevning. Zeolitt 5A ble brukt som adsorbent. For en spesifisert fangstrate på 90.0 % oppnådde prosessen en renhet på 96.4 % med et strømforbruk på 1.3 MJ/kg_{CO2}. Virkningsgraden til kraftverket falt 16.6 prosentpoeng fra 45.3 % til 28.7 % når CO_2-rensing basert på PSA ble introdusert. Til sammenligning oppnådde PCC kraftverket med absorpsjon en virkningsgrad på 33.4 %. Resultatene indikerer at CO_2-rensing basert på PSA som et alternativ til absorpsjon ikke er realistisk for PCC kraftverk.

PSA modellen i IGCC kraftverket bestod av syv kolonner og var en tolv-trinns Skarstrom prosess med fire trykkutjevningstrinn og "activated carbon" som adsorbent. Prosessen oppnådde en fangstrate på 86.3 % og en renhet på 87.8 % med neglisjerbart energiforbruk. PSA prosessen oppnådde ikke målet på 90 % fangstrate og 95.5 % renhet. På grunn av den lave renheten er det usikkert om transport og lagring av CO_2 er i det hele tatt mulig. Virkningsgraden til kraftverket falt 12.5 prosentpoeng fra 47.3 % til 34.8 %. Til sammenligning oppnådde IGCC kraftverket med absorpsjon en virkningsgrad på 36.4 %. Resultatene viste at CO_2-fangst med PSA for IGCC kraftverk ikke klarte å oppnå like bra resultater som absorpsjon. PSA teknologien kan likevel ha et potensial dersom renheten til CO_2 kan økes, og er derfor mer lovende enn PSA for PCC kraftverk.

List of Figures

Figure 1: CO_2 capture processes (Bolland, 2012) 2
Figure 2: PSA cycle steps 9
Figure 3: Heat transfer coefficient correlations 24
Figure 4: Adsorption isotherm (Agarwal, 2010) 25
Figure 5: Brunauer's classification of isotherms 26
Figure 6: Adsorption reactor 30
Figure 7: PSA cycle and time schedule front stage 39
Figure 8: PSA cycle and time schedule tail stage 40
Figure 9: PSA plant setup 41
Figure 10: PSA cycle and time schedule 48
Figure 11: Effect of PE step times on performance 53
Figure 12: Purity and recovery from simulation runs 54
Figure 13: Accounting of CO_2 (Bolland, 2012) 58
Figure 14: PCC plant layout (European benchmarking task force, 2008) 59
Figure 15: PCC plant layout with CO_2 capture by PSA 62
Figure 16: Losses associated with CO_2 capture 66
Figure 17: IGCC plant layout (European benchmarking task force, 2008) 73
Figure 18: IGCC plant layout with CO_2 capture by PSA 78
Figure 19: Breakdown of losses due to adsorption of syngas fuel 84
Figure 20: Increased emissions by additional formation of CO_2 85
Figure 21: Steam integration with gasifier island and gas cleanup system 87
Figure 22: Losses associated with CO_2 capture 89
Figure 23: CO_2 as fuel preparation gas (Botero, 2014) 92

List of Tables

Table 1: Post-combustion PSA configurations from literature[A] 10
Table 2: Pre-combustion PSA configurations from literature[a] 11
Table 3: Summary of main equations for PSA model 31
Table 4: Boundary conditions 32
Table 5: Process parameter definitions (Liu, et al., 2011) 35
Table 6: Reactor model variables 35
Table 7: Parameters for calculating molecular diffusivity 36
Table 8: CO_2 quality recommendations 38
Table 9: DYNAMIS quality recommendations (de Visser, et al., 2008) 38
Table 10: Flue gas composition 42
Table 11: Reactor bed parameters 42
Table 12: Fitting parameters for Langmuir adsorption isotherm 43
Table 13: Transport parameters 43
Table 14: Flow rates and step times 45
Table 15: PSA performance 46
Table 16: Detailed power consumption 46
Table 17: Thermoflex feed composition 47
Table 18: Initial step times 50
Table 19: Flow rates 50
Table 20: Reactor bed parameters 50
Table 21: Fitting parameters for Sips adsorption isotherm 51
Table 22: Transport parameters 52
Table 23: Flow rates and step times 55
Table 24: PSA performance 55
Table 25: Compositions leaving the PSA column 55
Table 26: Composition of air (European benchmarking task force, 2008) 57
Table 27: Coal parameters (European benchmarking task force, 2008) 57
Table 28: Stream table for PCC without CO_2 capture 59
Table 29: Steam turbine parameters 60
Table 30: PCC operational performance 60
Table 31: Operational performance PCC with CO_2 capture by absorption 61
Table 32: Accounting of CO_2 61
Table 33: Stream table for PCC with CO_2 capture by PSA 62
Table 34: Operational performance of PCC with CO_2 capture by PSA 63
Table 35: Accounting of CO_2 64
Table 36: Summary of losses associated with CO_2 capture 65
Table 37: Effect of feed pressure 67
Table 38: Step times and flow rates 68
Table 39: Performance PSA process 68
Table 40: Power consumption 68
Table 41: Losses associated with CO_2 capture by PSA 68

Table 42: Operational performance relaxed constraints 69
Table 43: Accounting of CO_2 relaxed constraints 69
Table 44: Size and number of columns 70
Table 45: Summary PCC simulations 72
Table 46: Summary CO_2 accounting 72
Table 47: Stream data for IGCC without CO_2 capture 73
Table 48: Gasifier input 74
Table 49: Gas turbine parameters 75
Table 50: HRSG and steam turbine parameters 75
Table 51: IGCC operational performance 76
Table 52: Operational performance IGCC with CO_2 capture by absorption 77
Table 53: Accounting of CO_2 77
Table 54: Stream table for IGCC with CO_2 capture by PSA 78
Table 55: Gas turbine parameters 79
Table 56: HRSG and steam turbine parameters 80
Table 57: Operational performance of IGCC with capture by PSA 81
Table 58: Accounting of CO_2 81
Table 59: Recovered exhaust heat and steam integration 87
Table 60: Accounting of losses due to CO_2 capture 88
Table 61: Size and number of columns 90
Table 62: Summary IGCC simulations 91
Table 63: Summary CO_2 accounting 91
Table 64: Syngas feed composition with CO_2 as fuel preparation gas 92
Table 65: Composition of CO_2-rich gas mixture [mol%] 93

Table of Content

Preface i
Abstract ii
Sammendrag iii
List of Figures iv
List of Tables v
Table of Content vii
Nomenclature ix
1 Introduction 1
1.1 Risk Assessment 3
1.2 Thesis Scope and Outline 3
2 Adsorption 4
2.1 PSA Process 4
3 Mathematical Modelling of PSA Processes 12
3.1 Introduction 12
3.2 Mass Transfer 13
3.3 Component Mass Balance 16
3.4 Overall Mass Balance 19
3.5 Momentum Balance 20
3.6 Energy Balance 20
3.7 Adsorption Isotherms 24
3.8 Valves 28
4 PSA Model 30
4.1 Post-Combustion 39
4.2 Pre-Combustion 46
5 Power Plant Simulations 56
5.1 PCC without CO_2 Capture 59
5.2 PCC with CO_2 Capture by Absorption 60
5.3 PCC with CO_2 Capture by PSA 62
5.4 Discussion of PCC Simulations 64
5.5 IGCC without CO_2 Capture 73
5.6 IGCC with CO_2 Capture by Absorption 76

5.7 IGCC with CO_2 Capture by PSA 77
5.8 Discussion of IGCC Simulations 82
6 Conclusion 94
7 Further Work 95
8 Works Cited 96
9 Appendix 100
9.1 Appendix A: PSA Simulation Results 100
9.2 Appendix B: PCC Simulation Flow Sheets 101
9.3 Appendix C: IGCC Simulation Flow Sheets 104
9.4 Appendix D: Losses Associated with CO_2 Capture Pre-Combustion 107

Nomenclature

Abbreviations

1D	One dimensional
ASC	Advanced supercritical
ASU	Air separation unit
CCS	Carbon capture and storage
CPU	Central processing unit
DECARBit	Decarbonize it
EQ	Pressure equalization step
ESP	Electrostatic precipitator
FP	Feed pressurization step
FVPSA	Fractionated vacuum pressure swing adsorption
GE	General Electric
gPROMS	general Process Modeling System
HHV	Higher heating value
HP	High pressure
HRSG	Heat recovery steam generator
IGCC	Integrated gasification combined cycle
IP	Intermediate pressure
IPCC	Intergovernmental Panel on Climate Change
LDF	Linear driving force
LHV	Lower heating value
LP	Low pressure
MEA	Monoethanolamine
mole%	Mole percentage
PCC	Pulverized coal combustion
ppm	Parts per million
PSA	Pressure swing adsorption
SLPM	Standard liter per minute
SPECCA	Specific energy consumption for CO_2 avoided
TSA	Temperature swing adsorption
vol%	Volume percentage
VPSA	Vacuum pressure swing adsorption
WGS	Water gas shift
wt%	Weight percentage

Roman Symbols

a	Adsorbent surface area per volume of bed	[m^2/m^3]
a_i	The number of adsorbent sites occupied by one molecule	[-]
Bi	Mass Biot number	[-]
b	Equilibrium constant	[m^3/mol]
C	Gas phase concentration	[mol/m^3]
C_G	Total gas phase concentration	[mol/m^3]
$C_{p,ads}$	Molar specific heat of the adsorbed phase	[J/molK]
$C_{p,g}$	Mass specific heat capacity of the gas	[J/kgK]
$C_{p,s}$	Specific heat capacity of the solid	[J/kgK]
$C_{p,w}$	Specific heat capacity of the wall	[J/kgK]
C_p	Molar specific heat capacity of the gas	[J/molK]
C_{por}	Concentration in macropore	[mol/m^3]
C_{por}^s	Concentration on the adsorbent surface	[mol/m^3]
D_{ax}	Axial dispersion coefficient	[m^2/s]
D_c	Micropore (crystal) diffusivity	[m^2/s]
D_c^0	Limiting diffusivity at infinite temperature	[m^2/s]
$D_{i,j}$	Binary molecular diffusivity	[m^2/s], [cm^2/s]
D_k	Knudsen diffusivity	[m^2/s]
D_m	Molecular diffusivity	[m^2/s]
D_p	Macropore diffusivity	[m^2/s]
D_s	Surface diffusivity	[m^2/s]
d_b	Internal diameter of column	[m]
d_p	Mean pore diameter	[m]
d_{pa}	Particle diameter	[m]
E_a	Activation energy of micropore diffusion	[kJ/mol]
H_{ads}	Heat of adsorption	[J/mol]
h_f	Film heat transfer coefficient	[W/m^2K]
h_w	Film heat transfer coefficient between gas and wall	[W/m^2K]
K	Adsorption equilibrium constant	[m^3/kg], [1/Pa]
K'	Adsorption equilibrium constant	[molm^3/kgJ]
K_0	Adsorption equilibrium constant at infinite temperature	[m^3/kg]
K_0'	Adsorption equilibrium constant at infinite temperature	[molm^3/kgJ]
k_{LDF}	LDF mass transfer coefficient	[1/s]
k_g	Film mass transfer coefficient	[m/s]
k	Boltzmann constant	[J/K]
L	Bed length	[m]
M	Molecular weight	[g/mol], [kg/mol]
$\dot{m}$	Mass flow rate	[kg/s]
N_c	Number of components	[-]

N_s	Surface flux	[Mol/m^{2}s]
Nu	Nusselt number	[-]
$\dot{n}_{in}$	Mole flow rate entering column	[mol/s]
$\dot{n}_{set}$	Mole flow rate set value	[mol/s]
$n_{depress}$	Number of moles leaving the depressurization step	[mol]
n_{press}	Number of moles entering the pressurization step	[mol]
P	Pressure	[Pa], [kPa] [Bar], [atm]
Pr	Prandtl number	[-]
P_{high}	Highest pressure in PSA cycle	[kPa]
P_{eq}	Equalization pressure in pressure equalization steps	[kPa]
P_{low}	Lowest pressure in PSA cycle	[kPa]
Q	Flow rate	[SLPM]
q	Adsorbed phase concentration	[mol/kg]
q^*	Adsorbed phase concentration in equilibrium state	[mol/kg]
q_m	Saturation limit concentration Multisite Langmuir	[mol/kg
q_s	Saturation limit concentration	[mol/kg]
R	Ideal gas constant	[J/molK], [kJ/molK]
Re_p	Reynolds number	[-]
R_{pa}	Particle radius	[m]
r_b	Internal radius of column	[m]
r_c	Micropore or crystal radius	[m]
r	Radial distance in particle	[m]
Sh	Sherwood number	[-]
Sc	Schmidt number	[-]
s	The Sips model exponent	[-]
s_1	Parameter for Sips exponent	[-]
s_2	Parameter for Sips exponent	[1/K]
s_{ref}	Parameter for Sips exponent	[-]
T	Bulk gas phase temperature	[K]
T^*	Temperature for diffusion collision integral	[K]
T_∞	Ambient temperature	[K]
T_p	Solid temperature	[K]
T_s	Temperature of the gas at the surface of adsorbent	[K]
T_w	Wall temperature	[K]
t	Time	[s]
t_w	Thickness of the column wall	[m]
U	Global external heat transfer coefficient	[W/m^{2}K]
u_s	Superficial velocity	[m/s]
u	Interstitial velocity	[m/s]

V_{sp}	Valve set point	[-]
V_{sp}^{act}	Actual valve set point	[-]
W_{ads}	Weight of adsorbents	[kg]
x_i	Pressure reduction parameter	[-]
y_f	Mole fraction	[-]

Greek Symbols

α_w	Ratio of the internal surface area to the volume of the column wall	[1/m]
α_{wl}	ratio of the logarithmic mean surface area of the column shell to the volume of the column wall	[1/m]
γ	Heat capacity ratio $\gamma = C_p/C_v$	[-]
ΔE	Effective bond energy	[kJ/mol]
ΔH	Change in isosteric heat of adsorption/enthalpy	[kJ/mol]
ΔU	Change in internal energy	[kJ/mol]
Δt	Residence time at each site	[s]
$\frac{\partial Q'}{\partial t}$	Heat transfer rate	[W/m^3]
ε	Bed void fraction	$[m_{gas}^3/m_{tot}^3]$
$\varepsilon_{i,j}^L$	Characteristic Lennard-Jones energy parameter	[J]
ε_p	Adsorbent particle void fraction	[-]
ε_t	Total void fraction	[-]
η	Efficiency	[-]
Θ	Parameter for the Sips equilibrium constant	[J/mol]
θ	Parameter for the adsorption saturation limit	[J/mol]
θ_s	Surface fractional coverage	[-]
λ	Heat axial dispersion coefficient	[W/mK]
λ_{fl}	Thermal conductivity of the gas	[W/mK]
λ_{av}	Average distance between sites	[m]
μ	Viscosity	[Pas]
v	Vibration frequency	[1/s]
ρ_b	Density of bed	[kg/m^3]
ρ_g	Gas density	[kg/m^3]
ρ_p	Particle density	[kg/m^3]
ρ_w	Wall density	[kg/m^3]
$\sigma_{i,j}$	Characteristic Lennard-Jones length parameter	[Å]
τ	Tortuosity factor	[-]
τ_v	Time constant	[-]
χ	CO_2 emission index	[kg_{CO2}/kWh_{LHV}]
Ω	Parameter for the Sips equilibrium constant	[1/Pa]
Ω_D	Diffusion collision integral	[-]

ω	Parameter for the adsorption saturation limit	[mol/kg]

Chemical Symbols

Ar	Argon
CH_4	Methane
CO	Carbon monoxide
CO_2	Carbon dioxide
COS	Carbonyl sulfide
H_2	Hydrogen
H_2O	Water
H_2S	Hydrogen sulfide
N_2	Nitrogen
O_2	Oxygen
SO_2	Sulfur dioxide

1 Introduction

Global warming due to CO_2 emissions is a widespread public concern. The annual CO_2 emissions have increased by 80 % between 1970 and 2004, and the growing environmental concerns have prompted action from international governments, resulting in organizations such as Intergovernmental Panel on Climate Change (IPCC) and the Global Climate Change Initiative (D'Alessandro, et al., 2010). Anthropologic CO_2 emissions have increased the global atmospheric CO_2 concentration from a preindustrial value of 280 ppm (Samanta, et al., 2011) to the current value of 401 ppm (CO2now.org, 2014). Estimates show that the global emissions could lead to a 2.4-6.4 °C increase in earth's average temperature by the year 2100 (Brúder, 2012). Cost effective large scale Carbon Capture and Storage (CCS) is a central strategy to meet the world's increasing energy demand, while at the same time reducing the global emissions to the atmosphere (D'Alessandro, et al., 2010). CO_2 should be captured from large point sources such as power plants, and stored below ground in large reservoirs (Working Group III of IPCC, 2005). The main focus of CCS today is coal based power plants (Samanta, et al., 2011).

A modern power plant with CCS could potentially reduce the CO_2 emissions to the atmosphere by 80-90 %. The drawback is that CCS can increase the cost of electricity by 0.01-0.05 US$/kWh or by 20-70 US$/tonne CO_2 avoided and increase the heat rate for a power plant by 25-40 %. Existing methods for CCS are not cost-effective, and provide incentives for more effective capture processes and materials (Working Group III of IPCC, 2005), (D'Alessandro, et al., 2010). Integration of capture, transport and storage has been demonstrated in several industrial applications, but not yet at a commercial large scale power plant. There are, however two large scale power plants with CCS planned to start up in 2014 (Global CCS Institute, 2013). Carbon capture by pre-combustion and post-combustion are considered economical feasible under specific conditions, but they are not mature market technologies (Working Group III of IPCC, 2005).

The search for energy efficient CO_2 capture has led to many different concepts and power plant designs. The three main principles for capturing carbon from power plants are pre-, post- and oxy-fuel combustion capture. In the context of coal power plants, pre-combustion capture is applicable to IGCC plants, while oxy-combustion and post-combustion capture is applicable to conventional coal power plants. Each application involves different gas separation technologies which impose distinct requirements and constraints for materials (Samanta, et al., 2011). The main principles for capturing CO_2 are illustrated in figure 1.

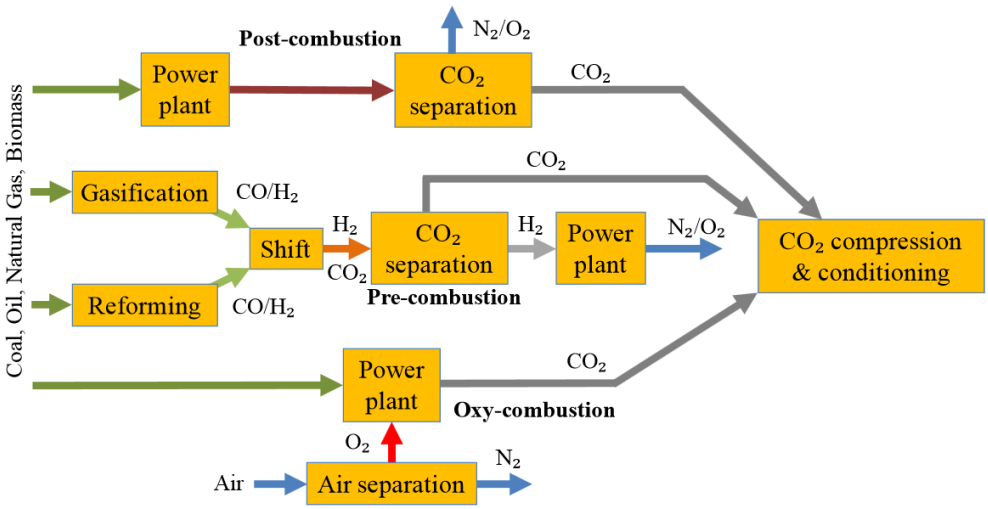

Figure 1: CO_2 capture processes (Bolland, 2012)

The pre-combustion CO_2 capture is not as mature as the post-combustion, but it introduces significant advantages. The CO_2 concentration in a typical pre-combustion process is 36 mole% and the pressure is typically 30 bar. These favorable conditions can reduce the heat rate increase to 10-16 %, which is about half compared to post-combustion capture. The downside is that pre-combustion capture is only applicable for new power plants since the CO_2 capture is an integrated part of the process (D'Alessandro, et al., 2010). Gas turbines running on hydrogen are also a challenge, and it requires research and development before well-functioning hydrogen gas turbines becomes available (Bolland, 2012).

For post-combustion capture of CO_2 from flue gas, a major difficulty is the low pressure of the flue gas. The concentration of CO_2 is low, about 15 mole%, and must be captured from a high volume gas stream at atmospheric pressure (D'Alessandro, et al., 2010). Post-combustion CO_2 capture can be retrofitted to existing power plant, but is expected to lead to higher costs and significantly reduced overall efficiency compared to newly built plants (Working Group III of IPCC, 2005), (D'Alessandro, et al., 2010). Post-combustion CO_2 capture technology has been employed in the industry for several years, based on separation of CO_2 from gas streams in natural gas and refinery off-gases by the use of amine absorbers (Samanta, et al., 2011).

A state of the art amine-based regenerative chemical absorption process using monoethanolamine (MEA) is highly energy demanding due to the high regeneration requirement. It is estimated that the cost of electricity increases with 80 % when CO_2 capture process with an aqueous 30 wt% MEA is used in a coal power plant (Samanta, et al., 2011). The process also requires a large amount of makeup due to thermal and oxidative degradation of the amine. The amine-based absorption process is often used as a benchmark to compare new CO_2 capture technologies (Choi, et al., 2009), (Samanta, et al., 2011).

Existing methods are not cost-effective enough to be implemented in large scale. Amongst the many processes suggested for CO_2 capture, the adsorption process has shown promise and there is a growing interest for it as an alternative. Potential advantages such as reduced

energy requirement, greater capacity and better selectivity may be achieved. The success of the adsorption process depends on the process design, the solvent material and the interaction between these (Samanta, et al., 2011).

1.1 Risk Assessment

In this thesis, there has been no laboratorial work or excursions. Therefore, it has not been performed a risk assessment for the work regarding this thesis.

1.2 Thesis Scope and Outline

This thesis is a continuation of the previous work conducted in the project thesis. Previous work investigated the effect of carbon capture by PSA on a PCC and IGCC power plant. The main drawback of the analysis was that the PSA process was not modeled and the performance was based on literature data. Literature data such as purity, recovery and power consumption was used. The main objective of this thesis is to develop a dynamic model of the PSA process for the pre- and post-combustion case and integrate the model with the power plant models. The PSA process is to be optimized to achieve the target recovery and purity, while minimizing the power consumption. Optimization of the PSA process will reduce the energy penalty of CCS. The goal is to estimate the net power plant efficiencies for both the pre- and post-combustion case. In addition to the energy assessment, the size and number of PSA columns required to accommodate the flue gas will be estimated. A full assessment of the performance and an evaluation of the feasibility of PSA as a technology for decarbonisation will be carried out.

This thesis will include a literature review on PSA modeling and a definition of a suitable dynamic model to represent the performances of a PSA cycle. The simulation tool gPROMS (general Process Modeling System) will be used to model the PSA process. Thermoflow's software Steam Pro, GT Pro and Thermoflex will be used to model the power plants. The PSA model and power plant model will be linked together by macros in Microsoft Excel.

2 Adsorption

Adsorption is a process where molecules accumulate on the surface of a solid material, in contrary to absorption where the molecules are taken up by the bulk volume of the sorbent. The process arises as a consequence of attractive forces. The nature of the bonds depends on the species involved, but adsorption is generally classified in either physisorption or chemisorption. Physisorption is characterized by weak van der Waals forces, where no chemical bonds are formed. In chemisorption, on the other hand, the molecules undergo a chemical reaction where covalent bonds are formed (Hedin, et al., 2010).

Solid adsorbents are typically employed in cyclic processes of adsorption and desorption. In the desorption stage, the adsorbed gas is released from the solid. Desorption is usually induced by a pressure swing or a temperature swing. Both types are relevant for CO_2 capture purposes (Hedin, et al., 2010). PSA and the majority of other practical separation processes are based on physisorption. (Ruthven, et al., 1994). Pressure swing is usually utilized for physisorption, while temperature swing is used for chemisorption. The advantage of adsorption processes compared to the amine-based absorption is the lower energy requirement of the regeneration. Amine-based absorbents contain large amounts of water, which have high heating capacity. A large amount of makeup is also required to due thermal and oxidative degradation (D'Alessandro, et al., 2010), (Samanta, et al., 2011).

The PSA is based on the fact that gases tend to attract to the adsorbents under high pressure. A higher pressure results in more adsorbed gas and when pressure is reduced the gas is released, or desorbed. PSA can be used to separate gases because some gases are attracted more strongly to the surface than others. As the PSA is a cyclic operation, the vessels can be set up in a batch or as a continuous operation. For CO_2 capture in power plants, a continuous operation is of great importance. This requires several vessels which are operated at different stages in the process such that there is a continuous gas feed from the power plant to the PSA process (Bolland, 2012).

The Temperature Swing Adsorption (TSA) relies on regeneration by an increase in temperature. For any given pressure, the adsorption capacity is decreased as the temperature is increased. A relatively small increase in temperature can have large effects, and it is generally possible to desorb any component provided the temperature is high enough. TSA is usually more energy demanding than PSA since the chemical bonds are stronger than the van der Waals forces, and harder to break (Samanta, et al., 2011).

A disadvantage with adsorption compared to other separation technologies is that more treatment of the gas feed before the separation is required, as most adsorbents are very sensitive to water and heat, and can also be affected by sulfur oxides and H_2S. The gas stream has to be cooled and dried, and possibly cleaned (Samanta, et al., 2011), (Choi, et al., 2009).

2.1 PSA Process

Swing adsorption processes like PSA uses set of fixed beds connected by valves so that the gas stream can be shifted between these beds. The beds therefore undergo several cyclic

steps and there is a swing between the sorption and desorption. TSA normally uses fluidized bed reactors, and the beds are not themselves subjected to the temperature swing, but rather the gas itself. This is a more complex setup than for PSA, which uses several beds. The number of beds and the number of steps determine if the PSA process can be continuous or if it is a batch operation (Bolland, 2012).

2.1.1 PSA and VPSA

There were two types of PSA processes that were investigated in this thesis. The main difference between these two processes is the difference in desorption pressure – atmospheric or sub-atmospheric. In PSA cycles with sub-atmospheric desorption, the desorption pressure is usually around 0.1 atm as seen in several experiments and simulations (Liu, et al., 2011), (Na, et al., 2002), (Takamura, et al., 2001). This type of PSA process is also sometimes referred to as Vacuum Pressure Swing Adsorption (VPSA). The reason for utilizing a sub-atmospheric pressure is to achieve a larger pressure swing, thus increasing the performance. Although the vacuum pumps, which are necessary to perform this operation, require power, it is the obvious choice of PSA cycle for post-combustion capture. The explanation is that since the flue gas has atmospheric pressure, a small pressurization to around 1.5 bar may be necessary as seen in the reviewed cycles in table 1. However, by using near vacuum desorption, the energy penalty can be reduced as additional compression of the atmospheric flue gas would be far more energy demanding then the vacuum suction required for sub-atmospheric desorption.

For pre-combustion CO_2 capture by PSA, atmospheric desorption pressure may be utilized as the feed pressure from the incoming syngas after the Water Gas Shift (WGS) reaction can be between 20-70 bar (Bolland, 2012). Hence, the necessary pressure swing is provided by the high pressure syngas. Because pressurization of the feed gas and near vacuum pressure desorption is not needed, the PSA process may not require power. In that aspect the PSA process is advantageous as it has already been mentioned that the absorption technology is very energy consuming.

2.1.2 CO_2 Capture Challenges

This thesis aims to model a PSA process that can achieve at least 90 % CO_2 recovery for both the pre- and post-combustion case. Recovery is the same as capture rate. The CO_2 recovery is defined as (Khajuria, 2011):

$$\frac{Amount\ of\ CO_2\ in\ the\ product\ stream}{Amount\ of\ CO_2\ in\ the\ feed\ stream} \quad (1)$$

The captured CO_2 should also have a high level of purity. The goal is to achieve a purity of at least 95.5 % for both the pre- and post-combustion case which is recommended by DYNAMIS (de Visser, et al., 2008). The CO_2 purity is defined as (Khajuria, 2011):

$$\frac{Amount\ of\ CO_2\ in\ the\ product\ stream}{Total\ amount\ of\ product\ stream} \quad (2)$$

Strong arguments for a high purity CO_2 capture are to keep compression duties as low as possible as well as size reduction of equipment related to handling, storage and

compression of CO_2. The most important argument is the fact that there is a limit to the concentration of impurities that can be tolerated for transport and storage (de Visser, et al., 2008). Table 9 in section 4 provides information about the DYNAMIS recommendations for tolerated levels of impurities. Although a specific aim for power consumption of the PSA process has not been set, it should be as low as possible in order to compete with the major capture technologies such as absorption separation. Another important process requirement is the ability to maintain a continuous flow of syngas or flue gas.

Historically, the PSA process has been used to obtain high raffinate product purity. The raffinate is defined as the less adsorbed species. The strongly adsorbed species, also called extract product, is usually a byproduct with large impurities. The PSA cycle can be modified to achieve a higher purity of the adsorbed species. However, this increases the capital cost and increase the complexity of the PSA process (Ruthven, et al., 1994). Choi, et al. (2003) and Liu, et al. (2011) also show that modifications to achieve higher extract purity are successful, but also result in decreasing the extract capture rate. There is therefore often a trade-off between extract capture rate and purity.

When capturing CO_2 for CCS purposes the CO_2 is usually the strongly adsorbed species on many adsorbents, including zeolites (Liu, et al., 2011) and activated carbons (Lopes, et al., 2009). CO_2 is therefore the component that is subject to adsorption and not nitrogen or hydrogen. That means that in the context of CO_2 capture, CO_2 is the extract product, and the challenge is to combine high CO_2 capture rate with high CO_2 purity.

The CO_2 concentration of the feed gas is important for the PSA process. A high CO_2 concentration is beneficial with regards to obtaining both high CO_2 purity and high CO_2 recovery. If the CO_2 concentration in the feed gas is above 25 mole%, 99 mole% purity combined with over 70 % recovery is achievable with a single stage PSA process. When the CO_2 concentration ranges between 10-15 mole%, it is difficult to obtain high purity and high recovery with a single stage PSA (Park, et al., 2002). It is therefore easier to achieve the required purity and recovery when capturing the CO_2 in syngas obtained from gasification as this typically contains around 38 mole% CO_2 (Bolland, 2012).

Another general feature of the PSA process, which is a challenge for large scale CO_2 capture, is the scaling characteristics. For other separation methods, the capital cost is non-linear with respect to throughput. This is not the case with PSA as the throughput is proportional to the capital cost. This means that when the overall costs are taken into consideration, PSA is economically favorable for small scale separation (Ruthven, et al., 1994). However, as the PSA has potential advantages compared to other separation methods such as low energy requirement and easy operation, this may outweigh the downside of an increased capital cost (Takamura, et al., 2001).

The capacity of several attractive adsorbents such as zeolites and activated carbons decrease significantly when subjected to moisture (Choi, et al., 2009). Flue gas typically contains 7-9 mole% water vapor and therefore needs to be dried before the adsorption process (Bolland, 2012). One method is to cool the flue gas below the dew point temperature of the water in order to remove the water with a scrubber. This process will

require extra equipment, which increases the capital costs. In addition, auxiliary power demand associated with pumping of cooling water and flue gas pressure loss in the heat exchanger can be expected. The typical water vapor fraction from coal gasification is very low (0.2 mole%) (Bolland, 2012), so the pre-combustion PSA process in an IGCC power plant does not face the same problems. In addition to water removal, contaminants such as H_2S may have to be removed if the adsorbent material cannot tolerate it (D'Alessandro, et al., 2010).

2.1.3 PSA Cycle Steps

The basic PSA cycle principle is to have two or more beds that undergo cyclic adsorption and desorption (Bolland, 2012). However, as the operating cycle is critical to the performance, there have been many different attempts to modify the basic cycle. This includes adding cycle steps, the number of beds (Ruthven, et al., 1994) and even adding another PSA stage, meaning that the adsorbed product passes through a secondary PSA process (Liu, et al., 2011).

There are several factors that determine how the process should be modified such as the nature of adsorption selectivity (equilibrium or kinetics) and the trade-off between CO_2 purity and recovery.

The typical steps in a PSA cycle are:

1) Feed pressurization: This step is also called pressurization. The pressure in the bed is increased to the feed pressure as fresh feed gas is introduced co-currently into the bed. The product end is closed during this step in order to achieve the rise in pressure. The pressurization can also be counter-current, but then with the raffinate gas entering counter-current into the bed (Liu, et al., 2011). If the latter step is employed this is carried out prior to the co-current pressurization with the feed gas, with the purpose of improving the purity and recovery of the raffinate product (Ruthven, et al., 1994).

2) Feed step: This step is also called the adsorption step, and usually follows the pressurization step. The feed gas is passed through the adsorbent at the highest cycle pressure level with the product side valve open. This step causes the raffinate gas to become enriched in the less adsorbed species as the strongly adsorbed species are taken up by the adsorbents (Rodrigues, et al., 1988). It is important that the feed stops before breakthrough is reached. Breakthrough can be said to be occurring when the concentration of the strongly adsorbed species in the raffinate product starts to increase dramatically. It is therefore very important to select the correct feed step time in order to achieve high recovery (Choi, et al., 2003). During the adsorption step the pressure can either be kept at a constant level or be allowed to be slightly reduced. By reducing the pressure the recovery of the raffinate gas is increased (Ruthven, et al., 1994). For CO_2 PSA this should mean that the purity of the adsorbed CO_2 would increase, but at the expense of the recovery.

3) Pressure equalization: During this step the pressure between two beds is equalized by connecting a high pressure bed with a low pressure bed. The high pressure bed goes through a depressurization, which starts before breakthrough of the strongly adsorbed species (Liu, et al., 2011). The low pressure bed is pressurized. This step saves energy since the work needed for the pressurization step can be reduced (Choi, et al., 2003).

4) Desorption: The desorption can be performed with different modes of operations. One is to have counter-current desorption with raffinate purge, which was the method of choice in the basic Skarstrom cycle (Ruthven, et al., 1994). This is done by using a fraction of the raffinate product to flush the void spaces in the bed. By doing this one can ensure that the raffinate at the end of the bed, which is recovered in the next cycle, is completely free of the strongly adsorbed species. This result is increased extract recovery at the expense of decreased extract purity (Ruthven, et al., 1994). Counter-current purging is often carried out at the lowest cycle pressure, but it is also possible to employ this step at intermediate pressures (Liu, et al., 2011).

   An alternative to purging is to use a counter-current evacuation, also known as blowdown (Ruthven, et al., 1994). During the evacuation step the extract product is recovered. With the blowdown step a high extract purity and recovery can be obtained. The disadvantage with this step compared to the raffinate purging is that when evacuation is performed at near vacuum pressure the increase in the recovery of the raffinate is at the expense of additional mechanical energy needed for the evacuation step (Ruthven, et al., 1994). It should be noticed that blowdown and purge may be used in the same PSA cycle

5) Rinse step: The rinse step is a form of purging, but instead of purging with the raffinate product the extract product is used. This step often follows the pressure equalization step as seen in several papers (Choi, et al., 2003), (Na, et al., 2002). The aim is to improve the extract product purity when less adsorbing (lighter) species are co-adsorbed with the more strongly adsorbed (heavier) species (Ruthven, et al., 1994). The rinse step is carried out by using a fraction of the adsorbed gas and recycling it co-currently into the bed. The rinse can be performed with the valve at the other end of the bed first closed, then open (Choi, et al., 2003), or open during the entire step (Na, et al., 2002). As with the adsorption step time, the rinse step time is important to optimize. If the rinse is allowed to proceed for too long time, the recovery of the extract product is significantly decreased as a large portion of the heavy species disappears with the raffinate (Na, et al., 2002).

Figure 2 shows the cycle steps discussed above. The feed pressurization (FP), feed, rinse and the depressurization part of the pressure equalization (EQ) step are co-current. The

blowdown, purge and pressurization part of pressure equalization are counter-current. It should be pointed out that not all of these steps are necessary to perform a PSA cycle, but when aiming for a high CO_2 recovery and purity, some of these steps may be necessary to include. This applies in particular for post-combustion CO_2 recovery.

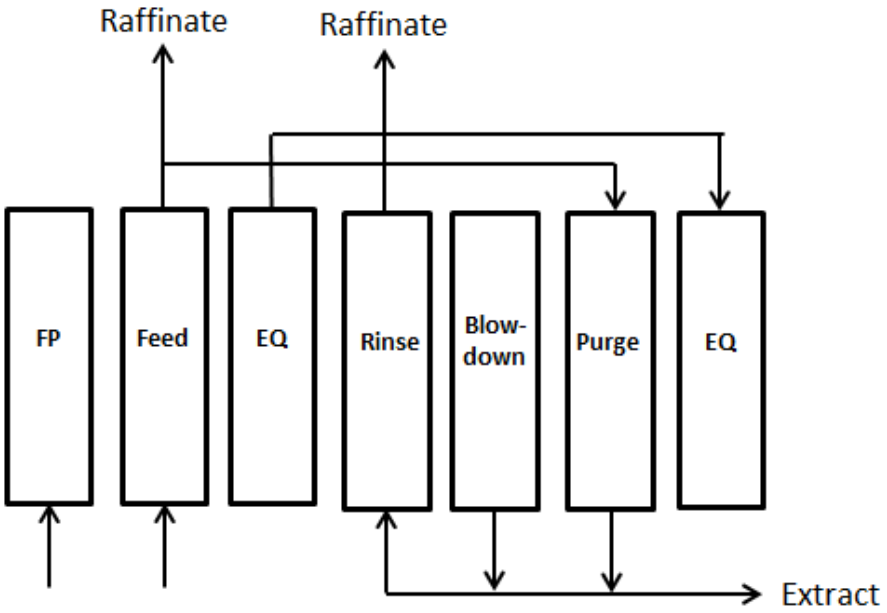

Figure 2: PSA cycle steps

2.1.4 Choice of PSA Cycle for Modeling

A number of PSA cycle configurations have been reviewed. The review culminated in two tables summarizing the performance achieved in the literature. Table 1 shows the overview of cycles considered for post-combustion capture. The best performing cycle was the two-stage PSA cycle with zeolite 5A as adsorbent by Liu, et al. (2011). The front stage was a three-bed and five-step Skarstrom cycle with rinse and the tail stage was a two-bed and six-step Skarstrom cycle with pressure equalization.

Table 2 shows the overview of cycles considered for pre-combustion capture. The best performing cycle was the seven-bed, twelve-step Skarstrom PSA cycle with four pressure equalization steps and activated carbon as adsorbent by Casas, et al. (2012).

These two cycles made up the basis for modeling in gPROMS. The modeling of the PSA processes followed the parameters and assumptions by the authors to as large extent as possible. However, the main goal was to achieve a high CO_2 purity and recovery combined with low power consumption. Deviations from the original cycles regarding cycle times, flow rates, pressure levels and configuration was necessary in order to optimize the performance.

Table 1: Post-combustion PSA configurations from literature[A]

Cycle configuration	Cycle type/description	Cycle step sequence[b]	Ads[c]	P_H atm	P_L atm	Study type	CO_2 feed conc. %.	CO_2 prod. Purity %	CO_2 rec. %	Feed flow rate[d]	Ref.
3-bed 7-step	VPSA with rinse and pressure equalization	fPR, AD, PEo, cRN, oRN, EVn, PEn	13X	1.5	0.05	Exp	13	90.0	78.0	10 LPM	(Choi, et al., 2003)
4-step	VPSA with rinse recycle and raffinate pressurization	rPR, AD, oRN, EVn	AC	1.2	0.1	Sim	17	90	85	-	(Kikkindes, et al., 1993)
3-bed 6-step	VPSA with pressure equalization and rinse-recycle	fPR, AD, PEo, oRN, EVn, PEn	AC	1.97	0.1	Exp	13	99	59	83 LPM	(Na, et al., 2002)
2-bed 4 step	Skarstrom VPSA	fPR, AD, Bn, Pn,	5A	1.48	0.1	Sim	15	50.67	95.04	0.8 SLPM	(Liu, et al., 2011)
2-bed 6-step	Skarstrom VPSA with pressure equalization	fPR, AD, PEo, Bn, Pn, PEn	5A	1.48	0.1	Sim	15	58.23	93.62	0.8 SLPM	(Liu, et al., 2011)
3-bed 5-step	Skarstrom VPSA with rinse	fPR, AD, oRN, Bn, Pn	5A	1.48	0.1	Sim	15	69.15	98.92	0.8 SLPM	(Liu, et al., 2011)
4-bed 7-step	Skarstrom VPSA with pressure equalization and rinse	fPR, AD, oRN, PEo, Bn, Pn, PEn	5A	1.48	0.1	Sim	15	77.14	91.46	0.8 SLPM	(Liu, et al., 2011)
Two-stage: 3-bed 5-step and 2-bed 6-step	Front VPSA: Skarstrom with rinse Tail VPSA: Skarstrom with pressure equalization	Front: fPR, AD, oRN, Bn, Pn Tail: fPR, AD, PEo, Bn, Pn, PEn	5A	1.48	0.1 and 0.15	Sim	15	96.05	91.05	0.8 SLPM	(Liu, et al., 2011)
4-bed 8-step	Skarstrom VPSA with pressure equalization and rinse	fPR, AD, oRN, PEo, EVn, Pn, PEn, 0	67 % NaX 33 % NaA	1.18	0.1	Exp	13	58.80	91.59	-	(Takamura, et al., 2001)
4-bed 8-step	Skarstrom VPSA with pressure equalization and rinse	fPR, AD, oRN, PEo, EVn, Pn, PEn, 0	NaX	1.18	0.1	Exp	13	56.93	87.96	-	(Takamura, et al., 2001)
2-bed 4-step	Skarstrom VPSA	fPR, AD, Bn, Pn	13X	1.13	0.07	Sim	10	55	87	135 LPM	(Park, et al., 2002)
2-bed 6-step	Skarstrom VPSA with pressure equalization	fPR, AD, PEo, Bn, Pn, PEn	13X	1.13	0.07	Sim	10	64	85	135 LPM	(Park, et al., 2002)
3-bed 5-step	Skarstrom VPSA with rinse	fPR, AD, oRN, Bn, Pn	13X	1.13	0.07	Sim	10	64	89	135 LPM	(Park, et al., 2002)
3-bed 8-step	VPSA with pressure equalization and rinse	fPR, AD, Bo, PEo, cRN, oRN, EVn, PEn	AC	1.5	0.1	Exp	17	91.2	46.1	10 SLPM	(Na, et al., 2001)
2-bed 4-step	Skarstrom VPSA	fPR, AD, Bn, Pn	13X	13.3	0.88	Sim	15	71.9	94.4	-	(Ko, et al., 2005)
2-bed 4-step	FVPSA	fPR, AD, Bo, EVn	13X	6.7	0.69	Sim	15	90.0	93.8	-	(Ko, et al., 2005)

[A]The main performance parameters have been CO_2 purity and recovery. Some of the performance numbers given in this table have been stated as the best performance in the originating journal articles. Other numbers have been read from result graphs from the respective experiments or simulations. [b] Cycle step abbreviation legend: fPR = feed pressurization, rPR = raffinate pressurization, AD = adsorption, PEo = co-current pressurization, PEn = counter-current pressurization, cRN = closed end rinse step, oRN = open end rinse step, Bo = co-current blowdown, Bn = counter-current blowdown, EVn = counter-current evacuation, Pn = counter-current purge, 0 = null step. [c] Adsorbent abbreviation legend: 13X = zeolite 13X, AC = activated carbon, 5A = zeolite 5A, NaX = NaX-type zeolite, NaA =NaA-type zeolite. [d] Feed flow rate dimensions: SLPM = standard liter per minute, LPM = liter per minute.

Table 2: Pre-combustion PSA configurations from literature[a]

Cycle configuration	Cycle type/description	Cycle step sequence[b]	Ads[c]	P_H atm	P_L atm	Study type	CO_2 feed conc. %.	CO_2 prod. Purity %	CO_2 rec. %	Feed flow rate[d]	Ref.
2-bed 6-step	Skarstrom PSA with pressure equalization	fPR, AD, PEn, Bn, Pn, PEo	AC	19.74	0.99	Exp.	50	92.6 ±5.7	88.0 ± 5.4	1.2 LPM	(Schell, et al., 2013)
6-bed 10-step	Skarstrom PSA with 3 pressure equalization steps, co-current blowdown	fPR, AD, PEo, PEo, PEo, Bo, Pn, PEo, PEo, PEo	AC	33.56	0.99	Sim.	40	93.1	90.3	1.2 LPM	(Casas, et al., 2012)
6-bed 10-step	Skarstrom PSA with 3 pressure equalization steps, co-current blowdown	fPR, AD, PEo, PEo, PEo, Bo, Pn, PEo, PEo, PEo	AC	33.56	1.97	Sim.	40	86.5	85	1.2 LPM	(Casas, et al., 2012)
6-bed 10-step	Skarstrom PSA with 3 pressure equalization steps, co-current blowdown	fPR, AD, PEo, PEo, PEo, Bo, Pn, PEo, PEo, PEo	AC	24.68	0.99	Sim.	40	93.4	90	1.2 LPM	(Casas, et al., 2012)
5-bed 8-step	Skarstrom PSA with 2 pressure equalization steps	fPR, AD, PEo, PEo, Bn, Pn, PEo, PEo	AC	33.56	0.99	Sim.	40	89.4	90	1.2 LPM	(Casas, et al., 2012)
7-bed 12-step	Skarstrom PSA with 4 pressure equalization steps	fPR, AD, PEo, PEo, PEo, PEo, Bo, Pn, PEo, PEo, PEo, PEo	AC	33.56	0.99	Sim.	40	95.3	90	1.2 LPM	(Casas, et al., 2012)

For table description, see table 1.

3 Mathematical Modelling of PSA Processes

3.1 Introduction

PSA processes consists of several beds interacting with each other as gas flows from one bed to another, as in pressure equalization, rinse and purge. There are two main approaches when modeling PSA processes; the unibed and multibed method. The unibed method takes advantage of that all the beds have the same physical dynamic behavior, and consequently simulates one bed for all operating steps in the cycle. The simplest, and not so realistic, strategy for the unibed method is to use average and fixed gas compositions for the streams that connect two columns together. A more realistic approach is to store the solution from one step in the cycle, and use the solution in a later step, which imitates the interaction between the beds. On the other hand, the multibed approach simulates all the beds and the interaction between these, but simulates only a portion of the cycle. This is a more complex setup and is more computationally demanding. Ancillary equipment, such as valves, mass-flow controllers and regulators may also be included in the simulations to study how the entire PSA unit will work together (Agarwal, 2010), (Liu, et al., 2011).

PSA processes always operate under transient conditions, and the boundary conditions change through the steps of the cycle. Consequently, the PSA process will never reach steady state. However, the PSA process can operate under what is called cyclic steady state. At cyclic steady state, the conditions are identical at the beginning and end of a cycle for all beds, and may take from several hundred to several thousands of cycles to reach. The process itself is dynamic, but the results repeat itself from one cycle to the next (Agarwal, 2010).

A model should be designed for its purpose. It should be as simple as possible, while still accounting for the essential mechanisms involved. The model can be on a macro, micro and molecular scale with mechanisms as convection, dispersion, diffusion, migration, adsorption, reaction and desorption. In reactors there will be gradients in both radial and axial direction for temperature, concentration, pressure and velocity. The fundamental approach would be to model all the mechanisms involved and interactions between phenomena of different scales. However, assumptions are often made to formulate simplified criteria and thus reducing the computational time and complexity of the mathematical model (Jakobsen, 2011).

There are in principle two ways of modeling a fixed bed reactor, which are the pseudo homogeneous and the heterogeneous models. Pseudo homogeneous models do not account explicitly for the existence of the adsorbents, in contrast to heterogeneous models which does. A heterogeneous model requires additional conservation equations for the fluid phase and fluid inside particle pores. Pseudo homogeneous models are used when the temperature and concentration difference between the gas and adsorbent surface are small. Heterogeneous models are used when this simplification is not valid (Jakobsen, 2011).

The mathematical model of a fixed-bed PSA process includes the following:

- Mass transfer
- Component mass balance
- Overall mass balance
- Momentum balance
- Energy balance for the wall, solid and gas
- Nonlinear multicomponent adsorption equilibrium isotherms
- Boundary conditions

3.2 Mass Transfer

Most adsorbents are porous particles with large surface area to ensure a high capacity, which results in a large number of pores. The adsorbate molecules diffuse into the pores to fully utilize the adsorption sites. Several types of diffusion mechanisms may become dominant, and at times some mechanisms can compete or cooperate (Suzuki, 1990). The adsorption process occurs in sequence; the adsorbate diffuses from the bulk gas phase to the surface of the adsorbent, followed by diffusion from the surface into the macropores, and finally diffuses further into the micropores before getting adsorbed. Due to this, there are three different mass transfer resistances which are external film resistance, macropore diffusive resistance and micropore diffusive resistance (Agarwal, 2010).

3.2.1 External Transport Processes

Film Resistance

The external film resistance is due to a laminar boundary layer around the surface of the adsorbent, which limits the mass and heat transfer rate. The boundary layer is caused by the no-slip, or continuity condition at the surface. The significance of the resistance depends on the boundary layer thickness, which depends on the hydrodynamic conditions (Karger, et al., 2012). The transport processes are represented by film coefficients which are defined according to the linear laws of Fick and Fourier (Yang, 1986).

The mass transfer, based on per unit volume of bed is given by (Yang, 1986):

$$\frac{\partial C_i}{\partial t} = k_g a\left(C^s_{por,i} - C_i\right) \quad i = 1, \ldots, N_c \tag{3}$$

Here, C_i is the gas phase concentration of the ith component [mol/m^3], k_g is the film mass transfer coefficient [m/s], a is adsorbent surface area per volume of bed [m^2/m^3], $C^s_{por,i}$ is the concentration of the ith component on the adsorbent solid surface [mol/m^3] and N_c is the number of components.

The heat transfer, based on per unit volume of bed is given by (Yang, 1986):

$$\frac{\partial Q'}{\partial t} = h_f a(T_s - T) \tag{4}$$

Here, $\frac{\partial Q'}{\partial t}$ is the rate of heat transfer [W/m^3], h_f is the film heat transfer coefficient [W/m^{2}K], T_s is the temperature of the gas at the surface of the adsorbent [K] and T is the bulk temperature of the gas [K].

For a flowing fluid, the film becomes thinner and the film coefficients become larger. The film coefficients vary in a complex manner around the particle. There are correlations that can be used to calculate the coefficients around the particle, but average values are often used in practice. The average film mass transfer coefficient can be obtained from the Sherwood number given by (Yang, 1986), (Lopes, et al., 2009):

$$Sh = \frac{2k_g R_{pa}}{D_m} \tag{5}$$

R_{pa} is the particle radius [m] and D_m is the molecular diffusivity [m^2/s].

When axial dispersion is included in the modeling, the Sherwood number can be found from this equation (Yang, 1986), (Lopes, et al., 2009):

$$Sh = 2.0 + 1.1Sc^{\frac{1}{3}} Re_p^{0.6} \tag{6}$$

Here, Sh, Sc and Re is Sherwood, Schmidt and Reynolds numbers, respectively. The Reynolds number is given by (Lopes, et al., 2009):

$$Re_p = \frac{\rho_g u_s d_{pa}}{\mu} \tag{7}$$

Here, ρ_g is the gas density [kg/m^3], u_s is the superficial velocity [m/s], d_{pa} is the particle diameter [m] and μ is the gas viscosity [Pas].

The Schmidt number is given by (Lopes, et al., 2009), (Yang, 1986):

$$Sc = \frac{\mu}{\rho_g D_m} \tag{8}$$

The film heat transfer coefficient can be obtained from the Nusselt number (Yang, 1986):

$$Nu = \frac{2h_f R_{pa}}{\lambda_{fl}} \tag{9}$$

λ_{fl} is the thermal conductivity of the gas [W/mK].

The external film resistances are typically smaller than the internal transport resistances and are often negligible in PSA processes (Karger, et al., 2012), (Agarwal, 2010), (Lopes, et al., 2009).

3.2.2 Internal Transport Processes

Macropore Diffusion - Knudsen and Molecular Diffusion

The macropores act as a highway for the adsorbate molecules to reach the interior of the particle. In such a case, molecular diffusion or Knudsen diffusion takes place, or a

combination of both. All adsorbents consist of large surface area which is located inside the particles. The gas must penetrate into the porous structure during adsorption and penetrate out during desorption (Yang, 1986). Diffusion in the gas phase results from collisions. In a large pore, diffusion occurs mainly by bulk molecular diffusion mechanisms, since collisions between diffusing molecules occur more frequently than collisions between molecules and the pore wall. This type of diffusion is called molecular diffusion. The resistance depends on the relative magnitude of the pore diameter and the free mean path of the adsorbate (Karger, et al., 2012). In a multicomponent system, the molecular diffusivity is given by Chapman-Enskog equation (Lopes, et al., 2009), (Solsvik & Hugo A., 2011):

$$D_{m,i} = \frac{1 - y_{f,i}}{\sum_{j=1, i \neq j}^{N_c} \frac{y_{f,j}}{D_{i,j}}} \quad i = 1, \dots, N_c \tag{10}$$

Here, D_m is molecular diffusivity [m^2/s], $y_{f,i}$ is the mole fraction and $D_{i,j}$ is the binary molecular diffusivity [m^2/s].

The binary molecular diffusivity is given by (Pooling, et al., 2000):

$$D_{i,j} = \frac{0.00266\, T^{\frac{3}{2}}}{M_{ij}^{0.5} P \sigma_{ij}^2 \Omega_D} \tag{11}$$

Here, $D_{i,j}$ has the unit [cm^2/s], $M_{ij} = 2(\frac{1}{M_i} + \frac{1}{M_j})^{-1}$ where M is molecular weight [g/mol], $\sigma_{ij} = 0.5(\sigma_i + \sigma_j)$ is the characteristic Lennard-Jones length parameter [Å], Ω_D is the diffusion collision integral [-] and P is pressure [bar]. Ω_D is given by (Pooling, et al., 2000):

$$\Omega_D = \frac{A}{(T^*)^B} + \frac{C}{exp(DT^*)} + \frac{E}{exp(FT^*)} + \frac{G}{exp(HT^*)} \tag{12}$$

Here, $T^* = kT/\varepsilon_{ij}^L$, $\varepsilon_{ij}^L = \sqrt{\varepsilon_i^L \varepsilon_j^L}$ is the characteristic Lennard-Jones energy parameter [J], *k* is the Boltzmann constant [J/K] and A to G are constants.

On the other hand, when the free mean path is much larger than the pore diameter, Knudsen diffusion dominates the transport. The collisions between the gas and pore wall becomes more dominant than collisions between molecules. The Knudsen diffusivity is given by (Lopes, et al., 2009), (Suzuki, 1990):

$$D_{k,i} = 48.5 d_p \sqrt{\frac{T}{M_i}} \quad i = 1, \dots, N_c \tag{13}$$

Here, D_k is Knudsen diffusivity [m^2/s], d_p is the mean pore diameter [m] and M is molecular weight [kg/mol].

In the intermediate case when the magnitude of the free mean path and pore diameter is of the same order, both mechanisms for diffusion are important (Yang, 1986). The macropore

diffusivity is then given by Bosanquet's equation which combines Knudsen and molecular diffusivity (Lopes, et al., 2009):

$$\frac{1}{D_{p,i}} = \tau\left(\frac{1}{D_{m,i}} + \frac{1}{D_{k,i}}\right) \quad i = 1, \dots, N_c \tag{14}$$

Here, D_p is macropore diffusivity [m^2/s], τ is the tortuosity factor which accounts for non-ideal effects [-].

Micropore Diffusion

A surface gradient exists on the pore wall and the flux associated with this is called micropore diffusion or surface diffusion. Surface diffusion can be important in the total flux in a porous material if the surface area and surface concentration is high, which can occur in PSA processes. It can sometimes be convenient to lump the surface diffusion into the macropore diffusivity, however a problem arises as surface diffusivity is strongly dependent of the concentration, while the macropore diffusivity is assumed constant. Surface diffusion takes place by the hopping of molecules between adsorption sites (Yang, 1986).

The surface diffusivity can be related to the surface concentration and flux (Yang, 1986):

$$N_s = -D_s \frac{dC_i}{dr} \tag{15}$$

Here, N_s is the surface flux [mol/m^{2}s], r is the radial distance in the particle [m] and D_s is the surface diffusivity [m^2/s]. It is strongly dependent of the surface fractional coverage (θ_s) and can be expressed by:

$$\frac{D_{s,\theta}}{D_{s,\theta=0}} = \frac{1}{1-\theta_s} \tag{16}$$

The surface diffusivity is given by the Einstein equation:

$$D_s = \frac{\lambda_{av}{}^2}{2\Delta t} \tag{17}$$

Here, λ_{av} is the average distance between sites [m], and Δt is the residense time at each site [s] given by:

$$\frac{1}{\Delta t} = ve^{-\Delta E/RT} \tag{18}$$

Here, v is vibration frequency [1/s] of the bonding that holds the molecule to the site [1/s], ΔE is the effective bond energy [kJ/mol] and R is the ideal gas constant [kJ/molK].

3.3 Component Mass Balance

The complete mathematical model of the mass balance must include three equations. One balance for the gas phase, one balance inside each particle, since the concentration within the particle is changing with the radius, and one equation to couple the equations at the particle surface.

The mass balance for the particle is given by (Yang, 1986):

$$D_{p,i}\left(\frac{\partial^2 C_{por,i}}{\partial r^2}+\frac{2}{r}\frac{\partial C_{por,i}}{\partial r}\right)=\frac{\partial C_i}{\partial t} \quad i=1,\dots,N_c \tag{19}$$

The mass balance for the bulk gas is given by (Yang, 1986):

$$\frac{\partial C_i}{\partial t}+\frac{(1-\varepsilon)}{\varepsilon}k_g a\left(C_i-C^S_{por,i}\right)+\frac{\partial(uC_i)}{\partial z}=D_{ax}\frac{\partial^2 C_i}{\partial z^2} \quad i=1,\dots,N_c \tag{20}$$

Equations (19) and (20) are coupled by the continuity at the particle surface by this equation (Yang, 1986):

$$D_{p,i}\left(\frac{\partial C_{por,i}}{\partial r}\right)_{r=R_{pa}}=k_g\left(C_i-C^S_{por,i}\right) \quad i=1,\dots,N_c \tag{21}$$

In equations (19), (20) and (21), ε is bed void fraction $[m^3_{gas}/m^3_{tot}]$, $C_{por,i}$ is the gas concentration in the macropores [mol/m^3], u is the interstitial gas velocity [m/s] and D_{ax} is the axial dispersion coefficient [m^2/s].

The solution of a system as described with mass balance equations for the bulk gas and within the particle requires a lot of CPU time. Reduced models which neglect the concentration gradient within the particle are often used. This can be achieved by assuming average solid loading for the entire particle and relating the adsorption rate in the particle to the equilibrium concentration as follows (Yang, 1986):

$$\frac{\partial q_i}{\partial t}=f(q_i^*) \tag{22}$$

Here, q_i is the adsorbed phase concentration [mol/kg] and q_i^* is the adsorbed phase concentration at equilibrium [mol/kg].

Equation (22) replaces equation (21) and is also used to replace the second term of equation (20). This eliminates the need for equation (19). There are several models used in the literature depending on the complexity needed in the model, and based on assumptions regarding the mass transfer resistances.

Using the principle in equation (22) and assuming an average gas concentration within the particle and a bi-dispersed particle with macro- and micropores, Liu, et al (2011) presented the three following balances:

$$\varepsilon\frac{\partial C_i}{\partial t}+\frac{(1-\varepsilon)k_g a}{1+Bi_i}\left(C_i-C_{por,i}\right)+\frac{\partial(u_s C_i)}{\partial z}=\varepsilon\frac{\partial}{\partial z}\left(D_{ax}\frac{\partial C_i}{\partial z}\right) \quad i=1,\dots,N_c \tag{23}$$

$$\varepsilon_p\frac{\partial C_{por,i}}{\partial t}=\varepsilon_p\frac{15D_{p,i}}{R^2_{pa}}\frac{Bi_i}{(1+Bi_i)}\left(C_i-C_{por,i}\right)-\rho_p\frac{\partial q_i}{\partial t} \quad i=1,\dots,N_c \tag{24}$$

$$\frac{\partial q_i}{\partial t}=\frac{15D_{c,i}}{r_c^2}(q_i^*-q_i) \quad i=1,\dots,N_c \tag{25}$$

Equation (23) is a mass balance for the bulk gas phase. The first term represents accumulation of solute in the fluid. The second term represents the flux of material due to a concentration gradient between the bulk gas and the gas in the macropores. The third term represents the amount of solute flowing in and out by convection to the section *dz* of the bed. The fourth term represents axial dispersion of solute in the bed. The latter is often neglected due to the fact that numerical dispersion will add to the physical dispersion, causing the concentration fronts to lose sharpness, i.e. numerical smearing of the solution (Agarwal, 2010).

Equation (24) is a mass balance for the gas in the macropores. The first term represents accumulation of solute in the macropore. The second term represents the flux of material due to a concentration gradient between the bulk gas and the gas in the macropores. The third term represents the mass that is adsorbed or desorbed in the micropores. The third term in equation (24) is obtained from equation (25) which is called the LDF equation for the micropores. The micropores act as a sink/source when gas is adsorbed/desorbed.

In equation (23), the axial dispersion coefficient is given by (Lopes, et al., 2009):

$$D_{ax,i} = (0.45 + 0.55\varepsilon)D_{m,i} + 0.35R_{pa}u \quad i = 1, \dots, N_c \tag{26}$$

In equation (24), ε_p is the adsorbent particle void fraction [-], ρ_p is the particle density [kg/m^3] and Bi_i is the mass Biot number given by (Liu, et al., 2011):

$$Bi_i = \frac{k_g R_{pa}}{5\varepsilon_p D_{p,i}} \tag{27}$$

In equation (25), $D_{c,i}$ is the micropore diffusivity [m^2/s] and is given by (Lopes, et al., 2009):

$$\frac{D_{c,i}}{r_c^2} = \frac{D_{c,i}^0}{r_c^2} e^{-\frac{E_a}{RT}} \tag{28}$$

Here, $D_{c,i}^0$ is the limiting diffusivity at infinite temperatures [m^2/s], E_a is the activation energy of micropore diffusion [kJ/mol] and r_c is micropore or crystal radius [m].

Equation (25) can also be given as (Azevedo & Rodrigues, 1999), (Agarwal, 2010):

$$\frac{\partial q_i}{\partial t} = k_{LDF,i}(q_i^* - q_i) \quad i = 1, \dots, N_c \tag{29}$$

Here, k_{LDF} is the LDF mass transfer coefficient [1/s]. The equation can be used if the LDF mass transfer coefficient has been measured in experiments, which is the case for the pre-combustion PSA process by Casas, et al. (2012).

The mass balance for the macropores, equation (24), can be completely avoided if the film resistance and macropore resistance are assumed negligible. Then the concentrations in the macropores and in the bulk gas becomes equal ($C_i = C_{por,i}$). For activated carbons and zeolites, Lopes et al. (2013) showed that macropore resistance and film resistance are in fact negligible compared to axial dispersion and micropore resistance. This allows for the use of the micropore LDF model only. This is also partially confirmed by Choi et al. (2009) stating

that micropore diffusion through crystals dominates the overall mass transfer for some zeolites such as zeolite 5A.

By the use of these reduced models, the new bulk gas mass balance can be written as (Ribeiro, et al., 2008):

$$\varepsilon\frac{\partial C_i}{\partial t}+(1-\varepsilon)\left(\varepsilon_p\frac{\partial C_i}{\partial t}+\rho_p\frac{\partial q_i}{\partial t}\right)+\frac{\partial(u_sC_i)}{\partial z}=\varepsilon\frac{\partial}{\partial z}(D_{ax}\frac{\partial C_i}{\partial z})\quad i=1,\dots,N_c \tag{30}$$

The first, fourth and fifth terms were explained earlier. The second term accounts for accumulation of solute in the macropore. The third term accounts for the adsorption or the flux of material into the adsorbent and replaces the second term in equation (23).

This equation can be written in a more compact form given the relation:

$$\varepsilon_t=\varepsilon+(1-\varepsilon)\varepsilon_p \tag{31}$$

Here ε_t is the total void fraction [-], including both the voids in the bed and in the macropores.

The final two balances which were used in the PSA models then become:

$$\varepsilon_t\frac{\partial C_i}{\partial t}+(1-\varepsilon)\rho_p\frac{\partial q_i}{\partial t}+\frac{\partial(u_sC_i)}{\partial z}=\varepsilon\frac{\partial}{\partial z}(D_{ax}\frac{\partial C_i}{\partial z})\quad i=1,\dots,N_c \tag{32}$$

$$\frac{\partial q_i}{\partial t}=\frac{15D_{c,i}}{r_c^2}(q_i^*-q_i)\quad i=1,\dots,N_c\qquad Post-combustion$$

$$\frac{\partial q_i}{\partial t}=k_{LDF,i}(q_i^*-q_i)\quad i=1,\dots,N_c\qquad Pre-combustion$$

3.4 Overall Mass Balance

The overall mass balance is used to calculate the velocity for all axial positions in the bed and is given by:

$$\varepsilon\frac{\partial C_G}{\partial t}+\frac{\partial(u_sC_G)}{\partial z}=-(1-\varepsilon)\sum_{i=1}^{N_c}k_ga\left(C_i-C_{por,i}\right) \tag{33}$$

The first term represents accumulation and the second term represents flow in and out by convection as before. The third term accounts for the flux of material into the adsorbent.

The total gas concentration is given by:

$$C_G=\sum_{i=1}^{N_c}C_i\qquad or\qquad C_G=\frac{P}{RT} \tag{34}$$

Here, C_G is the total gas phase concentration [mol/m^3].

The mole fraction is given by:

$$y_{f,i} = \frac{C_i}{C_G} \tag{35}$$

Like the component mass balance, the overall mass balance requires an additional mass balance within the particle. It can be simplified further in the same manner as the component mass balance using the principle in equation (22). The simplified overall mass balance is given by:

$$\varepsilon \frac{\partial C_G}{\partial t} + \varepsilon_p (1-\varepsilon) \sum_{i=1}^{N_c} \frac{\partial C_{por,i}}{\partial t} + \frac{\partial (u_s C_G)}{\partial z} = -(1-\varepsilon)\rho_p \sum_{i=1}^{N_c} \frac{\partial q_i}{\partial t} \tag{36}$$

The second term, which represents accumulation in the macropore, can be rewritten together with the bulk gas accumulation term. The macropore resistance is assumed negligible which means that the concentration in the pore is the same as the bulk gas. The final overall mass balance is then reduced to (Casas, et al., 2012):

$$\varepsilon_t \frac{\partial C_G}{\partial t} + \frac{\partial (u_s C_G)}{\partial z} = -(1-\varepsilon)\rho_p \sum_{i=1}^{N_c} \frac{\partial q_i}{\partial t} \tag{37}$$

3.5 Momentum Balance

The gas in the packed column experiences a pressure drop due to viscous losses and drop in kinetic energy. The Ergun equation can be used to model this pressure drop, and is given by (Ribeiro, et al., 2008):

$$\frac{\partial P}{\partial z} = -\frac{150\mu(1-\varepsilon)^2}{\varepsilon^3 d_{pa}^2} u_s - \frac{1.75(1-\varepsilon)\rho_g}{\varepsilon^3 d_{pa}} |u_s| u_s \tag{38}$$

The first term represents losses due to viscous flow (laminar part), while the second term represents the drop in kinetic energy (turbulent part). Often pressure drop is assumed negligible, so that an overall mass balance to obtain the velocity profile can be avoided and a constant or linear velocity profile can be used instead. This can be acceptable for processes with low Reynolds number (Agarwal, 2010). The pressure drop is assumed instantaneous. The term $|u_s|u_s$ is to account for co-current as well as counter-current flow.

The relationship between the superficial gas velocity (u_s) and interstitial velocity (u) is given by:

$$u_s = \varepsilon u \tag{39}$$

3.6 Energy Balance

Adsorption is an exothermic process and the change in temperature will have an impact on the adsorption equilibrium behavior. It is therefore important to take heat effects into account in order to achieve accurate adsorption modeling. The generated heat is transported by conduction between the adsorbent particles and by convection in the bulk

gas phase (Agarwal, 2010). The variation of temperature depends on the heat of adsorption, the bulk phase transport properties and the thermal characteristics of the bed, such as conductivity. The temperature difference between the bulk gas phase and the adsorbent particles is often neglected and a thermal equilibrium between these is assumed (Agarwal, 2010). When this is the case a pseudo homogeneous model can be established. When it cannot be neglected a heterogeneous is established, which takes this into account with an extra energy balance equation for the solid sorbent. The complete energy balance, when assuming that the temperature in the solid is uniform, includes three energy equations, one for each phase (gas, solid and wall) (Ribeiro, et al., 2008). The energy balance for the solid sorbent, considering a spherical pellet, derived from Ribeiro, et al. (2008), is given by:

$$(1-\varepsilon)\left[\varepsilon_p \sum_{i=1}^{n} C_{por,i}\, C_{p,i} + \rho_p \sum_{i=1}^{n} q_i\, C_{p,ads,i} + \rho_p C_{p,s}\right]\frac{\partial T_p}{\partial t} \tag{40}$$
$$= \rho_b \sum_{i=1}^{n} (-H_{ads})_i \frac{\partial q_i}{\partial t} + (1-\varepsilon) a h_f \left(T - T_p\right)$$

Here, C_p is the molar specific heat at constant pressure [J/molK], ρ_b is the bed density [kg/m^3], $C_{p,ads,i}$ is the molar specific heat in the adsorbed gas phase [J/molK], $C_{p,s}$ is the solid specific heat capacity [J/kgK], T_p is the temperature of the solid [K] and H_{ads} is the heat of adsorption [J/mol].

The first term denotes how the solid temperature changes with time when including the gas component in the macropores, the adsorbed gas and the solid itself. The second term denotes the heat of adsorption, which is the heat that is produced; hence the negative sign in front of H_{ads}. The third term denotes the energy that would be leaving the solid particle due the temperature difference between the gas and the solid. This term equals zero in the pseudo homogeneous model.

The energy balance for the gas phase derived from Ribeiro, et al. (2008) and Casas, et al. (2012) is given by:

$$\frac{\partial}{\partial z}\left(\lambda \frac{\partial T}{\partial z}\right) + \varepsilon_t \frac{\partial P}{\partial z} - u_s C_G C_p \frac{\partial T}{\partial z} - (1-\varepsilon) a h_f \left(T - T_p\right) \tag{41}$$
$$- \frac{4 h_w}{d_b}(T - T_w) - \varepsilon C_G C_p \frac{\partial T}{\partial t} = 0$$

Here, λ is the heat axial dispersion coefficient [W/mK], h_w is the film heat transfer coefficient between the gas and the wall [W/m^{2}K], d_b is the internal bed diameter [m], and T_w is the temperature of the wall [K].

The first term denotes heat axial dispersion, which describes the heat transfer in axial direction (Jakobsen, 2011). The second term describes the change in pressure. The third term describes the convection. The fourth term denotes the heat that enters the bulk gas phase from the solid due heat produced by adsorption, which gives a temperature

difference between the gas and the solid. The fifth term denotes the heat dissipated to the wall and the sixth term describes heat accumulation in the gas.

The heat axial dispersion coefficient (λ) is given by (Lopes, et al., 2009):

$$\lambda = \lambda_{fl}(7 + 0.5Re_p Pr) \tag{42}$$

Here, Pr is the Prandtl number and λ_{fl} is the thermal conductivity of the gas [W/mK].

The Prandtl number is given by (Jakobsen, 2011):

$$Pr = \frac{C_{p,g}\mu}{\lambda_{fl}} \tag{43}$$

Here, $C_{p,g}$ is the specific heat capacity per mass of the gas [J/kgK].

The energy balance for the wall is given by (Ribeiro, et al., 2008), (Liu, et al., 2011):

$$C_{p,w}\,\rho_w\,\frac{\partial T_w}{\partial t} = \alpha_w h_w(T - T_w) - \alpha_{wl}U(T_w - T_\infty) \tag{44}$$

Here $C_{p,w}$ is the specific heat capacity of the wall [J/kgK], ρ_w is the wall density [kg/m^3], α_w is the ratio of internal surface area to the volume of the wall [1/m], α_{wl} is the ratio of the logarithmic mean surface area of the column shell to the volume of the column wall [1/m], U is the global external heat transfer coefficient [W/m^{2}K] and T_∞ is the ambient temperature [K].

The first term denotes the rate of heat accumulation in the wall, which is explained by the energy exchange between the bulk gas and the wall, and the temperature difference between the wall and the surroundings. In some models the entire system is assumed to be in thermal equilibrium. This is a reduction, which neglects the temperature difference between the gas and the wall, thus further simplifying the energy balance.

The alpha parameters in equation (44) are given by (Liu, et al., 2011):

$$\alpha_w = \frac{d_b}{t_w(d_b + t_w)} \tag{45}$$

$$\alpha_{wl} = \frac{1}{(d_b + t_w)\ln(\frac{d_b + t_w}{d_b})} \tag{46}$$

Here, d_b is the internal diameter of the reactor [m] and t_w is the thickness of the reactor wall [m].

The energy equations that have been presented are governing equations for a general 1D model with heat axial dispersion only. As this study will use the pseudo homogeneous model for further study, the energy balance is reduced from three to two equations, and there is no need for a separate energy balance equation for the solid. This is a valid assumption since at cyclic steady state the temperature profiles of the bulk gas and solid

adsorbent are almost identical (Ribeiro, et al., 2008). Combining the energy balance for the solid and the gas phase gives (Ribeiro, et al., 2008):

$$\frac{\partial}{\partial z}\left(\lambda\frac{\partial T}{\partial z}\right)+\varepsilon_t\frac{\partial P}{\partial z}-u_s C_G C_p\frac{\partial T}{\partial z}$$
$$-\left[\varepsilon_t C_G C_p+(1-\varepsilon)\left(\rho_p\sum_{i=1}^{n}q_i\,C_{p,ads,i}+\rho_p C_{p,s}\right)\right]\frac{\partial T}{\partial t} \qquad (47)$$
$$+\rho_b\sum_{i=1}^{n}(-H_{ads})_i\frac{\partial q_i}{\partial t}=0$$

It should be noted that the term with $C_{por,i}$ was combined with the $\varepsilon_t C_G C_p$ term. This was done because the mass balance has been simplified to neglect macropore resistance and film resistance. Hence, it complies with the assumption that the concentration in the macropore equals the concentration in the bulk gas.

The energy balance for the solid and gas phase was similar in the pre- and post-combustion model. However, in the post-combustion model the term $\varepsilon_t\frac{\partial P}{\partial z}$, which denotes the pressure drop, was removed from the energy balance. This was because it was not included in the reference paper for post-combustion capture by Liu, et al. (2011).

It can be noticed that the term including the film heat transfer coefficient at the wall has been removed. This is because adiabatic conditions were assumed for both the pre-combustion and post-combustion case. By letting the film heat transfer coefficient h_w = 0, and the global external heat transfer coefficient $U=0$, the wall temperature becomes constant. Figure 3 shows various film heat transfer correlations as a function of the column diameter. From this it can be seen that for small sized columns there is a significant heat transfer. However, as the goal was that the result should reflect a full size column, adiabatic conditions were a valid assumption. Moreover, several papers simulating with small sized columns assume adiabatic conditions, including the papers from Casas, et al. (2012) and Ribeiro, et al. (2008). Casas, et al. (2012) argued that adiabatic conditions are realistic in industrial PSA plants. The energy balance for the wall was therefore reduced to:

$$\frac{\partial T_w}{\partial t}=0 \qquad (48)$$

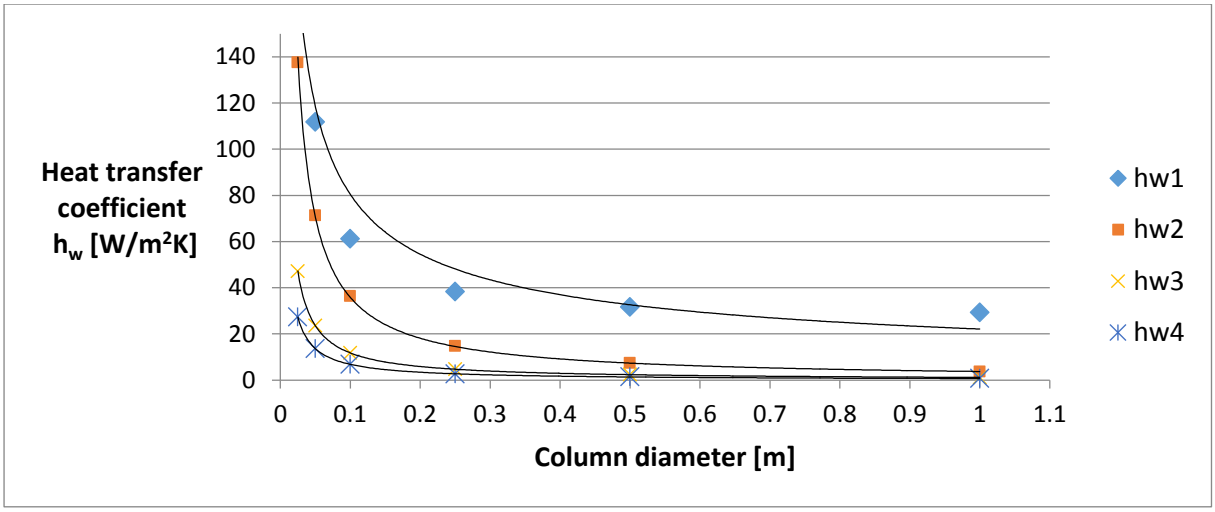

Figure 3: Heat transfer coefficient correlations

hw1: Froment and Wasch's correlation (Froment, et al., 2011), hw2: Leva's correlation (Casas, et al., 2012), hw3: Wakao and Kaguei's correlation (Bandari, et al., 2012), hw4: Wilson's correlation (Bandari, et al., 2012).

3.7 Adsorption Isotherms

The adsorption isotherm is fundamentally important for designing adsorption processes. When the adsorbent and the gas has been in contact for a sufficient amount of time, equilibrium occurs. In this state no more gas can be adsorbed unless the pressure or temperature is changed. The relationship between the total pressure and the amount adsorbed at constant temperature is called the adsorption isotherm (Agarwal, 2010). It is given by:

$$q^* = f(p) \tag{49}$$

It expresses the amount adsorbed at equilibrium and at constant temperature, where q^* [mol/kg] is only a function of partial pressure. Figure 4 shows how pressure and temperature affects adsorption, and it becomes clear from the figure that high pressures and low temperatures facilitates adsorption, while low pressures and high temperatures facilitates desorption. The reason why adsorption is favored at low temperatures is explained by the fact that it is an exothermic reaction: According to Le Chatelier's principle for a reversible process at equilibrium, increasing the temperature (adding heat to the system) causes the system to compensate by removing this excess heat. This is done by desorbing some of the adsorbed components (endothermic reaction) (Laughlin, 2009).

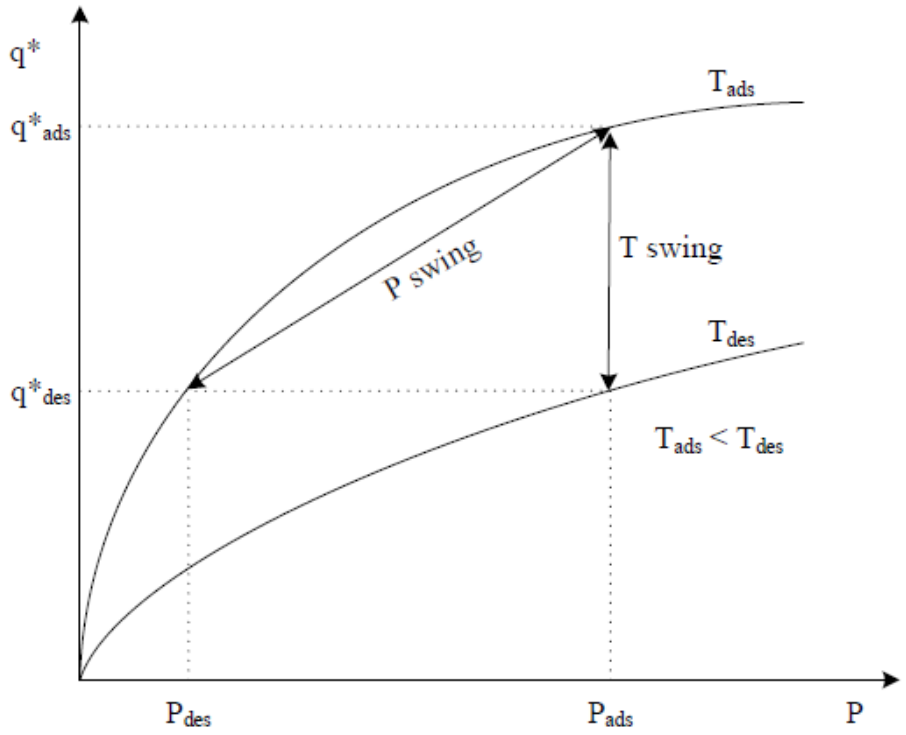

Figure 4: Adsorption isotherm (Agarwal, 2010)

At low pressures or concentrations the equilibrium relationship follows Henry's Law (Ruthven, et al., 1994):

$$q^* = K'P \qquad or \qquad q^* = KC \tag{50}$$

K' [molm^3/kgJ] and K [m^3/kg] are Henry's constants, also known as the adsorption equilibrium constants and they follow the vant Hoff relations given as (Ruthven, et al., 1994):

$$K' = K'_0 e^{-\Delta H/RT} \qquad or \qquad K = K_0 e^{-\Delta U/RT} \tag{51}$$

Here, K'_0 [molm^3/kgJ] and K_0 [m^3/kg] are the adsorption equilibrium constants at infinite temperature. ΔH is the change in enthalpy and ΔU is the change in internal energy. The change in enthalpy is explained by the relation:

$$\Delta H = \Delta U - RT \tag{52}$$

Here, ΔH and ΔU has the unit [kJ/mol]. Since ΔH and ΔU is negative for an exothermic reaction, the above equations shows that Henry's constant decreases with increasing temperature (Ruthven, et al., 1994).

At higher concentrations (pressures) the isotherm curve deviates from the linear relationship given by Henry's Law as can be seen in graph i and ii in figure 5.

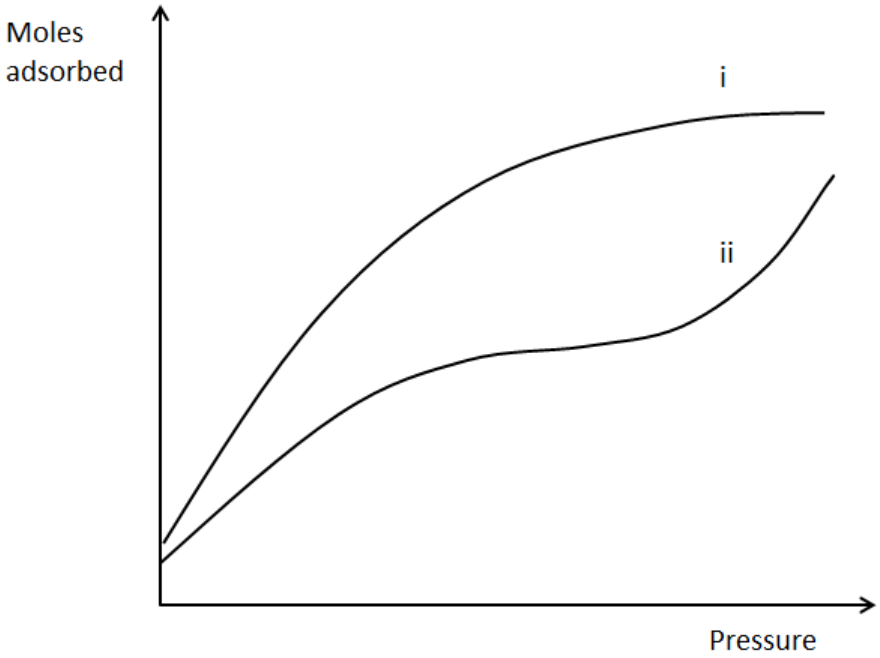

Figure 5: Brunauer's classification of isotherms

The two most common forms of isotherms from Brunauer's classification can be seen in figure 5. Type i behavior can be seen where the saturation limit corresponds to complete filling of the micropores. The plateau indicates a complete coverage of a monolayer. Type ii behavior can be seen on non-porous solids and represents an indefinite multi-layer which is filled up after the monolayer, hence the rapid incline after the plateau. The isotherm does not have a saturation limit (Imtiaz, 2002).

3.7.1 Langmuir Isotherm

The simplest and most used isotherm model for adsorption is the Langmuir isotherm. It is classified as type i in figure 5. The ideal Langmuir model is given by:

$$\frac{q^*}{q_s} = \frac{bC}{1 + bC} \tag{53}$$

In this equation q_s is the saturation limit [mol/kg] and b is an equilibrium constant [m^3/mol], which is directly related to Henry's constant ($K = bq_s$). It can be seen that for low concentrations the equation approximates a linear expression, which is in correspondence to Henry's law, while for high concentrations the equation shows an asymptotic behavior as q^* approaches q_s. The Langmuir isotherm model can be derived by considering the mass balance between occupied and unoccupied sites (Ruthven, et al., 1994). The model assumes that the adsorbed layer is only one molecule in thickness, a monolayer adsorption. It assumes no interaction between the neighboring adsorbed molecules, and homogeneous adsorption, meaning that each adsorption site has equal affinity for the adsorbate (Foo & Hameed, 2010).

3.7.2 Freundlich Isotherm

The Freundlich isotherm is regarded as an empirical model, and is also classified as type i shown in figure 5. The Freundlich equation is given as (Ruthven, et al., 1994):

$$q^* = bC^{\frac{1}{n}}, \qquad n > 1.0 \tag{54}$$

The Freundlich isotherm model has two parameters as the Langmuir model, but it does not reduce to Henry's law in the low concentration region. In order to increase the flexibility as an empirical correlation, the Langmuir-Freundlich isotherm can be used (Ruthven, et al., 1994):

$$\frac{q^*}{q_s} = \frac{bC^{\frac{1}{n}},}{1 + bC^{\frac{1}{n}},} \tag{55}$$

This equation has three parameters and has no sound theoretical basis (Ruthven, et al., 1994). However, it solves the issue in the Freundlich model of not having a finite adsorption limit.

3.7.3 Sips Isotherm

The Sips isotherm is similar to the Langmuir-Freundlich isotherm. The multisite Sips isotherm was used in the reference paper by Casas, et al. (2012), and was therefore chosen to be used in the pre-combustion model.

$$\frac{q_i^*}{q_{si}} = \frac{(K_i P_i)^{S_i}}{1 + (K_i P_i)^{S_i}} \quad i = 1, \dots, N_c \tag{56}$$

The Sips isotherm, like the Langmuir-Freundlich isotherm, has a finite adsorption limit, which strengthens its accuracy in the high concentration area. The Sips isotherm was reported to give a higher accuracy than the Langmuir isotherm for activated carbon in the low pressure area (Casas, et al., 2012).

The sips isotherm for a multicomponent model is given by (Casas, et al., 2012):

$$\frac{q_i^*}{q_{si}} = \frac{(K_i P_i)^{S_i}}{1 + \sum_{j=1}^{n} (K_j P_j)^{S_j}} \quad i = 1, \dots, N_c \tag{57}$$

Here, q_{si} is the saturation limit [mol/kg], S_i and S_j are the Sips exponent for the ith and jth component [-], respectively, and K_i and K_j are the adsorption equilibrium constants for the for the ith and jth component, respectively [1/Pa]. The adsorption equilibrium constant is given by (Casas, et al., 2012):

$$K_i = \Omega_i \exp\left(\frac{-\Theta_i}{RT}\right) \quad i = 1, \dots, N_c \tag{58}$$

Here, Ω_i [1/Pa] and Θ_i [J/mol] are parameters for the temperature dependent description of the adsorption equilibrium constant K_i.

The equation for the saturation limit is given by (Casas, et al., 2012):

$$q_{si} = \omega_i \exp\left(-\frac{\theta_i}{RT}\right) \quad i = 1, \dots, N_c \tag{59}$$

Here, ω_i [mol/kg] and θ_i [J/mol] are parameters for the temperature dependent description of the saturation limit q_{si}.

The Sips exponents are given by (Casas, et al., 2012):

$$s_i = s_{1i} \arctan\left(s_{2i}\left(T - T_{ref,i}\right)\right) + s_{ref,i} \quad i = 1, \dots, N_c \tag{60}$$

Here, s_{1i} [-], s_{2i} [1/K] and $s_{ref,i}$ [-] are parameters for the temperature dependent description of the Sips exponent.

3.7.4 Multisite Langmuir Isotherm

It was proposed from Nitta et al. (1984) (cited by Marathe (2006)) that the adsorbent had a fixed number of sites (q_s) and that one adsorbed molecule could occupy a number (a_i) of sites depending on its size. The saturation capacity for each adsorbate gas therefore becomes:

$$q_{m,i} = \frac{q_s}{a_i} \quad i = 1, \dots, N_c \tag{61}$$

The ideal Langmuir isotherm in equation (53) can be rewritten and expressed by:

$$\frac{q^*}{q_s} = bC\left(1 - \frac{q^*}{q_s}\right) \tag{62}$$

By adding the combinatorial factor, which is the number of distinguishable ways of combining N adsorbed molecules over M sites, the multisite Langmuir isotherms can be written as (Nitta, et al., 1984), (Liu, et al., 2011):

$$\frac{q_{,i}^*}{q_{m,i}} = a_i K_i P_i \left(1 - \sum_i \frac{q_{,i}^*}{q_{m,i}}\right)^{a_i} \quad i = 1, \dots, N_c \tag{63}$$

It was observed that the reference paper for the post-combustion modeling (Liu, et al. 2012) incorporated the a_i into K_i, creating a different value for the adsorption equilibrium constant ($a_i K_i = K$). As the multisite Langmuir model was used in the simulation by Liu, et al. (2011), it was the choice for the post-combustion modeling.

3.8 Valves

The flow rates of the feed, purge and rinse are controlled according to the valve characteristic given by (Liu, et al., 2011):

$$\tau_v \frac{\partial V_{sp}^{act}}{\partial t} = V_{sp} - V_{sp}^{act} \tag{64}$$

Here, τ_v is a time constant [-], V_{sp}^{act} is the actual set point of the valve [-] and V_{sp} is the set point of the valve which is used to control the valve [-].

4 PSA Model

A one-dimensional pseudo homogeneous model for a fixed bed reactor has been developed. The reactor is a cylinder or length L and diameter d. The model accommodated both co-current and counter-current flow. Co-current flow was defined as flow from z = 0 in the direction of z = L, and counter-current flow vice versa. As a convention, z = 0 was defined as the inlet, and z = L as the outlet of the reactor.

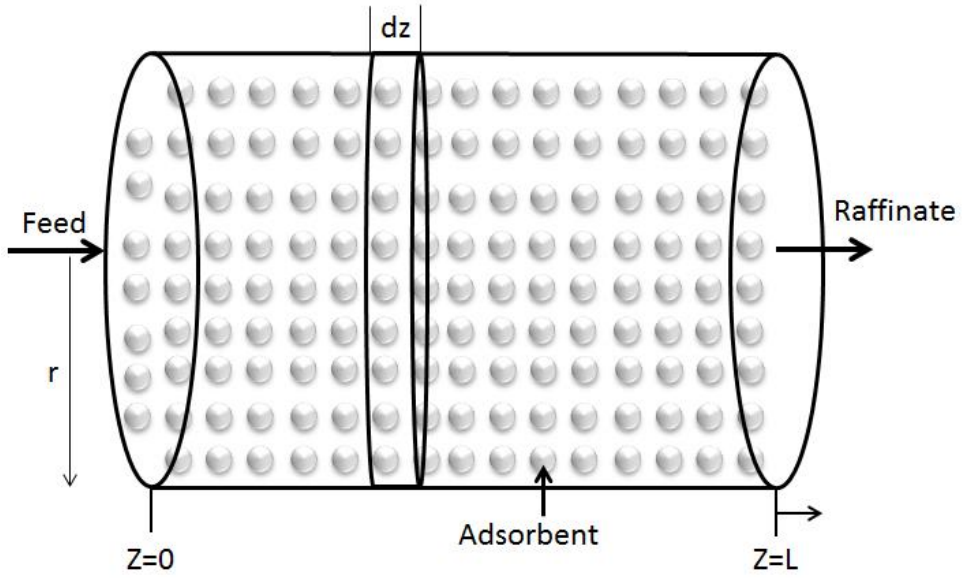

Figure 6: Adsorption reactor

The following model assumptions were used in the modeling:

- Pseudo homogeneous model.
- Post-combustion - three components considered, CO_2, N_2 and Ar.
- Pre-combustion - three components considered, CO_2, H_2 and N_2.
- Bi-dispersed particle with macro- and micropores.
- Adsorbent particle with micropore mass transfer resistance described by the LDF model for micropores.
- Macropore resistance neglected
- External film mass and heat transfer resistance neglected.
- All radial gradients are neglected (temperature, pressure, concentrations and velocity).
- The bulk density of the solid phase is constant.
- Post-combustion - adsorption is modeled by multisite Langmuir isotherm.
- Pre-combustion - adsorption is modeled by Sips isotherm.
- Gas phase follows ideal gas law.
- Momentum balance described by Ergun's equation.
- Constant cross sectional area and uniform void fraction in the column.
- Adiabatic conditions

Table 3 summarizes the main equations used in the modeling of the PSA process. Additional equations were used to evaluate variables and parameters which were needed to solve this system of equations, as described earlier.

Table 3: Summary of main equations for PSA model

Component mass balance – post-combustion

$$\varepsilon_t \frac{\partial C_i}{\partial t} + (1-\varepsilon)\rho_p \frac{\partial q_i}{\partial t} + \frac{\partial (u_s C_i)}{\partial z} = \varepsilon \frac{\partial}{\partial z}\left(D_{ax} \frac{\partial C_i}{\partial z}\right) \quad i = 1, \dots, N_c$$

Component mass balance – pre-combustion

$$\varepsilon_t \frac{\partial C_i}{\partial t} + (1-\varepsilon)\rho_p \frac{\partial q_i}{\partial t} + \frac{\partial (u_s C_i)}{\partial z} = \varepsilon D_{ax} \frac{\partial^2 C_i}{\partial z^2} \quad i = 1, \dots, N_c$$

Overall mass balance

$$\varepsilon_t \frac{\partial C_G}{\partial t} + \frac{\partial (u_s C_G)}{\partial z} = -(1-\varepsilon)\rho_p \sum_{i=1}^{N_c} \frac{\partial q_i}{\partial t}$$

LDF equation for micropore - post-combustion

$$\frac{\partial q_i}{\partial t} = \frac{15 D_{c,i}}{r_c^2}(q_i^* - q_i) \quad i = 1, \dots, N_c$$

LDF equation for micropore - pre-combustion

$$\frac{\partial q_i}{\partial t} = k_{LDF}(q_i^* - q_i) \quad i = 1, \dots, N_c$$

Multisite Langmuir isotherm - post-combustion

$$\frac{q_{,i}^*}{q_{m,i}} = a_i K_i P_i \left(1 - \sum_i \frac{q_{,i}^*}{q_{m,i}}\right)^{a_i} \quad i = 1, \dots, N_c$$

Sips isotherm - pre-combustion

$$\frac{q_i^*}{q_{si}} = \frac{(K_i P_i)^{S_i}}{1 + \sum_{j=1}^{n} (K_j P_j)^{S_j}} \quad i = 1, \dots, N_c$$

Momentum balance - Ergun equation

$$\frac{\partial P}{\partial z} = -\frac{150\mu(1-\varepsilon)^2}{\varepsilon^3 d_{pa}^2} u_s - \frac{1.75(1-\varepsilon)\rho_g}{\varepsilon^3 d_{pa}} |u_s| u_s$$

Energy balance - Solid and gas phase – Post-combustion

$$\frac{\partial}{\partial z}\left(\lambda\frac{\partial T}{\partial z}\right) - u_s C_G C_p \frac{\partial T}{\partial z} + \rho_b \sum_{i=1}^{n}(-H_{ads})_i \frac{\partial q_i}{\partial t} - \left[\varepsilon_t C_G C_p + (1-\varepsilon)\left(\rho_p \sum_{i=1}^{n} q_i\, C_{p,ads,i} + \rho_p C_{p,s}\right)\right]\frac{\partial T}{\partial t} = 0$$

Energy balance - Solid and gas phase – Pre-combustion

$$\frac{\partial}{\partial z}\left(\lambda\frac{\partial T}{\partial z}\right) + \varepsilon_t \frac{\partial p}{\partial z} - u_s C_G C_p \frac{\partial T}{\partial z} + \rho_b \sum_{i=1}^{n}(-H_{ads})_i \frac{\partial q_i}{\partial t} - \left[\varepsilon_t C_G C_p + (1-\varepsilon)\left(\rho_p \sum_{i=1}^{n} q_i\, C_{p,ads,i} + \rho_p C_{p,s}\right)\right]\frac{\partial T}{\partial t} = 0$$

Energy balance - Wall

$$\frac{\partial T_w}{\partial t} = 0$$

Molecular diffusion

$$D_{m,i} = \frac{1 - y_{f,i}}{\sum_{j=1, i\neq j}^{N_c} \frac{y_{f,j}}{D_{i,j}}} \quad i = 1, \dots, N_c$$

Axial Dispersion

$$D_{ax,i} = (0.45 + 0.55\varepsilon)D_{m,i} + 0.35\frac{d_{pa}}{2}u \quad i = 1, \dots, N_c$$

Heat axial dispersion

$$\lambda = \lambda_{fl}(7 + 0.5 Re_p Pr)$$

The boundary conditions change throughout the cycle. The appropriate boundary conditions for each of the steps were taken from Ribeiro, et al. (2008) and are listed in table 4:

Table 4: Boundary conditions

Feed – Co-current	
Inlet, z = 0	Outlet, z = L
$\varepsilon D_{ax}\frac{\partial C_i}{\partial z} = -u_s\left(\frac{P y_{f,i}}{RT_{inlet}} - C_i\right)$	$\frac{\partial C_i}{\partial z} = 0$

$\lambda \frac{\partial T}{\partial z} + u_s C_p C_G (T_{inlet} - T) = 0$	$\frac{\partial T}{\partial z} = 0$
	$P = P_{outlet}$

Rinse – Co-current

Inlet, z = 0	Outlet, z = L
$\varepsilon D_{ax} \frac{\partial C_i}{\partial z} = -u_s (\frac{P y_{f,i}}{R T_{inlet}} - C_i)$	$\frac{\partial C_i}{\partial z} = 0$
$\lambda \frac{\partial T}{\partial z} + u_s C_p C_G (T_{inlet} - T) = 0$	$\frac{\partial T}{\partial z} = 0$
	$P = P_{outlet}$

Depressurization - Co-current

Inlet, z = 0	Outlet, z = L
$\frac{\partial C_i}{\partial z} = 0$	$\frac{\partial C_i}{\partial z} = 0$
$\frac{\partial T}{\partial z} = 0$	$\frac{\partial T}{\partial z} = 0$
$u_s = 0$	$P = P_{outlet}$

Null

Inlet, z = 0	Outlet, z = L
$\frac{\partial C_i}{\partial z} = 0$	$\frac{\partial C_i}{\partial z} = 0$
$u_s = 0$	$u_s = 0$
$\frac{\partial T}{\partial z} = 0$	$\frac{\partial T}{\partial z} = 0$

Blowdown - Counter-current

Inlet, z = L	Outlet, z = 0
$\frac{\partial C_i}{\partial z} = 0$	$\frac{\partial C_i}{\partial z} = 0$
$\frac{\partial T}{\partial z} = 0$	$\frac{\partial T}{\partial z} = 0$
$u_s = 0$	$P = P_{outlet}$

Blowdown - Co-current

Inlet, z = 0	Outlet, z = L
$\frac{\partial C_i}{\partial z} = 0$	$\frac{\partial C_i}{\partial z} = 0$
$\frac{\partial T}{\partial z} = 0$	$\frac{\partial T}{\partial z} = 0$
$u_s = 0$	$P = P_{outlet}$

Purge - Counter-current

Inlet, z = L	Outlet, z = 0
$\varepsilon D_{ax} \frac{\partial C_i}{\partial z} = -u_s(\frac{P y_{f,i}}{R T_{inlet}} - C_i)$	$\frac{\partial C_i}{\partial z} = 0$
$\lambda \frac{\partial T}{\partial z} + u_s C_p C_G (T_{inlet} - T) = 0$	$\frac{\partial T}{\partial z} = 0$
	$P = P_{outlet}$

Pressurization - Counter-current

Inlet, z = L	Outlet, z = 0
$\varepsilon D_{ax} \frac{\partial C_i}{\partial z} = -u_s(\frac{P y_{f,i}}{R T_{inlet}} - C_i)$	$\frac{\partial C_i}{\partial z} = 0$
$\lambda \frac{\partial T}{\partial z} + u_s C_p C_G (T_{inlet} - T) = 0$	$\frac{\partial T}{\partial z} = 0$
	$u_s = 0$

Pressurization - Co-current

Inlet, z = 0	Outlet, z = L
$\varepsilon D_{ax} \frac{\partial C_i}{\partial z} = -u_s(\frac{P y_{f,i}}{R T_{inlet}} - C_i)$	$\frac{\partial C_i}{\partial z} = 0$
$\lambda \frac{\partial T}{\partial z} + u_s C_p C_G (T_{inlet} - T) = 0$	$\frac{\partial T}{\partial z} = 0$
	$u_s = 0$

Feed pressurization – Co-current

Inlet, z = 0	Outlet, z = L

$\varepsilon D_{ax}\frac{\partial C_i}{\partial z} = -u_s(\frac{Py_{f,i}}{RT_{inlet}} - C_i)$	$\frac{\partial C_i}{\partial z} = 0$
$\lambda\frac{\partial T}{\partial z} + u_s C_p C_G(T_{inlet} - T) = 0$	$\frac{\partial T}{\partial z} = 0$
$P = P_{outlet}$	$u_s = 0$

The definitions of key process parameters are given in table 5:

Table 5: Process parameter definitions (Liu, et al., 2011)

$$Purity_{CO_2} = \frac{\int_0^{t_{blow}} u_s C_{CO_2}|_{z=0} A_{bed} dt + \int_0^{t_{purge}} u_s C_{CO_2}|_{z=0} A_{bed} dt}{\int_0^{t_{blow}} u_s C_{tot}|_{z=0} A_{bed} dt + \int_0^{t_{purge}} u_s C_{tot}|_{z=0} A_{bed} dt}$$

$$Recovery_{CO_2} = \frac{\int_0^{t_{blow}} u_s C_{CO_2}|_{z=0} A_{bed} dt + \int_0^{t_{purge}} u_s C_{CO_2}|_{z=0} A_{bed} dt - \int_0^{t_{rinse}} u_s C_{CO_2}|_{z=0} A_{bed} dt}{\int_0^{t_{feed+FP}} u_s C_{CO_2}|_{z=0} A_{bed} dt}$$

$$Productivity_{CO_2} = \frac{\int_0^{t_{blow}} u_s C_{CO_2}|_{z=0} A_{bed} dt + \int_0^{t_{purge}} u_s C_{CO_2}|_{z=0} A_{bed} dt - \int_0^{t_{rinse}} u_s C_{CO_2}|_{z=0} A_{bed} dt}{W_{ads}\, t}$$

$$Specific\ Power_{CO_2} = \frac{\int_0^{t_{FP}+t_{feed}+t_{rinse}} Power_{blower} dt + \int_0^{t_{blow}+t_{purge}} Power_{vacuum} dt}{\int_0^{t_{blow}} C_{CO_2} u_s|_{z=0} A_{bed} dt + \int_0^{t_{purge}} u_s C_{CO_2}|_{z=0} A_{bed} dt - \int_0^{t_{rinse}} u_s C_{CO_2}|_{z=0} A_{bed} dt}$$

$$Power_{blower} = \frac{\gamma}{\gamma - 1} RT_{feed}[\left(\frac{P_{feed}}{P_{in}}\right)^{\frac{\gamma-1}{\gamma}} - 1] u_s(0) \pi r_b^2 \frac{P_{feed}}{RT_{feed}}$$

$$Power_{vacuum} = \frac{\gamma}{\gamma - 1} RT_{blow}[\left(\frac{P_{atm}}{P_{blow}}\right)^{\frac{\gamma-1}{\gamma}} - 1] u_s(0) \pi r_b^2 \frac{P_{blow}}{RT_{blow}}$$

Table 6 summarizes the most important reactor model variables and which equations were used to calculate them. MultiFlash is a physical property package in gPROMS.

Table 6: Reactor model variables

Variable	Equation	Variable	Equation
T	(47)	P	(38)
$D_{c,i}$	(28)	K_i	(51), (58)
D_{ax}	(26)	λ	(42)
q_i^*	(57), (63)	D_m	(10)
C_G	(34)	s_i	(60)
C_i	(32)	q_{si}	(59)
V_{sp}^{act}	(64)	Ω_D	(12)
$D_{i,j}$	(11)	$C_{p,ads,i}$	MultiFlash
q_i	(25), (29)	μ	MultiFlash
$y_{f,i}$	(35)	λ_{fl}	MultiFlash

u_s	(33)	$C_{p,g}$	MultiFlash
Re_p	(7)	$C_{p,i}$	MultiFlash
Pr	(43)		

The calculation of molecular diffusivity (D_m) had to be simplified in order to reduce computational time of the simulations. It should in principle be calculated at each position at all times in the reactor. Instead, an average was taken over the z-axis using 51 data points for all times. Then the variable was averaged over time for each step in the cycle, i.e. for feed, blowdown etc. Consequently, the variable was reduced to a set of parameters for each step which were used in the simulation. The parameters used to calculate molecular diffusivity are given in table 7:

Table 7: Parameters for calculating molecular diffusivity

Parameter	Value	Unit	Reference
A	1.06036	-	(Pooling, et al., 2000)
B	0.15610	-	(Pooling, et al., 2000)
C	0.19300	-	(Pooling, et al., 2000)
D	0.47635	-	(Pooling, et al., 2000)
E	1.03587	-	(Pooling, et al., 2000)
F	1.52996	-	(Pooling, et al., 2000)
G	1.76474	-	(Pooling, et al., 2000)
H	3.89411	-	(Pooling, et al., 2000)
k	$1.3805*10^{-23}$	J/K	(Pooling, et al., 2000)
ε^L/k	CO_2: 195.2 N_2: 71.4 H_2: 59.7 Ar: 93.3	K	(Pooling, et al., 2000)
σ	CO_2: 3.941 N_2: 3.798 H_2: 2.827 Ar: 3.542	Å	(Pooling, et al., 2000)

In addition to the governing equations and boundary conditions, the PSA process steps were also modeled according to:

Feed

The feed step was at P_{high} and was characterized by constant feed composition and the flow rate was set to:

$$\dot{n}_{in} = \dot{n}_{set} * V_{sp}^{act} \tag{65}$$

Here, $\dot{n}_{in}$ [mol/s] is the actual flow rate at any given time, $\dot{n}_{set}$ [mol/s] is the flow rate when the valve is fully open, and V_{sp}^{act} is the actual set point of the valve. $\dot{n}_{set}$ is input in the simulation.

Rinse

The rinse step was at P_{high} and the composition of the rinse stream was obtained by averaging the composition leaving the blowdown and purge step. The temperature was taken as an average of the temperature in the beginning and end of the blowdown and at the end of purge step. The flow rate was behaving as the feed flow rate given by equation (65), but with a different $\dot{n}_{set}$ value.

Pressure Equalization

The high pressure column was connected to a low pressure column, until the pressure was equalized to P_{eq}. The high pressure column was depressurized, and the low pressure column was pressurized in a linear fashion.

The unibed method, simulating only one bed for all the steps in the cycle, introduces a problem for the pressure equalization steps. The output compositions and mass leaving from the depressurization in one column should be used in the pressurization in another column. This can be solved by simulating the two steps separately, while assuring that the inlet and outlet conditions are consistent with each other. The temperature entering the low pressure column was taken as an average of the temperature in the beginning and the end of the depressurization step. The composition was taken as an average over the entire depressurization step. The final pressure of the two columns, P_{eq}, was determined by consistency in the mass balance between the beds. Only for the correct equilibrium pressure would the number of moles leaving the high pressure column be equal to the number of moles entering the low pressure column. The pressure was determined by iteration until the error was smaller than an acceptable tolerance. The error is given by:

$$error = \frac{n_{depress} - n_{press}}{n_{press}} \tag{66}$$

Here, $n_{depress}$ is the total number of moles leaving in the depressurization step and n_{press} is the total number of moles entering in the pressurization step.

Blowdown

Blowdown reduced the pressure from P_{high} or P_{eq} to P_{low} exponentially according to the equations:

$$P = P_{low} + (P_{high} - P_{low}) * \exp(-x_i * t) \tag{67}$$

$$P = P_{low} + (P_{eq} - P_{low}) * \exp(-x_i * t) \tag{68}$$

Equation (67) was used without pressure equalization and equation (68) was used with pressure equalization.

The x_i parameter determines the rate of pressure reduction. The choice of the parameter x_i is not critical, but it influences the outlet flow rate which affects the productivity of the process. Cases, et al. (2013) and Liu, et al. (2013) did not explicitly state the value they used.

The x_i parameter that was used is given in table 11 for post-combustion and in table 20 for pre-combustion.

Purge

The purge step was at P_{low}. For the pre-combustion case, the purge concentration and temperature was equal to the feed concentration and temperature. For the post-combustion case, the purge concentration was set equal to the averaged concentration leaving the exit of the column in the feed step. The temperature was an average between the start and end of the feed step. The flow rate was behaving as the feed flow rate given by equation (65), but with a different $\dot{n}_{set}$ value.

Feed Pressurization

The pressure was increased linearly from P_{low} (without pressure equalization) or P_{eq} (with pressure equalization) to P_{high}. The composition and temperature in the feed pressurization step was the same as in the feed step.

Performance Requirements PSA Process

Casas, et al. (2012) and Liu, et al. (2011), which were used as the reference papers for the PSA modeling, aimed for 95 % purity and 90 % recovery. There is currently a lack of standards regulating the composition of the high purity CO_2 gas stream for transport and storage (de Visser, et al., 2008). Table 8 summarizes some recommendations found in the literature. The recommendations by DYNAMIS (de Visser, et al., 2008) are widely accepted in the literature, and are shown in table 9. It also shows the acceptable concentrations of impurities, which had to be taken into consideration. The DYNAMIS performance targets were therefore used in the simulations, in addition to a 90 % recovery.

Table 8: CO_2 quality recommendations

Purity CO_2 [%]	Reference
>95.5	(de Visser, et al., 2008)
>95	(Andrei, et al., u.d.)
>90	(European Benchmarking Task Force, 2008)

Table 9: DYNAMIS quality recommendations (de Visser, et al., 2008)

Component	Concentration
H_2O	500 ppm
H_2S	200 ppm
CO	2000 ppm
CH_4	Aquifer < 4 vol.%, EOR < 2 vol.%
N_2	< 4 vol.% (all non-condensable gases)
Ar	< 4 vol.% (all non-condensable gases)
H_2	< 4 vol.% (all non-condensable gases)
CO_2	>95.5 %

4.1 Post-Combustion

4.1.1 Setup

It was observed from literature that the PSA cycles in general did not satisfy the performance targets, even with modifications such as vacuum desorption, rinse and pressure equalization steps. In order to increase the CO_2 purity and recovery Liu, et al. (2011) conducted simulations on a two-stage PSA cycle consisting of a "front" and "tail" PSA cycle. Using this configuration, they were able to reach a purity of 69.2 % after the front stage. The purity in the tail stage was further increased to 96.1 %. The total recovery was 91.1 %, with a 98.9 % recovery in the front stage and 92.0 % recovery in the tail stage. The process power consumption for the two-stage PSA cycle was 645.7 kJ/kg_{CO2} captured (Liu, et al., 2011). However, Liu, et al. (2011) did not account for the power consumption required to compress the feed gas to 1.5 bar and to compress the gas between the stages.

The post-combustion PSA model was based on data and parameters from the two-stage PSA process by Liu, et al. (2011) with some modifications. The front stage is presented in figure 7, which shows the pressure profile, the cycle steps and the time scheduling. It was a three-bed and five-step Skarstrom cycle with rinse. That means that there were three columns that underwent five cycle steps. The cycle steps were feed pressurization, feed, rinse, blowdown and purge. The three columns were operated at different stages in the cycle to ensure continuous feed as shown in figure 7. The front stage was designed to recover the majority of the CO_2 and deliver the CO_2 enriched stream to the tail cycle at a purity of around 50-60 %. Low specific power consumption was prioritized since the front stage had the highest flow rates entering. The CO_2-enriched stream that left the blowdown and purge step in the front stage was sent to the tail stage at 0.1 bar.

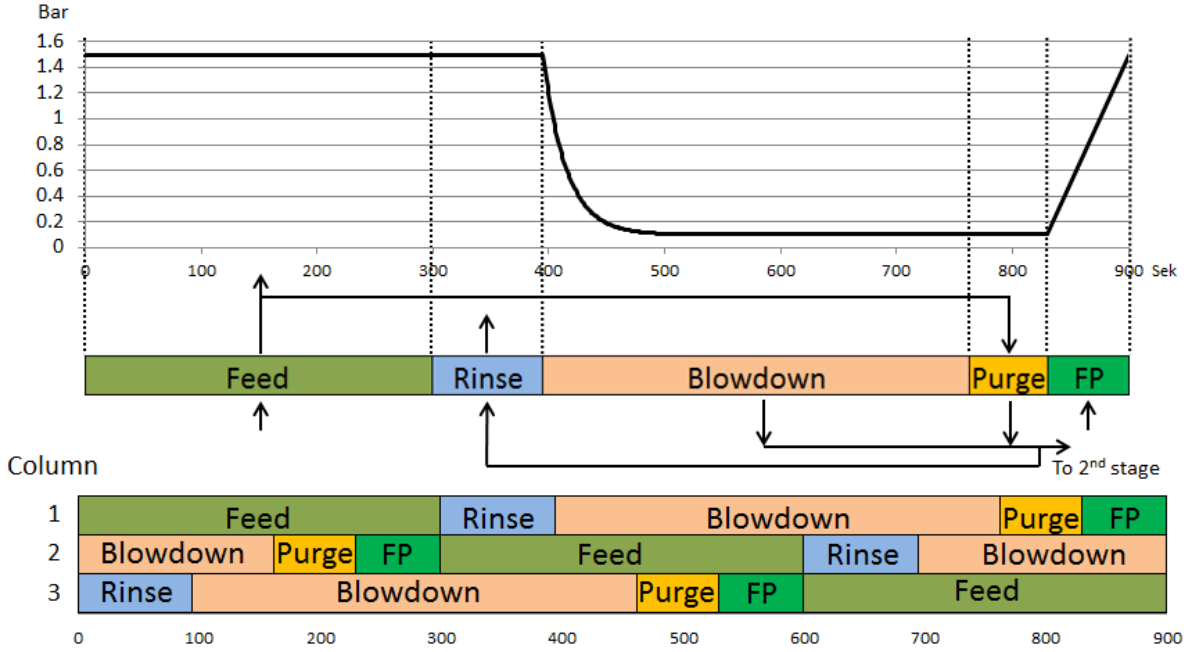

Figure 7: PSA cycle and time schedule front stage

The tail stage is presented in figure 8 and was a two-bed and five-step Skarstrom cycle with pressure equalization. It consisted of the steps feed pressurization, feed, pressure equalization and blowdown. The pressure equalization steps had to be synchronized for the two columns. One column was pressurized while the other was depressurized and it had to occur at the same time. The gas stream from the front stage at 0.1 bar was compressed to 1.5 bar prior to the tail stage in order to utilize a pressure swing also here. The tail stage was designed to increase the purity to above 95.5 %, while ensuring that the total capture rate did not drop below 90 %.

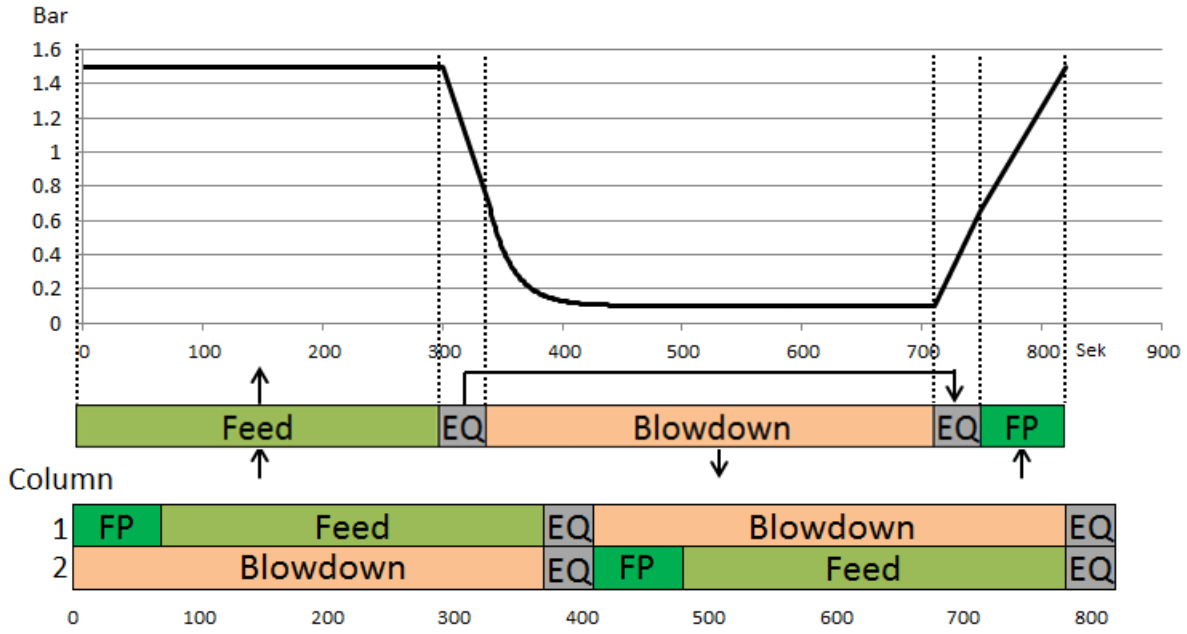

Figure 8: PSA cycle and time schedule tail stage

In a real plant there would be several trains of PSA processes to be able to accommodate all the flue gas. The gas leaving the front stages would be accumulated prior to being fed to the tail stages. This way the tail column could be roughly the same dimensions as the front column. The number of tail columns would on the other hand be less, since there was less gas to treat. Although it was not modeled, it was assumed that a tank handled the variations in flow rate and composition leaving the front stage. It could therefore be assumed that the flow rate and composition entering the tail stage was constant. The concentration entering the tail stage was given by the purity of each component obtained in the front stage. The simulations showed that a train ratio of two was practical when considering the amount of gas leaving the front stage and entering the tail stage. That means that two trains with three columns each were required per train of the tail stage with two columns each. The PSA plant setup is shown in figure 9. This process was later integrated with the PCC power plant. The number of trains required to accommodate all the flue gas and the sizing of the columns are discussed later. The number of trains may be varied according to the size of the power plant and the size of the columns, but the ratio between the front and tail stage will always be two.

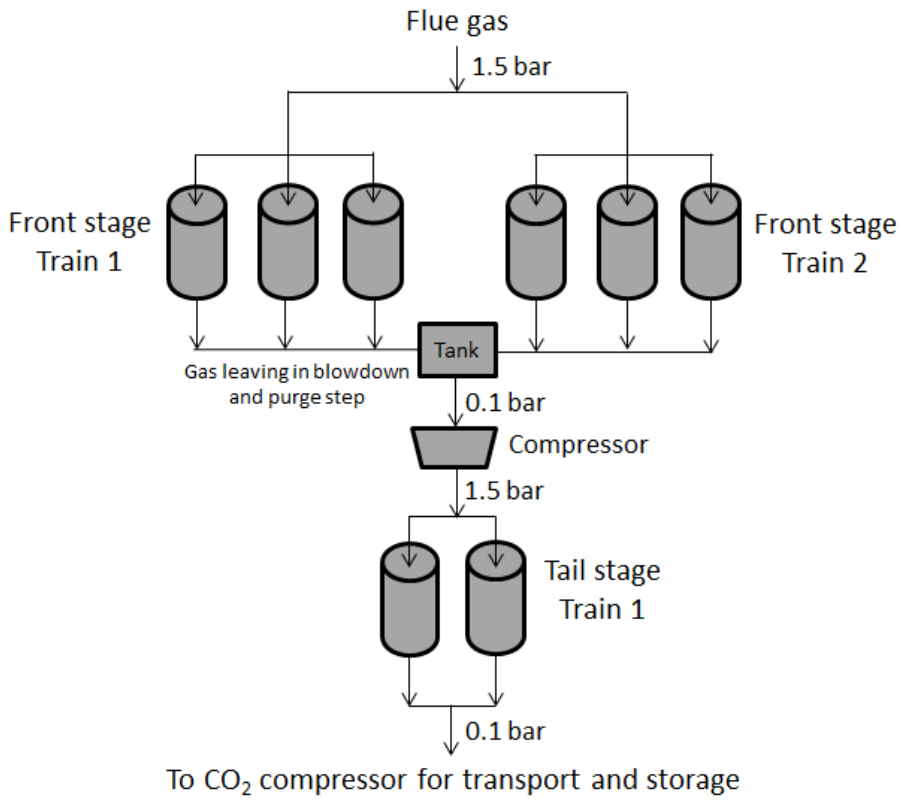

Figure 9: PSA plant setup

The simulations were performed with zeolite 5A as adsorbent and the fitting parameters for the Langmuir adsorption isotherm is given in table 12. The model equations have been discussed and are summarized in table 3. The boundary conditions are given in table 4, the reactor bed parameters are given in table 11 and the transport parameters are given in table 13.

Liu, et al. (2011) only considered CO_2 and N_2 in their model, and consequently there were only fitting and transport parameters for these components. The flue gas composition from the Thermoflex simulation of the PCC power plant is given in table 10. Due to lack of fitting and transport parameters for the Langmuir isotherms in the literature, some simplifications had to be made. SO_2 was neglected due to low mole fraction and lack of data. Oxygen and nitrogen have similar adsorption properties (Choi, et al., 2003).Consequently, their mole fractions were added together and treated as nitrogen. This way, one avoided using Langmuir data for oxygen from a different source which could be a cause of uncertainty. In the power plant, the amount of oxygen captured and its purity was calculated based on the capture rate of nitrogen. Argon flowed through the reactor without getting adsorbed. Some argon was still captured due to its presence in the column during the blowdown and purge steps.

Presence of water is always troublesome in PSA processes. There are very few studies in the literature treating this issue related to CO_2 capture. The studies that exist are mainly experimental, and almost nothing exist regarding modeling. Li, et al. (2008) found through experiments that water has a significant effect on the adsorbent capacity. A water zone

migrated a quarter of the way into the column before it stabilized, resulting in a "cold spot". CO_2 capture was still possible, but with lower performance. The capture rate of CO_2 dropped almost 20 % and the productivity by 22 % compared to a dry feed. The water in the vacuum stream was collected in the vacuum pump and removed. They argued that long term capture of CO_2 was possible without pre-drying of flue gas (Li, et al., 2008). However, one can argue that water should be removed prior to a PSA process to minimize performance penalty due to water. Another approach is to increase the length of the bed to compensate for the cold spot. In the simulations, water was removed to as large extent as possible by condensation, and the remaining water was neglected in the PSA process due to lack of modeling data. The mole fractions of the remaining components were equalized such that the sum became one. The resulting feed composition to the PSA process is given in table 11. It is given in mole%, which is the case for all composition tables unless otherwise specified.

Table 10: Flue gas composition

N_2	CO_2	O_2	Ar	SO_2	H_2O
77.87	14.27	4.62	0.94	0.004	2.31

A deviation from Liu, et al. (2011) was that they used the multibed approach, while in the simulations the unibed method was used. They also accounted for film mass and heat transfer resistance in the boundary layer surrounding the pellets. The macropore resistance was also accounted for, which resulted in a mass balance for the macropores and one LDF equation for the micropores. In these simulations macropore and film resistance were neglected as discussed in section 3.3. The mass balance and energy balance equations were modified accordingly. Liu, et al. (2011) also accounted for heat leaving to the wall and the surroundings. However, as explained in section 3.6, the parameters U and h_w were set to zero. According to Casas, et al. (2012), the purity and recovery of a PSA process is not affected by the size of the columns if the columns are adiabatic. Additionally, it is advantageous to simulate small scale to reduce the CPU time. Based on this, the column size given by Liu, et al. (2011) was used in the front stage of the simulations. For the tail stage, the radius had to be decreased slightly due to mass balance between the first and tail stage to ensure a train ratio of two.

Table 11: Reactor bed parameters

Parameter	Value	Unit	Reference
r_b	Front stage: 0.0235 Tail stage: 0.0217	m m	(Liu, et al., 2011)
L	0.202	m	(Liu, et al., 2011)
$C_{p,w}$	500	J/kgK	(Liu, et al., 2011)
ε_p	0.30	-	(Liu, et al., 2011)
ε	0.322	-	(Liu, et al., 2011)
ρ_w	8 238	kg/m^3	(Liu, et al., 2011)
ρ_p	1083	kg/m^3	(Liu, et al., 2011)

$C_{p,s}$	920	J/kgK	(Liu, et al., 2011)
d_{pa}	0.0027	m	(Liu, et al., 2011)
N_c	3	-	
x_i	0.05	-	
T_∞	298	K	(Liu, et al., 2011)
τ_v	0.5	-	(Liu, et al., 2011)
R	8.314	J/molK	
M	CO_2: 44 N_2: 28 Ar: 39.9	g/mol	
Feed composition	CO_2: 0.146 N_2: 0.844 Ar: 0.01	-	

Table 12: Fitting parameters for Langmuir adsorption isotherm

Parameter	Value	Unit	Reference
ΔH	CO_2: - 37.8530 N_2: - 19.4346	kJ/mol	(Liu, et al., 2011)
K_0	CO_2: $1.4680*10^{-7}$ N_2: $3.7885*10^{-7}$	kPa	(Liu, et al., 2011)
q_s	CO_2: 3.9188 N_2: 3.2793	mol/kg	(Liu, et al., 2011)
a_i	CO_2: 2.0589 N_2: 2.4604	-	(Liu, et al., 2011)

Table 13: Transport parameters

Parameter	Value	Unit	Reference
r_c	$2*10^{-6}$	m	(Liu, et al., 2011)
U	0	W/m^2K	
h_w	0	W/m^2K	
E_a	CO_2: -26.34 N_2: -6.28	kJ/mol	(Liu, et al., 2011)
$D_{c,i}^0$	CO_2: $5.9*10^{-11}$ N_2: $5.2*10^{-13}$	m^2/s	(Liu, et al., 2011)
$\frac{D_{c,i}^0}{r_c^2}$	CO_2: 14.75 N_2: 0.13	1/s	(Liu, et al., 2011)

4.1.2 Optimization

Optimization was necessary to achieve desired recovery and purity with an acceptable specific power consumption, productivity and power plant efficiency. The starting point for the optimization was the reference case by Liu, et al. (2011).

For the front stage, the only requirement which limited the relative step times was that the feed had to be continuous. At all times, one of the three columns needed to be in the feed step. Figure 7 shows an example of the time scheduling for the front stage. Mathematically it means that this equation should always be valid:

$$2 * t_{feed} = t_{rinse} + t_{blowdown} + t_{purge} + t_{FP} \quad (69)$$

This gave freedom to optimize the process over a wide range of step times to tune the process to the desired results.

Since the tail stage was a two-bed configuration with pressure equalization, the only limitation to the step times was that the pressure equalization steps had to be at the same time for both beds. Mathematically it means that this equation should always be valid:

$$t_{FP} + t_{feed} = t_{blowdown} + t_{purge} \quad (70)$$

This simple requirement also gave freedom to optimize the process over a wide range of step times to tune the process to the desired results. Due to the buffer tank between the front and tail stage, the feed did not have to be continuous, hence two beds were sufficient.

The optimization of a two-stage cycle was an iterative process since the performance of the front stage influenced the performance of the tail stage. The results illustrated that increasing the feed step time led to lower recovery, and slightly higher purity. When the feed step time was too long, breakthrough was reached and CO_2 was leaving the end of the column. Changing the flow rate had the same effect as changing the step time. It was the total amount of gas entering the PSA process that was important. The feed step could be used to make small adjustments in favor of either purity or recovery. The feed step time and flow rate will have influence on the number of columns required to accommodate all the flue gas, which should also be taken into consideration.

In the purge step, a portion of the raffinate gas was redirected back into the column which increased the recovery by flushing out the CO_2 from the bed. The simulations illustrated that adjusting the purge step time or flow rate was an effective way to control the recovery of the process. However; it was at the expense of reduced purity due to the high concentration of nitrogen in the raffinate gas. Increasing the purge step time increased the power consumption in the vacuum pump. A high recovery had to be balanced with the negative effect it had on the power plant.

Adjusting the rinse step time was an effective way of controlling the purity of the process. The rinse introduced a high purity gas stream from the blowdown and purge steps back into the column. It was used to produce a high purity region in the inlet of the column prior to the blowdown step, which increased the purity of the process. Unfortunately, this had a negative effect on the recovery. The gas had to be compressed from the vacuum pressure

0.1 bar to the inlet pressure of the column which was 1.5 bar. Consequently, the rinse step was power consuming and should be limited as much as possible. The rinse step also decreased the productivity as the extract product was decreased. On the other hand, it was necessary to achieve high purity, i.e. above 95.5 %.

The blowdown step was not able to manipulate the performance of the PSA process in any significant way. It was no point of prolonging the blowdown step after 0.1 bar had been reached, as this had no consequences for the performance. The blowdown step was used to balance the time scheduling ensuring that the feed was continuous. The pressure equalization steps were used to save power in the pressurization of the column. The equalization steps and pressurization steps were not useful for manipulating the performance of the process.

As discussed, there was a balance between recovery, purity and power consumption, and that there were often both positive and negative effects of manipulating a step time or flow rate. The large degree of freedom in the optimization made it possible to design a lot of well performing processes. Manipulating mainly the rinse and purge step made it possible to achieve a recovery and purity well above 95 %, but at the expense of high power consumption and low power plant efficiency. It is up to the designer whether purity, recovery or power consumption is valued most.

In the front stage the rinse and purge were set to the minimum possible to save power, while at the same time achieving the required purity and recovery. The blowdown was increased to ensure continuous feed flow. The purity was increased in the tail stage by lowering the purge step time. For the final cycle, the purge step was removed completely, making the tail stage a five-step process instead of a six-step process. The feed step time and flow rate for the tail stage were determined by the amount of gas available from the front stage. The flow rates and step times for the best performing cycle is shown in table 14 and the PSA performance is shown in table 15. This PSA process satisfied the DYNAMIS performance recommendations.

The power consumption of the front and tail stage was 1112 kJ/kg_{CO2}. This power consumption did not include the power consumption to compress the flue gas prior to the front stage. Including this, the resulting total specific power consumption was 1319 kJ/kg_{CO2}. Table 16 shows a detailed overview of the power consumption. The power consumption of 528 kJ/kg_{CO2} in the tail stage has been split up into recompression between the stages and tail stage without recompression.

Table 14: Flow rates and step times

Stage	Q_{feed} [SLPM]	Q_{purge} [SLPM]	Q_{rinse} [SLPM]	Feed [s]	Rinse [s]	EQ [s]	Blow [s]	Purge [s]	FP [s]
Front	0.8	0.2	0.4	300	95		367	68	70
Tail	0.52			300		40	370		70

Table 15: PSA performance

Stage	Rec CO_2 [%]	Rec N_2 [%]	Rec Ar [%]	Purity CO_2 [%]	Purity N_2 [%]	Purity Ar [%]	Power [kJ/kg_{CO2}]	Prod [mol_{CO2}/kgd]
Front	94.3	11.6	5.6	58.3	41.5	0.24	584	9.5*
Tail	95.5	5.1	2.8	96.4	3.6	0.01	528	31.9
Total	90.0	0.6	0.2	96.4	3.6	0.01	1112	7.0

*Based on the total amount of CO_2 captured in the front stage

Table 16: Detailed power consumption

	Specific power consumption [kJ/kg_{CO2}*]
Flue gas compression	207
Front stage	584
Tail stage (recompression only)	382
Tail stage (except recompression)	146
Total	1319

*Based on the total amount of CO_2 captured in the PSA process

As is shown in section 5.3, the power plant using this configuration achieved an efficiency of 28.7 %. To achieve a higher efficiency it was necessary to lower the purity requirement for the PSA process. The penalty in terms of power plant efficiency of having a purity of 96 % compared to 90 % was very high. The above process, which satisfied the requirements, was kept as the main model. An additional simulation with relaxed constraints (90 % purity) was performed as well, and is discussed in section 5.4.2.

The columns in the simulations were small scale. However, going full scale would increase the pressure drop in the column, since both superficial velocity and column length would be larger. The pressure drop was originally determined by Ergun's equation. In order to get an idea of the impact of an increased pressure drop on the overall performance of the plant, a simulation was performed with 0.1 bar pressure drop. This value has been considered reasonable for an actual power plant. This resulted in increased blower power consumption and lower net plant efficiency. The resulting final specific power consumption was 1354 kJ/kg_{CO2} and the power plant efficiency was 28.4 %. In comparison, the specific power consumption was 1319 kJ/kg_{CO2} and the power plant efficiency was 28.7 % when the pressure drop was calculated by Ergun's equation. This result illustrate that there is a small reduction in efficiency when going full scale, but it is not significant compared to the other losses associated with CO_2 capture.

4.2 Pre-Combustion

4.2.1 Setup

For pre-combustion, the seven-bed, twelve-step PSA cycle simulated by Casas, et al. (2012), was the best performing configuration found in literature. The pre-combustion model was therefore based on their parameters and configurations. Casas, et al. (2012) achieved 95.3

% purity and 90 % recovery using activated carbon as adsorbent. Because of the high feed pressure of 38.8 bar, there was no need for utilizing a sub-atmospheric desorption pressure. Instead, desorption was set to 1.0 bar and the energy penalty for compressing the CO_2 up to 110 bar was substantially decreased compared to the post-combustion case.

Compared to the mathematical model by Casas, et al. (2012), there were some modifications. The axial dispersion terms in the mass and energy balances, which were neglected by Casas, et al. (2012) in order to save computational time, were included in the model. It should be noticed that in the component mass balance equation in table 3 the axial dispersion coefficient should have been treated as a first order derivative, but due to numerical problems that was not possible. Several papers; (Casas, et al., 2012) and (Agarwal, 2010) either neglected the axial dispersion coefficient completely or treated it like a constant. This was done in order to save computational time and it had a negligible influence on the results (Casas, et al., 2012). Agarwal (2010) argued that adding the axial dispersion coefficient caused unwanted additional numerical smearing, which was not beneficial for the simulation. The modification of the component mass balance was therefore considered to be acceptable.

Casas, et al. (2012) modeled the PSA cycle with only two components: CO_2 and H_2 with a 40/60 composition. The Thermoflex simulation for the pre-combustion power plant gave the composition given in table 17. It shows that in reality there are several additional components that would be entering the PSA process. In the model N_2 was added as a third component and the PSA feed composition can be seen in table 20. The fractions of H_2 and CO_2 from the Thermoflex simulation were used, while N_2 made up the remaining fraction. One could argue that CO also could be included as a separate component based on its molar fraction in table 17 and that CO has higher adsorption capacity than N_2 for activated carbons (Park, et al., 2014), (Lopes, et al., 2009). However, the attempt to obtain the parameters for the Sips isotherm and the heat of adsorption was unsuccessful. The components CO, Ar, H_2O, CH_4, COS and H_2S were given the same adsorption characteristics as N_2. This was a simplification that was been made in order to avoid mass balance conflicts between Thermoflex and gPROMS. However, as CO, H_2O and CH_4 show very strong adsorption properties with activated carbon as an adsorbent (Lopes, et al., 2009), this was a reasonable assumption. As it was not successful to obtain exact data regarding the adsorption properties of Ar, COS and H_2S, giving them the same adsorption characteristics as N_2 was a more uncertain assumption. However, due to their relatively low molar fractions, this did not significantly increase the margin of error.

Table 17: Thermoflex feed composition

H_2	CO_2	N_2	CO	Ar	H_2O	CH_4	COS	H_2S
53.54	37.89	6.72	1.50	0.27	0.017	0.054	0.002	0.0001

The PSA cycle is shown in figure 10. It shows the pressure profile, cycle steps and time scheduling. It can be noticed that there are four pressure equalization steps. This was implemented in order to increase the purity of the product stream. As the blowdown was

conducted co-currently, the product that was first produced would have a composition similar to that of the feed. By utilizing the pressure equalization steps prior to the blowdown, the product with near feed composition was evacuated before the blowdown and purge, by sending it to the pressurization steps. It therefore helped increasing the purity (Casas, et al., 2012). It can be seen in figure 10 that the CO_2 was recovered in the blowdown and purge steps. The H_2-enriched syngas sent to the gas turbine was recovered in the feed step.

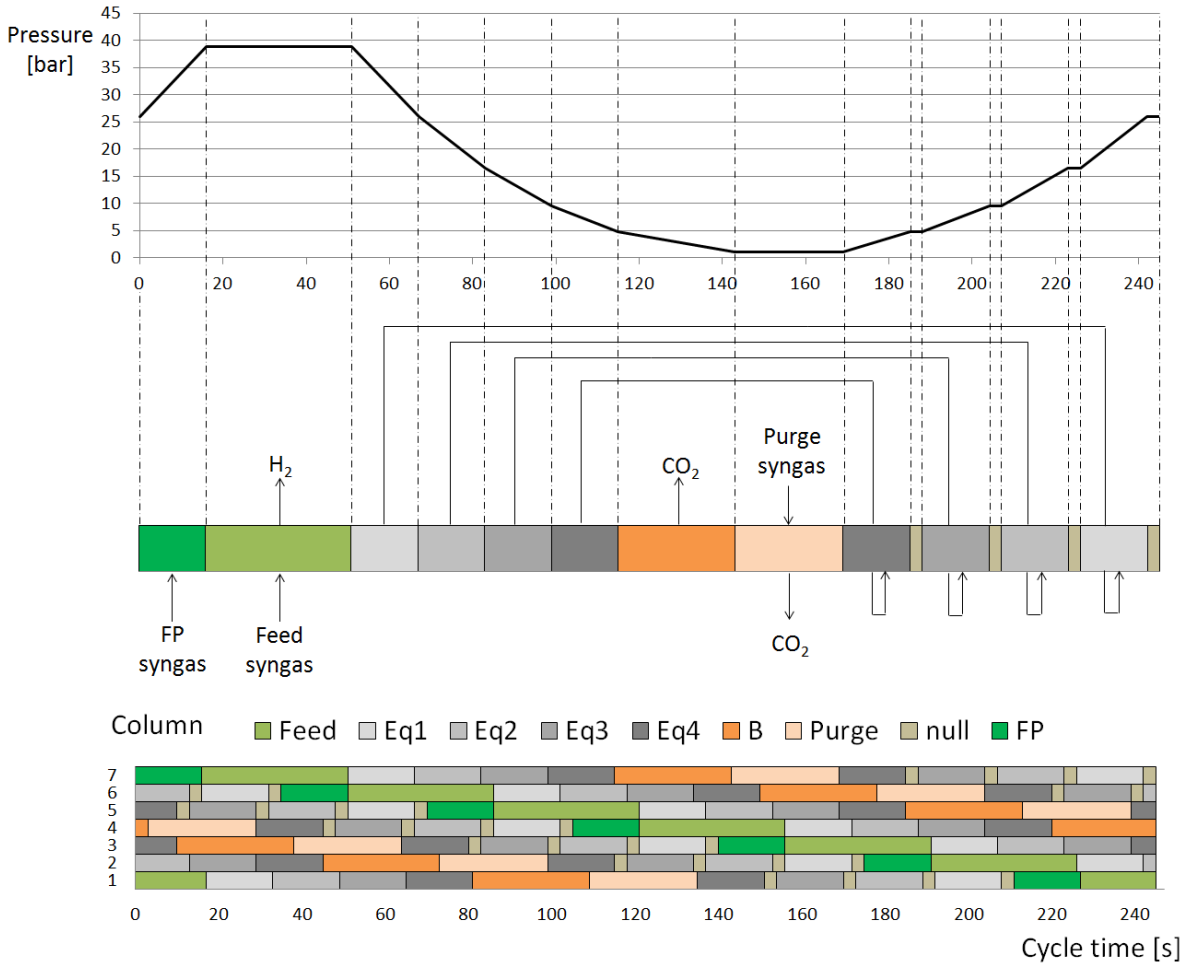

Figure 10: PSA cycle and time schedule

Legend: Feed = feed step, Eq1 = 1st pressure equalization step, Eq2 = 2nd pressure equalization step, Eq3 = 3rd pressure equalization step, Eq4 = 4th pressure equalization step, B = blowdown step, Purge = purge step, null = idle step, FP = feed pressurization step

For pre-combustion capture it was essential to optimize the cycle in order to achieve the required recovery and purity of CO_2. It was also important with regards to the power output from the gas turbine, which relied on a high recovery of H_2. A secondary goal was to achieve a high productivity in order to reduce the amount of adsorbents needed to perform the operation. Optimization was conducted by changing parameters which affected the performance of the cycle. The starting point for the optimization was based on Casas, et al. (2012). The parameters that were modified were the cycle step times, and the feed and

purge flow rate. Figure 10 shows an example of the time schedule for the seven-bed PSA cycle. The time scheduling was complex because there were seven beds and four pressure equalization steps in each cycle. In order to perform the pressure equalization it was important the bed which was depressurized was perfectly synchronized with the bed which was pressurized. It was also essential to ensure a continuous flow of syngas to the gas turbine.

Table 18 shows the step times for the reference case by Casas, et al. (2012) and the starting point for the simulation. It can be noted that the total idle time of 100 seconds was divided into three null steps of 33.3 seconds each. The null steps were implemented as they were necessary in order to synchronize the pressure equalization steps (Casas, et al., 2012). The base cycle by Casas, et al. (2012) had three pressure equalization steps. Unfortunately only the step times from this cycle were provided. It was therefore necessary to calculate new step times for the cycle with four pressure equalization steps. They had to correspond to the cycle time step constraints, and were as close to the reference case as possible.

The time scheduling constraints were as follows:

$$N_{columns}\, t_{feed} = t_{total} \tag{71}$$

This equation describes the necessary numbers of columns needed to guarantee a continuous flow of syngas feed to the PSA process and continuous flow of syngas to the gas turbine. As the number of columns was kept constant at seven, this gave a constant ratio between the total time and the feed step time. In addition it was discovered that the feed pressurization step time needed to be equal to the pressure equalization step times in order to synchronize the pressure equalization steps and to produce a continuous feed flow rate. By using that constraint equation (71) could be rewritten:

$$6\, t_{feed} = 9t_{eq} + 4t_{null} + t_{blow} + t_{purge} \tag{72}$$

For the pressure equalization steps to be synchronized, two extra equations were necessary. By keeping the previous constraints they could be written:

$$2\, t_{feed} - t_{eq} = t_{blow} + t_{purge} \tag{73}$$

$$t_{feed} = 2t_{eq} + t_{null} \tag{74}$$

With these three equations the relationship between the feed step, the pressure equalization step and the null step was determined. The relationship between the feed step, the pressure equalization step and total time of the blowdown and purge step was also determined. This effectively meant that when alternating the feed step and the pressure equalization step, the step time of the null steps and the purge and blowdown steps together were decided. As the total time of the blowdown and purge steps were given, changing the step time of the blowdown step was allowed, though within the time constraints given. This only affected the step time of the purge step and vice versa.

With the constraining equations fulfilled the starting point for further modification was given, which can be seen in table 18. It can be noticed that when the feed step time was kept at the same value as the reference, the blowdown and purge step times were increased by one second. The null steps were decreased by 1.3 seconds, but with four null steps instead of three the total idle time increased by 28 seconds. As already mentioned the feed pressurization step time needed to equal the pressure equalization step time and was therefore 4 seconds in the starting point. All of this increased the total cycle time by 40 seconds. To streamline the optimization process an Excel time schedule calculator was created. This automatically adjusted the step times of the feed pressurization, purge and null steps, when adjusting the length of the feed, pressure equalization and blowdown steps.

The reference case by Casas, et al. (2012) used a feed pressure of 34 bar. In contrast, the feed pressure in the simulations was set to 38.8 bar based in the results from the IGCC power plant in Thermoflex. If the feed volume flow rate from the reference plant was to be kept constant, the increased pressure would increase the molar flow rate. However, instead the molar flow rate in the starting point was set equal the reference case.

Table 18: Initial step times

	FP [s]	Feed [s]	EQ [s]	Blow [s]	Purge [s]	Idle [s]	Total [s]
Reference	2	40	4	50	24	100	240
Starting point	4	40	4	50	26	128	280

The initial feed and purge flow rates are given in table 19:

Table 19: Flow rates

$Q_{feed}\ [SLPM]$	$Q_{purge}\ [SLPM]$
38.98	1.72

The model equations have been discussed and are summarized in table 3 and the boundary conditions are given in table 4. The reactor bed parameters are given in table 20, the fitting parameters for the Sips isotherm in table 21 and the transport parameters in table 22:

Table 20: Reactor bed parameters

Parameter	Value	Unit	Reference
r_b	0.0125	m	(Casas, et al., 2012)
L	1.2	m	(Casas, et al., 2012)
ε_p	0.568	-	(Casas, et al., 2012)
ε	0.403	-	(Casas, et al., 2012)
ε_t	0.742	-	(Casas, et al., 2012)
ρ_p	850	kg/m^3	(Casas, et al., 2012)
ρ_s	1968	kg/m^3	(Casas, et al., 2012)
ρ_b	507	kg/m^3	(Casas, et al., 2012)
$C_{p.s}$	1000	J/kgK	(Casas, et al., 2012)

d_{pa}	0.003	m	(Casas, et al., 2012)
N_c	3	-	
R	8.314	J/molK	
τ_v	0.5	-	(Liu, et al., 2011)
x_i	0.25		
M	CO_2: 44 H_2: 2 N_2: 28	g/mol	
ΔH	CO_2: -26.0 H_2: -9.8 N_2: -16.3	kJ/mol	(Casas, et al., 2012) (Casas, et al., 2012) (Lopes, et al., 2009)
Feed composition	CO_2: 0.379 H_2: 0.535 N_2: 0.086	-	

The Sips parameters for all components given in table 21 were obtained from Schell, et al. (2012). For CO_2 and H_2 the parameters in table 21 were identical for Schell, et al. (2012) and Casas, et al. (2012).

Table 21: Fitting parameters for Sips adsorption isotherm

Parameter	Value	Unit	Reference
Ω_i	CO_2: 16.80 x 10^{-9} H_2: 6.97 x 10^{-10} N_2: 1.74 x 10^{-9}	1/Pa	(Schell, et al., 2012)
Θ_i	CO_2: -9159 H_2: -9826 N_2: -12 661	J/mol	(Schell, et al., 2012)
S_{1i}	CO_2: 0.072 H_2: 0 N_2: 0	-	(Schell, et al., 2012)
S_{2i}	CO_2: 0.106 H_2: 0 N_2: 0	1/K	(Schell, et al., 2012)
ω_i	CO_2: 1.38 H_2: 6.66 N_2: 2.82	mol/kg	(Schell, et al., 2012)

θ_i	CO_2: -5628 H_2: 0 N_2: -1706	J/mol	(Schell, et al., 2012)
$s_{ref.i}$	CO_2: 0.83 H_2: 0.96 N_2: 0.86	-	(Schell, et al., 2012)
$T_{ref.i}$	CO_2: 329 H_2: 273 N_2: 273	K	(Casas, et al., 2012) (Schell, et al., 2012)

Casas, et al. (2012) only provided the parameters for the linear driving force for CO_2 and H_2. The k_{LDF} for N_2 was calculated based on the ratio between the K_{LDF} for CO_2 and N_2 given by Lopes, et al. (2009). This yielded a k_{LDF} value for N_2 of 0.29. This is a rough approximation, but more detailed data was not available in the literature.

Table 22: Transport parameters

Parameter	Value	Unit	Reference
k_{LDF}	CO_2: 0.15	1/s	(Casas, et al., 2012)
	H_2: 1.0		(Casas, et al., 2012)
	N_2: 0.29		Based on (Lopes, et al., 2009)
h_w	0	W/m^{2}K	(Casas, et al., 2012)
U	0	W/m^{2}K	(Casas, et al., 2012)
T_∞	298	K	

4.2.2 Optimization

The results of the initial simulation showed that the performance was not satisfactory with regards to CO_2 purity. The purity was only 85.1 % while the recovery was acceptable at 90.2 %. In comparison, Casas, et al. (2012) achieved a purity of 95.3 % and a recovery of 90 % in the reference case. This mismatch in performance was investigated and it was due to dilution of N_2 in the syngas feed. By using the same feed gas composition as Casas, et al. (2012) the purity increased to 87.5 % while the recovery jumped to 97 %. By optimizing this cycle it should have been possible to achieve over 90 % purity by implementing measures that favors purity over recovery. It was beforehand believed that the higher feed pressure of 38.8 bar would compensate for the reduced CO_2 feed fraction since this gave CO_2 partial pressure of 14.7 bar compared to 13.6 bar in the reference case. However, the simulations illustrated that that was not the case. The cause for the poor performance was due to the fact that 40 % of all N_2 fed to the column was adsorbed. The adsorption of N_2 strongly competed with the adsorption of CO_2, and the feed fraction of N_2 was therefore decisive.

In order to improve the purity from the starting point the feed step time was increased and the purge step time was decreased. This did increase the purity by 1.2 percentage points; however the recovery dropped significantly to 83.8 %. Increasing the purge step time did

somewhat improve recovery, but the total results were still not satisfactory. Overall, it was observed that varying feed, purge and blowdown step times could not improve purity without significantly decreasing the recovery.

Changing the Pressure Equalization Step Time

The step time of the pressure equalization was investigated. By increasing the step time, it was observed that the evacuated amount of H_2 and N_2 decreased during the blowdown step, which increased the CO_2 purity. Increasing the time of the pressure equalization steps enabled an increase in purity of between 2 – 2.5 percentage points without decreasing the recovery. Several step times were experimented, all within the time constraints. However, increasing the step time to over 20 seconds yielded a rapid decrease in recovery, which can be observed in figure 11. A pressure equalization step time of 16 seconds proved to give the best output. It should be noted that in order to satisfy the strict time schedule, the pressure equalization step times could not be changed without changing the times of other steps. This means with regards to step time, one cannot observe the effect of only one parameter. The variation of other parameters might also have played a role in the performance.

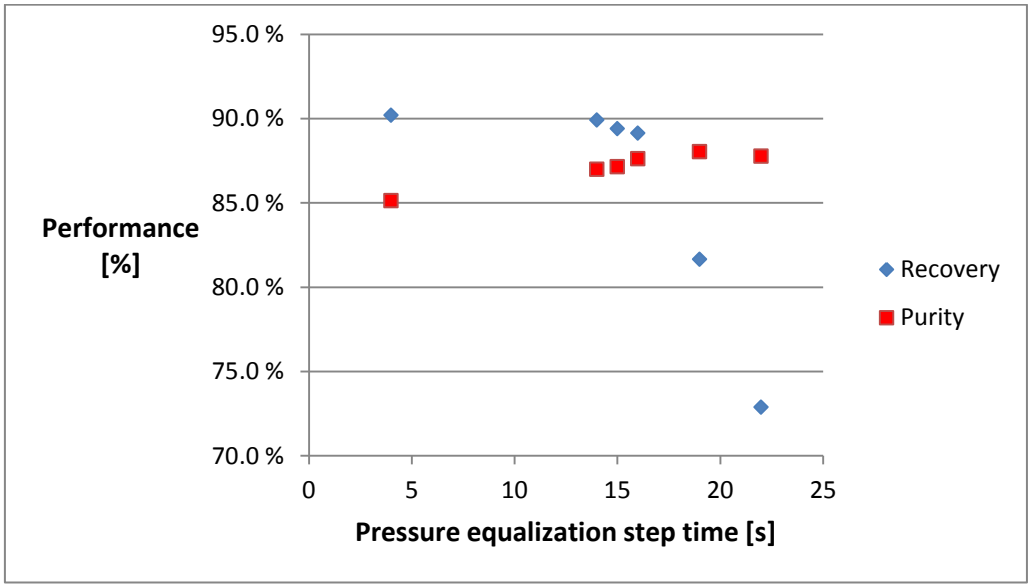

Figure 11: Effect of PE step times on performance

Finally, the feed and purge flow rates were modified. It was mainly experimented with a reduction of the purge flow rate as this enabled a higher purity, but unfortunately also gave a reduction in recovery. Increasing the feed flow rate increased the purity, but also led a rapidly decline in recovery due to breakthrough of CO_2. Figure 12 shows the CO_2 Recovery and purity from the various simulation runs, which are also given in table A1 in appendix A. During the optimization, it was observed that the correct intermediate pressures in the pressure equalization steps changed slightly. However, as correcting these four intermediate pressures was very time consuming, this was only done for the first run in the optimization and for the cycle chosen as the optimum point. The results shown in figure 12 can therefore be regarded more as indicators helping to choose the correct cycle, than final results themselves.

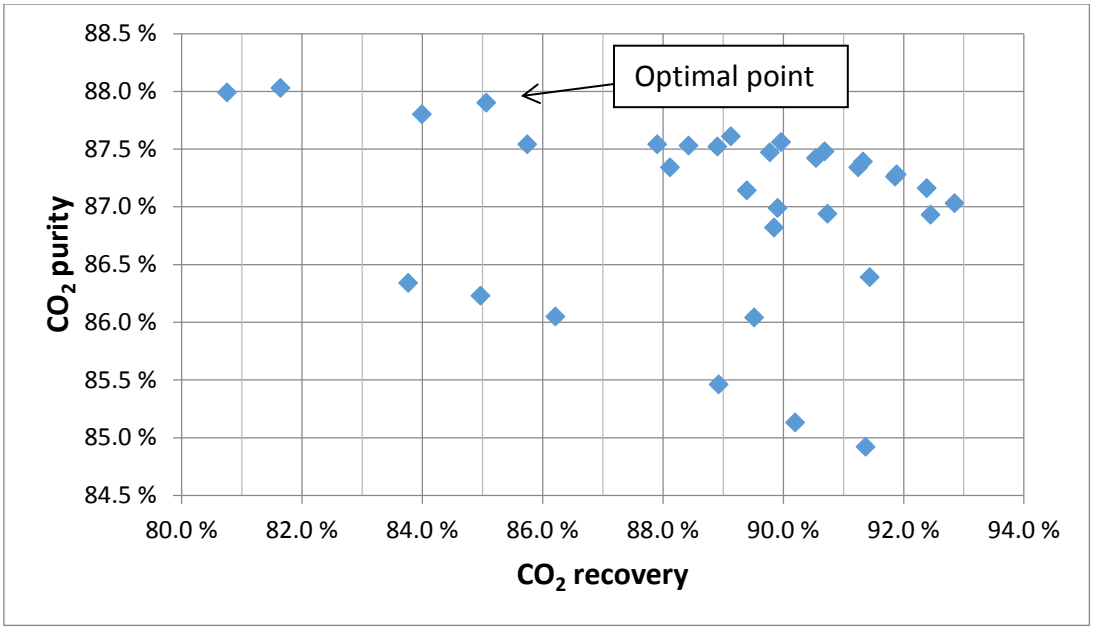

Figure 12: Purity and recovery from simulation runs

Figure 12 shows the optimal point of the cycle, table 23 shows the final flow rates and step times, table 24 shows the final results after correcting the intermediate pressures and table 25 shows the compositions leaving the PSA column. Note that compared to the optimal point in figure 12, the recovery increased, while the purity decreased slightly after correcting the intermediate pressures. The decision for this point was based on the fact that a high purity of CO_2 is essential for the feasibility of CO_2 transport and storage. Although simulations with slightly higher CO_2 purities were achieved, it offered a reasonable trade-off between purity and recovery. Moreover, connecting the preliminary results from gPROMS to Thermoflex showed that the net plant efficiency increased with higher CO_2 purities. This is reasonable since less H_2 was adsorbed in the PSA process. Although these were the best results achieved, according to DYNAMIS the CO_2 purity should be higher than 95.5 %. Moreover, the molar fractions of H_2 and N_2 shown in table 25 were above the proposed 4 vol% limit, while the CO fraction was 6.7 times the proposed 2000 ppm limit in table 9.

Due to the high mole fraction of hydrogen in the stream going to the CO_2 compressor, it was tested whether or not the stream had come to a chemical equilibrium. This was done in Aspen HYSYS using an equilibrium reactor for the CO-shift reaction:

$$H_2 + CO_2 \leftrightharpoons CO + H_2O \tag{75}$$

The results showed that with a constant temperature of 28 °C, corresponding to the temperature at the inlet and outlet of the compressor unit, the change in composition was negligible. The results illustrate that Thermoflex is giving the equilibrium compositions directly. During the transport, the heat loss depends on the ambient temperature. For a temperature drop from 28 °C to 15 °C the results showed a slight shift towards CO and H_2O with a 0.1 percentage point increase in molar fractions.

Table 23: Flow rates and step times

Q_{feed} [SLPM]	Q_{purge} [SLPM]	Feed [s]	EQ [s]	Blow [s]	Purge [s]	Null [s]	FP [s]	Tot [s]
42.88	0.86	35	16	28	26	3	16	245

Table 24: PSA performance

Recovery CO_2 [%]	Recovery N_2 [%]	Recovery H_2 [%]	Purity CO_2 [%]	Prod [mol_{CO2}/kg d]
86.3	33.5	3.2	87.8	19.0

Table 25: Compositions leaving the PSA column

	N_2	H_2	CO_2	CO	Ar	H_2S	H_2O	CH_4	COS
To Gas turbine	7.13	82.63	8.28	1.59	0.29	0.0	0.02	0.06	0.0
To CO_2 compressor	6.04	4.54	87.76	1.34	0.25	0.0	0.015	0.05	0.0

5 Power Plant Simulations

The effect of CO_2 capture by PSA on the power plants performance and efficiency has been investigated. Two types of power plants were studied, namely the IGCC plant (pre-combustion) and PCC plant (post-combustion). In order to do that, a reference power plant without CO_2 capture for both cases was needed. In addition, CO_2 capture by absorption is often used as a benchmark so that the performance of new technologies can be better evaluated. A total of six simulations were performed, which are:

1. PCC without CO_2 capture
2. PCC with CO_2 capture by absorption
3. PCC with CO_2 capture by PSA

4. IGCC without CO_2 capture
5. IGCC with CO_2 capture by absorption
6. IGCC with CO_2 capture by PSA

All simulations were performed according to DECARBit's recommendations (European Benchmarking Task Force, 2008). They define assumptions and parameters that should be applied in CCS simulations such that a comparison of different technologies is possible. The guidelines apply to ambient conditions, fuel, gasification, air separation, shift reaction, gas turbine, steam cycle, heat exchangers, equipment efficiencies, efficiency calculations, cycle definitions and cycle analysis. DECARBit has also performed simulations for the non-capture and capture by absorption cases. These simulations were used as a benchmark for the simulations to ensure that the power plants were state of the art.

The simulations were performed using the Thermoflow software GT Pro, Steam Pro and Thermoflex. The software's default parameters were used where the guidelines did not apply or were unspecified. The PSA processes were simulated in gPROMS and were linked to Thermoflow's software through macros in Excel. This way, the power plant performance with CO_2 capture was immediately obtained when optimizing and changing the PSA process in gPROMS.

Ambient Conditions

The ambient conditions and fuel characteristics were the same for all simulations:

- Pressure: 1.013 Bar
- Temperature: 15 °C
- Relative humidity: 60 %

The composition of air is given in table 26:

Table 26: Composition of air (European benchmarking task force, 2008)

Air composition		
Component	Volume fraction dry	Volume fraction 60 % humidity
O_2	20.95	20.74
CO_2	0.03	0.03
H_2O		1.01
N_2	78.09	77.29
Ar	0.93	0.93
Molecular weight	28.96	28.85

Fuel

There are three types of fuel that are representative of all fuels of interest in power generation with CCS. These are Bituminous Douglas Premium Coal, lignite and natural gas. The fuel used in the simulations was Bituminous Douglas Premium Coal. The composition, heating values and emissions are given in table 27:

Table 27: Coal parameters (European benchmarking task force, 2008)

Bituminous Douglas Premium Coal			
Approximate composition %		Ultimate composition %	
Fixed carbon	54.95	Carbon	66.52
Ash	14.15	Nitrogen	1.56
Volatiles	22.90	Hydrogen	3.78
Moisture	8.00	Total Sulfur	0.52
		Ash	14.15
HHV [MJ/kg]	26.19	Chlorine	0.009
LHV [MJ/kg]	25.17	Moisture	8.00
CO_2-emission [g/kWh$_{LHV}$]	349	Oxygen	5.46

Accounting of CO_2

When CO_2 capture is implemented in power plants, additional CO_2 is formed per unit of power output due to decreased plant efficiency. It is possible to characterize how much CO_2 is captured, emitted and avoided, and a complete accounting of CO_2 was performed according to the following:

$$CO_2\ captured = \frac{\chi}{\eta_{CO2}} \eta_{cap}\ [\frac{kg_{CO2}}{kWh_{work}}] \quad (76)$$

$$CO_2\ emitted = \frac{\chi}{\eta_{CO2}} (1 - \eta_{cap})\ [\frac{kg_{CO2}}{kWh_{work}}] \quad (77)$$

$$CO_2\ avoided = \frac{\chi}{\eta_{ref}} - \frac{\chi}{\eta_{CO2}}(1 - \eta_{cap})\ [\frac{kg_{CO2}}{kWh_{work}}] \quad (78)$$

$$\eta_{cap,e} = \frac{\frac{\chi}{\eta_{ref}} - \frac{\chi}{\eta_{CO2}}(1 - \eta_{cap})}{\frac{\chi}{\eta_{ref}}} = 1 - \frac{\eta_{ref}}{\eta_{CO2}}(1 - \eta_{cap}) \quad (79)$$

- χ: CO_2 emission index defined as $\chi = \frac{\dot{m}_{CO2}}{Q'}\ [\frac{kg_{CO2}}{kWh_{LHV}}]$, which is fuel dependent.
- η_{ref}: Efficiency of reference power plant without CO_2 capture.
- η_{CO2}: Efficiency of power plant with CO_2 capture.
- η_{cap}: Capture rate of CO_2, defined as the fraction of the formed CO_2 which is captured.
- $\eta_{cap,e}$: Capture efficiency, which is the ratio of CO_2 avoided and the emissions per unit power output of the reference plant. This is the most accurate measure to what extent CO_2 is captured in a power plant, as it takes into account the penalty of CO_2 capture.
- CO_2 captured: The amount of CO_2 which is captured per unit of power.
- CO_2 emitted: The amount of CO_2 emitted per unit of power.
- CO_2 avoided: The net reduction of CO_2 emissions per unit power output comparing a reference power plant without CO_2 capture with a similar plant with CO_2 capture.

Figure 13 illustrates the terms CO_2 captured, CO_2 avoided, CO_2 emitted and the additional CO_2 generated due to implementation of CO_2 capture:

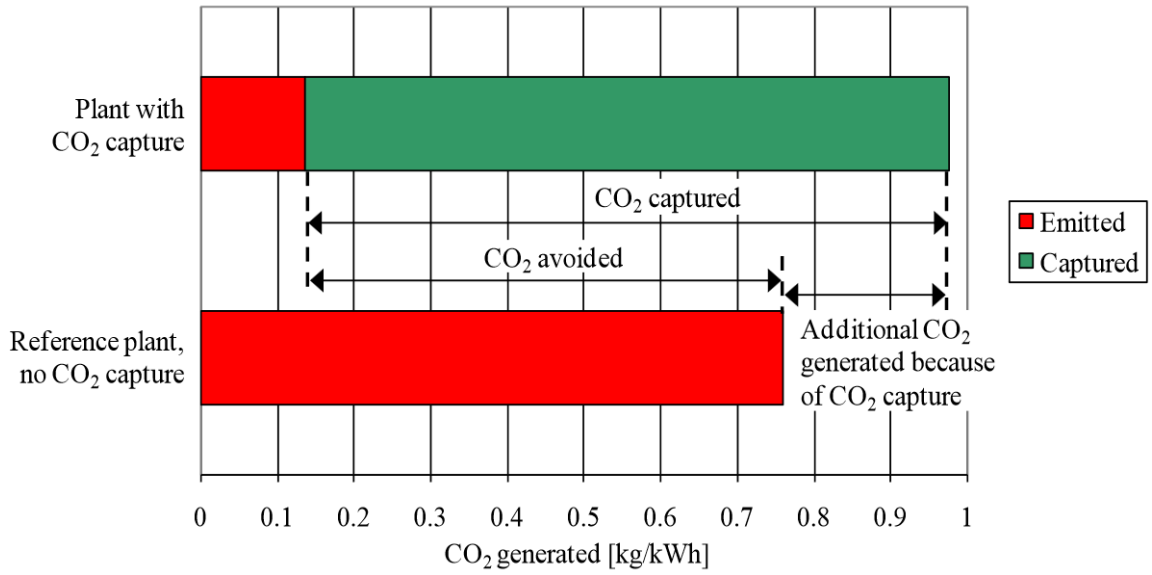

Figure 13: Accounting of CO_2 (Bolland, 2012)

5.1 PCC without CO_2 Capture

The PCC plant was based on an Advanced SuperCritical (ASC) boiler (93.5 % efficiency) and turbine with natural draft wet cooling tower. The steam turbine consisted of a High Pressure (HP) turbine, Intermediate Pressure (IP) turbine and Low Pressure (LP) turbine. Steam was bled from the turbine to a total of nine preheaters. There were two boiler feed pumps and the fired boiler had one pressure level and a single reheat. The plant layout is shown in figure 14, and corresponding streams are shown in table 28. The steam turbine parameters are presented in table 29 and a summary of the plants operational performance in given in table 30. The plant flow sheet is given in figure B1 in appendix B. The simulation was carried out using Steam Pro.

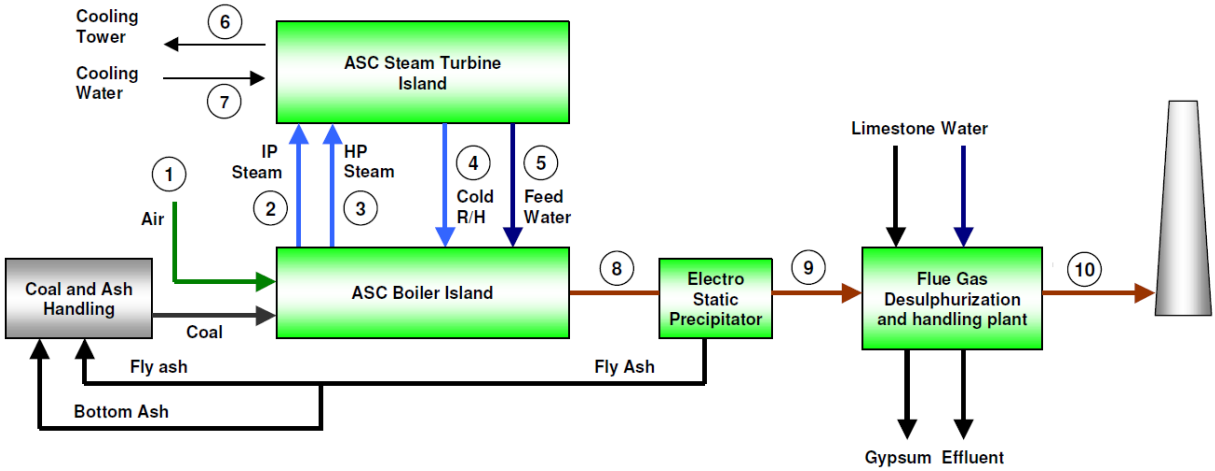

Figure 14: PCC plant layout (European benchmarking task force, 2008)

Table 28: Stream table for PCC without CO_2 capture

Stream composition and conditions									
Stream	Mass flow	T	P	Composition					
	Kg/s	°C	Bar	CO_2	N_2	O_2	Ar	SO_2	H_2O
Coal	66.17	25							
1	744.2	15		0.03	77.29	20.74	0.93		1.01
2	553.4	621.5	90.6						100
3	625.4	602.0	274.0						100
4	553.4	428.4	93.3						100
5	625.4	316.5	300.4						100
6	15440.0	29.2	1.9						100
7	15440.0	17.5	3.5						100
8	800.9	117.6	1.0	13.63	74.37	4.38	0.89	0.04	6.68
9	800.9	125.0	1.04	13.63	74.37	4.38	0.89	0.04	6.68
10	822.7	62.2	1.01	13.09	71.42	4.23	0.86	0.003	10.39

Table 29: Steam turbine parameters

Steam turbine	
Total turbine isentropic efficiency [%]	85.0
Total steam turbine output [MW]	825.6
Condenser pressure [Bar]	0.048
Turbine mechanical efficiency [%]	99.75
Miscellaneous ST auxiliary load [%]	0.35
Gear box efficiency [%]	98.5

Table 30: PCC operational performance

Operational performance		
	Simulation	DECARBit
Coal flow rate [kg/s]	66.2	65.8
Coal LHV [MJ/kg]	25.2	25.2
Net fuel input [MW_{th}]	1665.6	1657.8
Gross electrical output [MW]	825.6	819.0
Total auxiliary power consumption [MW]	71.2	64.7
Net electrical output [MW]	754.4	754.3
Net electrical efficiency [%]	45.3	45.5
Specific CO_2 emissions [kg/MWh_{net}]	769.2	763.0

As seen in table 30, the power plant achieved a net electrical output of 754.4 MW with an efficiency of 45.3 % and a specific CO_2 emission of 769.2 kg/MWh_{net} for a coal flow rate of 66.2 kg/s. The operational performance was quite close to the simulation performed by DECARBit. The simulated power plant itself and the assumptions were therefore realistic and state of the art. The performance of this power plant was used as a reference to evaluate the performance of the CO_2 capture processes.

5.2 PCC with CO_2 Capture by Absorption

The flow sheet of the PCC plant with CO_2 capture was quite similar to the regular PCC plant, except for the absorption process for CO_2 capture. The CO_2 was removed by chemical absorption using an amine based solvent, and a capture rate of 90 % was used. Steam was drawn from the LPT to provide heat in the stripper, which made the power plant different from the reference plant. The absorption process captured 12 383 $tonne_{CO2}$/day and the heat input was 458.6 MW. The total electricity consumption of the CO_2 separation and compression was 57.0 MW. The CO_2 was captured and compressed to 110 bar for transport. A CO_2 purity of 100 % for the captured CO_2 was used in the simulation as it was not possible to specify otherwise in Steam Pro. This assumption was however not far from the truth, as MEA based systems can achieve more than 99 % purity (Miller, 2010).

Since the focus of this report is not on absorption, only the main results are presented in table 31, the accounting of CO_2 in table 32, and a flow sheet is given in figure B2 in appendix B. The power plant obtained a net electrical output of 549.2 MW with an efficiency of 33.4 %. The efficiency dropped 11.95 percentage points from 45.3 % to 33.4 % when introducing CO_2 capture by absorption. The specific CO_2 emissions were reduced from 769.2 kg/MWh_{net} to 102.2 kg/MWh_{net} and the plant had a Specific Energy Consumption for CO_2 Avoided (SPECCA) of 4.3 MJ_{LHV}/kg CO_2. From table 31 it can be seen that the simulation was close to identical to the DECARBit simulation, which indicated that the power plant had a good performance and was realistic. The performance of the power plant with absorption was used as benchmark to evaluate the performance of the PSA process.

Table 31: Operational performance PCC with CO_2 capture by absorption

Operational performance		
	Simulation	DECARBit
Coal flow rate [kg/s]	65.4	65.8
Coal LVH [MJ/kg]	25.2	25.2
Net fuel input [MW_{th}]	1646.6	1646.7
Gross electrical output [MW]	683.9	684.2
CO_2 compressor power consumption [MW]	46.8	48
CO_2 separation power consumption [MW]	10.2	
Other power consumption [MW]	77.8	
Total auxiliary power consumption [MW]	134.8	135.0
Net electrical output [MW]	549.2	549.2
Net electrical efficiency [%]	33.4	33.4
CO_2 capture rate [%]	90	89
CO_2 capture efficiency [%]	86.4	85.1
CO_2 purity [%]	100	100
Specific CO_2 emissions [kg/MWh_{net}]	102.2	104.7
SPECCA [MJ/kg_{CO2}]	4.3	4.4

Table 32: Accounting of CO_2

Accounting of CO_2	
CO_2 captured [kg/MWh_{net}]	919.8
CO_2 avoided [kg/MWh_{net}]	667.0
CO_2 emitted [kg/MWh_{net}]	102.2
Total CO_2 formed [kg/MWh_{net}]	1022
Additional CO_2 [kg/MWh_{net}]	252.8
Additional fuel per kWh_{net} [%]	35.8

5.3 PCC with CO_2 Capture by PSA

The PCC power plant layout for CO_2 capture by PSA is given in figure 15 and the corresponding streams are given in table 33. The plant flow sheet is given in figure B3 and B4 in appendix B. The power plant was very similar to the reference plant, but with the addition of a dehumidification process, a flue gas compressor, a PSA process and a compressor for CO_2 transport. They were added at the end of the flow sheet after the desulfurization process since the gas going into the PSA process had to contain as little contaminants as possible. A dehumidification process was added upstream of the PSA process to remove the water due to its detrimental effect on the performance. The flue gas compressor was needed to increase the feed pressure of the PSA process to 1.5 bar. The rest of the plant was identical to PCC without CO_2 capture. The reference plant was simulated using Steam Pro while the plant with CO_2 capture by PSA was simulated using Thermoflex. It should be mentioned that there were some small corrections when going from Steam Pro to Thermoflex, which for example reduced the gross output with 0.4 MW and some other small changes.

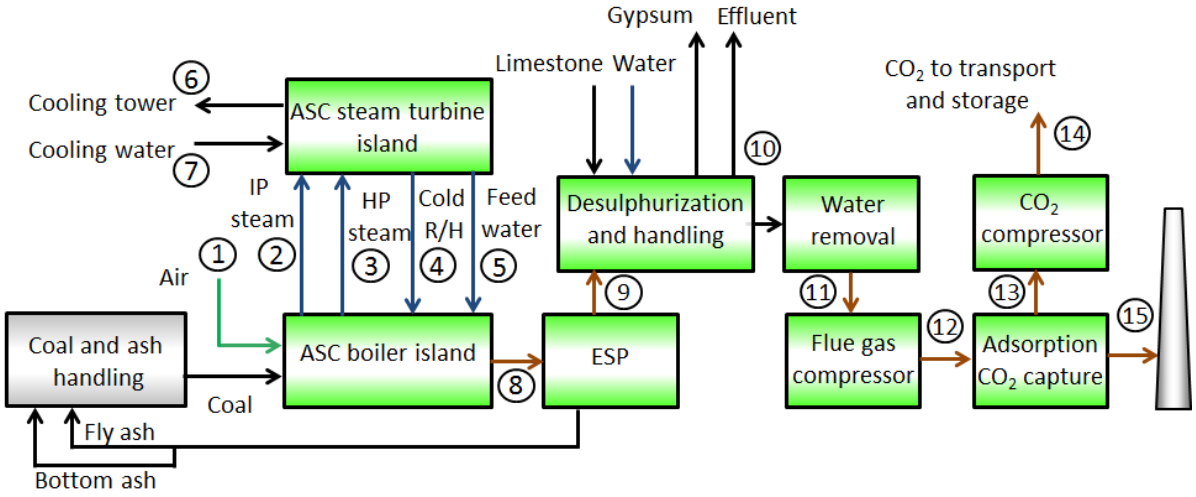

Figure 15: PCC plant layout with CO_2 capture by PSA

Table 33: Stream table for PCC with CO_2 capture by PSA

Stream composition and conditions									
Stream	Mass flow	T	P	Composition					
	Kg/s	°C	Bar	CO_2	N_2	O_2	Ar	SO_2	H_2O
Coal	66.17	25							
1	744.2	15		0.03	77.29	20.74	0.93		1.01
2	553.4	621.5	90.6						100
3	625.4	602.0	274.0						100
4	553.4	428.4	93.3						100
5	625.4	316.5	300.4						100
6	15 440.0	29.2	1.9						100
7	15 440.0	17.5	3.5						100
8	800.9	117.5	1.0	13.63	74.37	4.38	0.89	0.04	6.69
9	800.9	127.6	1.07	13.63	74.37	4.38	0.89	0.04	6.69

10	823.3	62.9	1.04	13.08	71.34	4.23	0.86	0.003	10.50
11	780.9	20.1	1.02	14.27	77.87	4.62	0.94	0.004	2.31
12	780.9	25.0	1.5	14.27	77.87	4.62	0.94	0.004	2.31
13	148.9	22.8	0.1	96.36	3.42	0.20	0.01		
14	148.9	28.0	110.0	96.36	3.42	0.20	0.01		
15	632.0	27.5	1.5	1.65	89.31	5.29	1.08	0.005	2.66

Water was partially removed prior to the PSA process by condensing the vapor. The water content of the stream that entered the dehumidification process was 10.5 mole%. The stream was cooled down to 20 °C, and the resulting mole fraction of water in the stream leaving the dehumidification process was 2.31 %. As mentioned in section 4.1.1, the effect of water on the PSA performance was neglected in the simulations due to lack of modeling data.

The operational performance of the plant is summarized in table 34 and the accounting of CO_2 is given in table 35. The efficiency dropped 16.6 percentage points from 45.3 % to 28.7 %. The performance and parameters for the boiler and steam turbine was identical to the reference plant and will not be repeated here.

Table 34: Operational performance of PCC with CO_2 capture by PSA

Operational performance	
Coal flow rate [kg/s]	66.2
Coal LHV [MJ/kg]	25.2
Net fuel input [MW_{th}]	1665.6
Gross electrical output [MW]	825.2
PSA power consumption [MW]	161.6
Flue gas compressor [MW]	30.2
CO_2 compressor [MW]	80.4
Total auxiliary power consumption [MW]	346.5
Net electrical output [MW]	478.7
Net electrical efficiency [%]	28.7
CO_2 capture rate [%]	90.0
CO_2 capture efficiency [%]	84.2
CO_2 purity [%]	96.4
Specific CO_2 emissions [kg_{CO2}/MWh_{net}]	121.6
SPECCA [MJ/kg_{CO2}]	7.1

Table 35: Accounting of CO_2

Accounting of CO_2	
CO_2 captured [kg/MWh_{net}]	1093.2
CO_2 avoided [kg/MWh_{net}]	647.6
CO_2 emitted [kg/MWh_{net}]	121.6
Total CO_2 formed [kg/MWh_{net}]	1214.8
Additional CO_2 [kg/MWh_{net}]	445.6
Additional fuel per kWh_{net} [%]	57.6

5.4 Discussion of PCC Simulations

5.4.1 Breakdown of Efficiency Losses due to CO_2 Capture

For PSA the efficiency dropped 16.6 percentage points from 45.3 % to 28.7 %, while for absorption the efficiency dropped 11.9 percentage points to 33.4 %. In this section, the penalty of CO_2 capture and where the main losses occur will be investigated for the absorption and PSA case.

For PSA, there were four main factors reducing the power plant efficiency, which were the compression of flue gas upstream the PSA process, the PSA process itself, the CO_2 compression and losses due to water removal. The CO_2 compression required a total of 80.4 MW which decreased the efficiency of the power plant with 4.8 percentage points. A high capture ratio will increase the power consumption due to a higher mass flow to the compressor, while a high purity will result in the opposite. The CO_2 compression power consumption for the PSA case was larger than for the absorption case due to a lower inlet pressure and lower purity. The inlet pressures were 0.1 bar and 1.7 bar for PSA and absorption, respectively. Increasing the vacuum pressure could decrease the power consumption in the CO_2 compressor, but it severely affected the performance of the PSA process, and was ruled out. Consequently, the CO_2 compression power consumption will always account for a significant reduction in power plant efficiency. With 96.4 % purity and 90 % capture rate, the energy saving potential was small since a capture rate of 90 % was desired and the purity was high. Increasing the purity further would require significantly higher blower energy consumption in the rinse step, which would have the opposite effect.

The flue gas compression from 1.02 bar to 1.50 bar required 30.2 MW which decreased the efficiency of the power plant with 1.8 percentage points. It would be advantageous to eliminate this loss by reducing the feed pressure of the PSA process. That would decrease the power consumption of the compressor, but affect the PSA performance. This was investigated in section 5.4.2.

The impact of the power requirement in the PSA process was significant. The process used a total of 161.6 MW, which decreased the efficiency of the power plant with 9.7 percentage points. Improvements in this process could have large energy saving potential. Based on the performed simulations, it was not possible to decrease the power consumption further without sacrificing either recovery or purity. The power consumption due to recompression

from 0.1 bar to 1.5 bar between the stages could be reduced by lowering the feed pressure or increasing the vacuum pressure. This was also investigated in section 5.4.2.

The losses associated with water removal were pressure losses and extra pumping work. The pressure loss in the heat exchanger was 2 %, which increased the power consumption of the fan upstream of the desulfurization process. This fan was used to overcome the pressure losses due to the downstream equipment. The total additional power consumption was 3.1 MW which decreased the efficiency of the power plant with 0.2 percentage points. The penalty of water removal was small compared to the other losses.

Adding these four contributions together resulted in an efficiency drop of 16.6 percentage points, which was the total plant efficiency drop when introducing CO_2 capture by PSA. Table 36 summarizes the above discussion.

For absorption, there were three main factors reducing the plant efficiency, which were CO_2 compression, auxiliary power consumption in the separation process and a reduction in gross power due to steam extraction to the stripper. The compression of CO_2 required a total of 46.8 MW and reduced the power plant efficiency by 2.84 percentage points. As mentioned, this was lower than for PSA due to a higher purity and a higher inlet pressure to the compressor. The purity of CO_2 was 100 %, so there was no potential of energy savings by increasing the purity. The power consumption in the separation process, not including CO_2 compression, was 10.2 MW. This was related to pumping work, and reduced the plant efficiency by 0.62 percentage points. When adding these two contributions, the resulting efficiency reduction was 3.46 percentage points. The rest of the decrease in efficiency was attributed to the loss in gross power due to steam extraction from the steam turbine. The gross output was reduced by 141.7 MW from 825.6 MW to 683.9, which reduced the efficiency by 8.51 percentage points. The sum of the efficiency losses was 11.95 %. Table 36 summarizes the above discussion and figure 16 shows the relative significance of the losses associated with CO_2 capture.

Table 36: Summary of losses associated with CO_2 capture

Technology	Absorption		PSA	
	Power consumption [MW]	Efficiency reduction [%-points]	Power consumption [MW]	Efficiency reduction [%-points]
CO_2 compression	46.81	2.84	80.4	4.8
CO_2 separation	10.23	0.62	161.6	9.7
Water removal			3.1	0.2
Flue gas compression			30.2	1.8
Gross output reduction		8.51		
Total	57.0	11.95	275.3	16.6

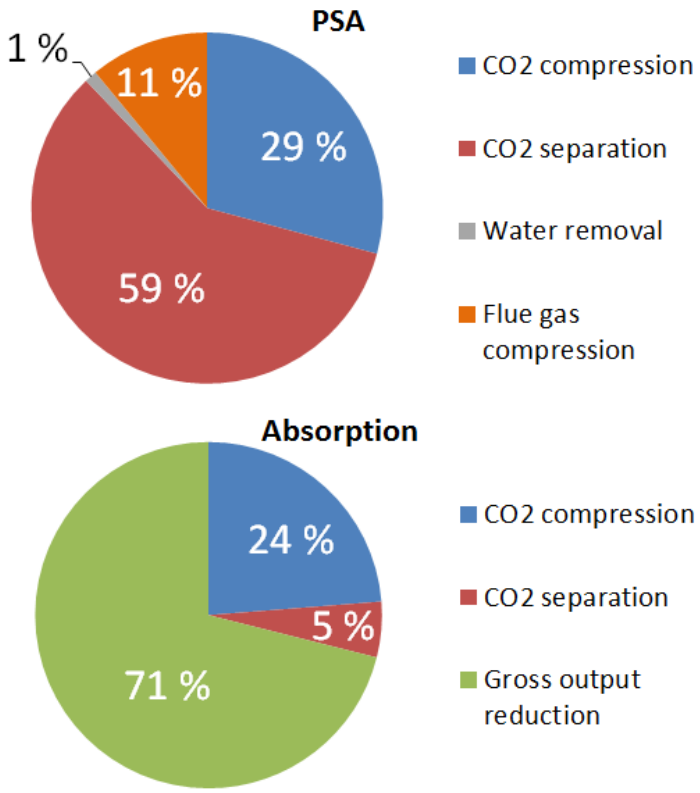

Figure 16: Losses associated with CO_2 capture

5.4.2 Relaxed Constraints

The power plant efficiency of 28.7 % was considerably lower than for absorption with 33.4 % efficiency. It was not possible to increase the power plant efficiency to an acceptable level and at the same time fulfill the DYNAMIS quality recommendations in table 9. Due to lack of standards regarding gas quality for CO_2 transport and storage, a lower purity than 95.5 % may be feasible. Assuming that a purity requirement of 90 % is sufficient; this section will investigate how much it is possible to increase the power plant efficiency based on this new constraint.

Assuming that everything apart from the PSA power consumption remained unchanged, a reduction of 528 kJ/kg_{CO2} from 1319 kJ/kg_{CO2} to 791 kJ/kg_{CO2} was required in order to obtain a net efficiency equal to the absorption case. That is a reduction of 40 % in power consumption. In comparison, the power consumption of the tail stage alone accounted for exactly 528 kJ/kg_{CO2}. In reality, the power consumption of the CO_2 compressor would depend on the capture rate and purity of the PSA process. High power plant efficiency can be achieved with low mass flow to the compressor, but that would be contradictory to the purpose of CCS. Table 16 indicates that it was not possible for the given PSA cycle to achieve the same plant efficiency as the absorption case. Major modifications of the PSA process and different strategies were needed.

The compression between the two stages was a significant contribution to the total power consumption. It depended on the feed pressure of the tail stage and the vacuum pressure of the front stage. The pressures were 1.5 bar and 0.1 bar, respectively. One possible

modification to decrease the power consumption was to increase the vacuum pressure. A simulation with a vacuum pressure of 0.2 bar showed that the recovery in the front stage dropped from 94.3 % to 65.2 %, which made it a poor solution.

Another modification was to reduce feed pressure of both columns. That would effectively reduce the power consumption of the feed compressor and the compressor between the stages due to lower pressure ratio. By holding the step times and flow rates constant and without optimization, the results in table 37 were obtained when changing the feed pressure. These results indicate that it should be possible to decrease the purity and increase the recovery so that 90 % can be achieved for both. The recovery of the tail stage could be increased by introducing purge again, and that would effectively trade purity for recovery. Table 37 also shows that very high purities could be combined with high power plant efficiency if the CO_2 recovery requirement was lowered.

Table 37: Effect of feed pressure

Feed pressure [Bar]	Power consumption [kJ/kg_{CO2}]	Recovery CO_2 [%]	Purity CO_2 [%]	Power plant efficiency [%]
1.5	1319	90.0	96.4	28.7
1.2	1124	84.2	99.1	31.6
1.1	1051	80.7	99.6	32.7
1.0	1026	76.2	99.8	33.6

Optimization showed that it was possible to achieve 90 % capture rate and purity with an inlet pressure of 1.02 bar. The flue gas compressor was removed completely and the power plant efficiency increased from 28.7 % to 32.3 %. From table 40, compared to table 16, it is clear that the compression work was significantly reduced. The results illustrate that an increase in purity came at a high cost. The lower purity requirement made it possible to lower the feed pressure, but also decrease the rinse step time in the front stage from 95 to 20 seconds. The purge step time did not only have to be increased in the front stage to maintain recovery, but purge also had to be added in the tail stage. The specific power consumption in the tail stage is about the same for both cases. The power saved in the compression prior to the tail stage was lost by adding purge to the cycle again. However, the net effect was significant; the total specific power was reduced from 1319 kJ/kg_{CO2} to 880 kJ/kg_{CO2}.

The step times and flow rates are given in table 38, the performance is given in table 39, the power consumption is given in table 40 and accounting of losses is given in table 41. The operational performance of the power plant with relaxed constraints is shown in table 42 and the accounting of CO_2 in table 43. The power plant efficiency was still lower than for absorption, and either the CO_2 purity or recovery requirement for the PSA process would have to be below 90 % to match it.

Table 38: Step times and flow rates

Stage	Q_{feed} [SLPM]	Q_{purge} [SLPM]	Q_{rinse} [SLPM]	Feed [s]	Rinse [s]	EQ [s]	Blow [s]	Purge [s]	FP [s]
Front	0.8	0.2	0.4	300	20		420	90	70
Tail	0.598	0.1		300		40	330	40	70

Table 39: Performance PSA process

Stage	Recovery CO_2 [%]	Recovery N_2 [%]	Recovery Ar [%]	Purity CO_2 [%]	Purity N_2 [%]	Purity Ar [%]	Power [kJ/kg_{CO2}]	Prod [mol_{CO2}/kgd]
Front	94.0	16.2	11.0	49.9	49.7	0.4	355	9.1*
Tail	95.8	10.1	6.4	90.4	9.5	0.05	525	21.0
Tot	90.0	1.6	0.7	90.4	9.5	0.05	880	6.1

*Based on the amount of CO_2 captured in the front stage

Table 40: Power consumption

	Specific power consumption [kJ/kg_{CO2}*]
Flue gas compression	0
Front stage	355
Tail stage (recompression only)	365
Tail stage (except recompression)	160
Total	880

*Based on the total amount of CO_2 captured in the PSA process

Table 41: Losses associated with CO_2 capture by PSA

	Power consumption [MW]	Efficiency reduction [%-points]
CO_2 compression	86.2	5.2
CO_2 separation	127.8	7.7
Water removal	3.1	0.2
Flue gas compression	0	0
Total	275.3	13.0

Table 42: Operational performance relaxed constraints

Operational performance	
Coal flow rate [kg/s]	66.2
Coal LHV [MJ/kg]	25.2
Net fuel input [MW_{th}]	1665.6
Gross electrical output [MW]	825.2
PSA power consumption [MW]	127.8
Flue gas compressor [MW]	0
CO_2 compressor [MW]	86.2
Total auxiliary power consumption [MW]	287.5
Net electrical output [MW]	537.7
Net electrical efficiency [%]	32.3
CO_2 capture rate [%]	90.0
CO_2 capture efficiency [%]	85.9
CO_2 purity [%]	90.4
Specific CO_2 emissions [kg/MWh_{net}]	108.5
SPECCA [MJ/kg_{CO2}]	4.9

Table 43: Accounting of CO_2 relaxed constraints

Accounting of CO_2	
CO_2 captured [kg/MWh_{net}]	973.1
CO_2 avoided [kg/MWh_{net}]	660.7
CO_2 emitted [kg/MWh_{net}]	108.5
Total CO_2 formed [kg/MWh_{net}]	1081.7
Additional CO_2 [kg/MWh_{net}]	312.5
Additional fuel per kWh_{net} [%]	40.3

5.4.3 Size of PSA Plant

The Ergun equation relates the superficial velocity to the pressure drop. A high velocity results in a large pressure drop. However, the advantage of a high velocity is that smaller column diameters or a reduced number of columns can be used. By solving the Ergun equation in gPROMS for a specified max allowable pressure drop, the max superficial velocity was obtained. The velocity was then used to calculate the area of the columns based on flue gas flow rate. The area of the columns also depended on the number of trains and columns. A low number of trains resulted in larger but fewer columns and vice versa. The maximum allowable pressure drop was set to 0.1 bar, which was considered an acceptable pressure drop in the columns.

As can be seen from the Ergun equation in table 3, the diameter of the adsorbent particle influences the pressure drop. A large diameter reduces the pressure drop and vice versa. In

the PSA simulations in section 4, the particle diameters were 3 mm and 2.7 mm for activated carbon and zeolite 5A, respectively. Based on technical specifications for commercial adsorbents, activated carbons are available at 5 mm (Limited, 2014) and zeolite 5A is available at 6 mm diameter (Alibaba, 2014). Larger particles would help reduce the column size. However, when scaling from lab/pilot size to full scale it is usual to keep the same particle diameters (Rodrigues, 2014). In addition, a larger particle size results in slower rate of adsorption which increases the contact time required for adsorption (Carbochem, 2014), and at a certain point, the mass transfer resistance within the particle becomes significant (Rodrigues, 2014). The size calculation was performed for both the large and small particles.

The length of the column would have to be decided based on the pressure drop, the optimized step times for the full scale column, breakthrough of CO_2 and process performance. Consequently, to be able to determine a suitable column length, simulations in full scale would have to be performed. Instead, the column length was set arbitrarily to 10 m and 15 m, and the diameter was calculated based on that. The goal was to get a rough estimate of the size of the columns and the whole PSA plant in order to be able to accommodate all the flue gas from the power plant. The mole flow rate for all cases in the front stage was 25.7 kmol/s and 5.9 kmol/s for the tail stage. This was based on the results from the power plant and the capture rates of the front stage. The pressure drop was 0.1 bar for all cases. The resulting number of columns and the diameters are given in table 44.

As discussed before, the PSA process was designed for a train ratio of two and that the tail columns would be roughly in the same dimensions as the front stage, only somewhat smaller. This is confirmed by the results in table 44. The results also show that a very high number of trains and large columns were required to accommodate the flue gas from the power plant. Depending on the number of trains and size of adsorbent particle, 120-160 columns of length 10-15 with a diameter of 5-12 meters may be necessary. This shows that the footprint of the PSA plant is huge, and indicates high investment costs. In any case, the size makes the PSA plant less attractive as a technology for decarbonisation. An alternative could be to treat only a fraction of the flue gas. That would reduce the size of the PSA plant and increase the power plant efficiency, but also reduce the total capture rate of CO_2 and increase the CO_2 emissions.

Table 44: Size and number of columns

	Column length 10 m							
Front Stage	2.7 mm particle				6 mm particle			
Number of trains	20	30	40	50	20	30	40	50
Number of columns	60	90	120	150	60	90	120	150
Column diameter [m]	15.0	12.2	10.6	9.5	10.4	8.5	7.4	6.6
Tail Stage								
Number of trains	10	15	20	25	10	15	20	25
Number of columns	20	30	40	50	20	30	40	50
Column diameter [m]	10.4	8.5	7.4	6.6	7.4	6.1	5.3	4.7

	Column length 15 m							
Front Stage	2.7 mm particle				6 mm particle			
Number of trains	20	30	40	50	20	30	40	50
Number of columns	60	90	120	150	60	90	120	150
Column diameter [m]	17.4	14.2	12.3	11.0	11.7	9.6	8.3	7.4
Tail Stage								
Number of trains	10	15	20	25	10	15	20	25
Number of columns	20	30	40	50	20	30	40	50
Column diameter [m]	12.1	9.9	8.6	7.7	8.3	6.8	5.9	5.3

5.4.4 Power Plant Comparison

The power plant simulation results are summarized in table 45 and the accounting of CO_2 is summarized in table 46. The power plant with CO_2 capture by PSA had an efficiency of 28.7 %, a CO_2 emitted of 121.6 kg/MWh_{net} and an additional fuel per kWh_{net} of 57.6 %. For the absorption case, the efficiency was 33.4 %, the CO_2 emitted was 102.2 kg/MWh_{net} and an additional fuel per kWh_{net} of 35.8 %. Even with an optimistic approach where water was not considered in the PSA process, the absorption process was superior in all aspects. The net power output, the plant efficiency, the CO_2 purity and the CO_2 capture efficiency were higher, while the specific CO_2 emission, SPECCA and additional fuel per kWh were lower. It is highly likely that the water which should be in the PSA process would decrease the power plant efficiency further.

The main drawback of CO_2 capture by PSA was the high power consumption due to compressing the flue gas and recompression between the stages. The advantage of the PSA process was that it did not require steam, and saved energy compared to absorption. An attempt to reduce the PSA power consumption was made. Lowering the purity to 90.4 % increased the power plant efficiency from 28.7 % to 32.3 %. A 90 % purity was easily achievable, and modifications to lower the power consumption was implemented. The feed pressure was lowered and the rinse step time was decreased, which was advantageous. The purge was increased to maintain the recovery, which was energy demanding. The decrease in purity increased the power consumption in the CO_2 compressor with 6 MW. Even with these modifications it was not possible to increase the plant efficiency enough to match the absorption case. If the efficiency was to be increased even further, the purity or recovery had to be decreased below 90 %. When everything is taken into account, the results indicate that PSA as a technology for decarbonisation as an alternative to absorption is not realistic.

In order to improve the performance of the power plant, a new PSA process configuration and new adsorbents may be necessary. The PSA processes in table 1 indicate that a single stage process is not sufficient to achieve the required purity and recovery. On the other hand, the simulated two stage process had too high power consumption. It is difficult to suggest a better cycle configuration that will have satisfy both the DYNAMIS quality recommendation and at the same time have low enough power consumption. An improvement of the adsorbent, such as better selectivity and water resistance, may make it possible to decrease the power consumption. The feed pressure and the step lengths of rinse and purge could be lowered while still achieving the required performance. Also, a water resistant adsorbent would obviously be beneficial for post-combustion.

Table 45: Summary PCC simulations

Operational performance				
	No capture	$PSA_{96\,\%}$	$PSA_{90\,\%}$	Absorption
Coal flow rate [kg/s]	66.2	66.2	66.2	65.4
Coal LHV [MJ/kg]	25.2	25.2	25.2	25.2
Net fuel input [MW_{th}]	1665.6	1665.6	1665.6	1646.6
Gross electrical output [MW]	825.6	825.2	825.2	683.9
Flue gas compressor [MW]		30.2		
CO_2 separation [MW]		161.6	127.8	10.2
CO_2 compressor [MW]		80.4	86.2	46.8
Total auxiliary [MW]	71.2	346.5	287.5	134.8
Net electrical output [MW]	754.4	478.7	537.7	549.2
Net electrical efficiency [%]	45.3	28.7	32.3	33.4
CO_2 capture rate [%]		90.0	90.0	90
CO_2 capture efficiency [%]		84.2	85.9	86.4
CO_2 purity [%]		96.4	90.4	100
Specific CO_2 emissions [kg/MWh_{net}]	769.2	121.6	108.5	102.2
SPECCA [MJ/kg_{CO2}]		7.1	4.9	4.3

Table 46: Summary CO_2 accounting

Accounting of CO_2			
	$PSA_{96\,\%}$	$PSA_{90\,\%}$	Absorption
CO_2 captured [kg/MWh_{net}]	1093.2	973.1	919.8
CO_2 avoided [kg/MWh_{net}]	647.6	660.7	667.0
CO_2 emitted [kg/MWh_{net}]	121.6	108.5	102.2
Total CO_2 formed [kg/MWh_{net}]	1214.8	1081.7	1022
Additional CO_2 [kg/MWh_{net}]	445.6	312.5	252.8
Additional fuel per kWh_{net} [%]	57.6	40.3	35.8

5.5 IGCC without CO_2 Capture

The design basis for the IGCC reference plant was based on the assumptions and parameters given by DECARBit. The modeled plant was compared to the benchmark IGCC plant in DECARBit to ensure that the model was realistic. The simulation was carried out using GT Pro and Thermoflex. A simplified plant layout of the IGCC power plant without CO_2 capture is given in figure 17. Important streams have been indicated with numbers, and their condition and composition are given in table 47.

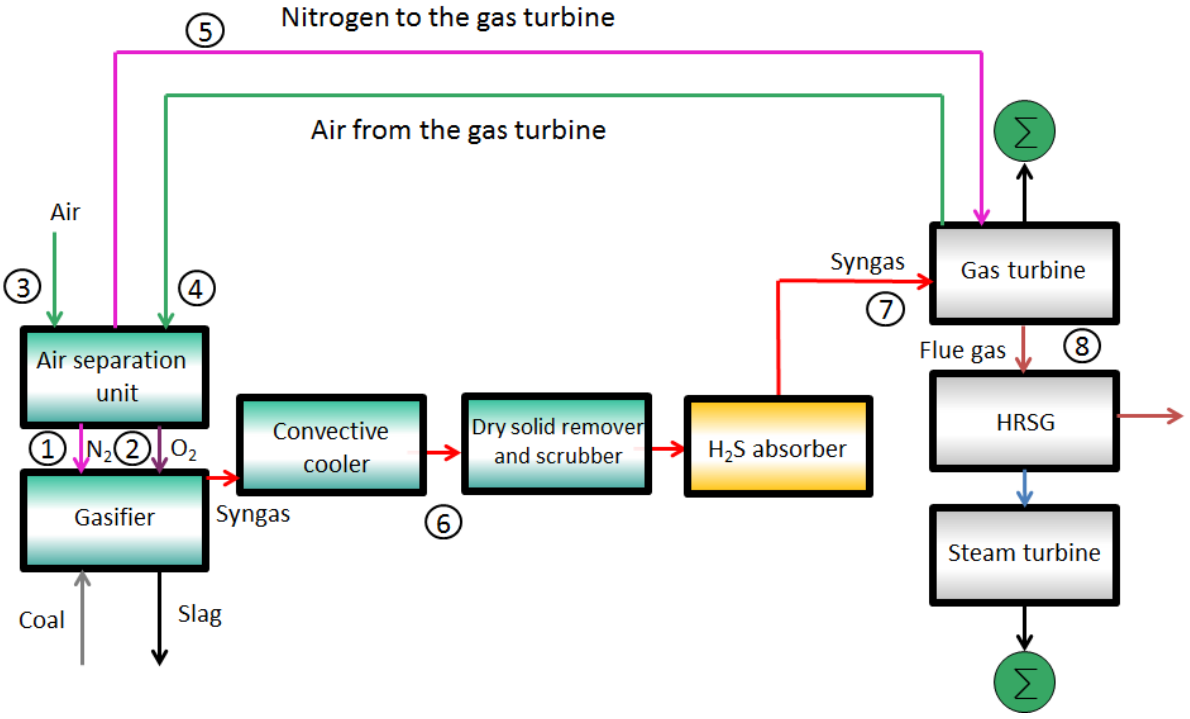

Figure 17: IGCC plant layout (European benchmarking task force, 2008)

Table 47: Stream data for IGCC without CO_2 capture

Stream compositions and conditions														
Stream	Mass flow	T	P	MW	Composition									
	Kg/s	°C	Bar	g/mol	N_2	H_2	CO_2	CO	O_2	Ar	H_2S	H_2O	CH_4	COS
1	7.34	114	88	28.02	100									
2	27.02	124.2	48		3.5				95	1.5				
3	55.84	15	1.01	28.85	77.29		0.03		20.74	0.93		1.01		
4	55.84	389.8	16.9	28.85	77.29		0.03		20.74	0.93		1.01		
5	33.28	223.6	30.4	28.02	100									
6	66.02	350.5	43.1	21.31	10.01	26.21	3.07	55.72		0.41	0.16	4.33	0.08	0.01
7	63.2	175.2	30.4	21.39	10.50	27.49	3.05	58.43		0.43		0.02	0.09	0.00
8	680.6	594.0	1.05		74.17		7.90		12.65	0.87		4.42		

The gasifier was an entrained flow oxygen-blown gasifier from Shell with convective cooler. The gasifier inputs are given in table 48:

Table 48: Gasifier input

	Gasifier input
Gasifier type	Entrained flow oxygen-blown gasifier from Shell with convective cooler
Flow rate of O_2	0.8124 t of O_2 /t of coal
Flow rate of N_2	0.2207 t of N_2 /t of coal
Flow rate of H_2O	0.10 t of H_2O/t of coal
Gasifier pressure	44 Bar
Carbon conversion	99 %
Quench temperature	900 °C

According to the guidelines the gasifier temperature should have been set at 1550 °C, but the software only allowed specifying either flow rate of O_2 or temperature, not both. The O_2 flow rate was specified and the resulting gasifier temperature became 1308 °C. The cold gas efficiency was 82.4 %. The stream parameters of the raw syngas are given as stream 6 in table 47.

The ASU was operated at a pressure of 10 bar. 50 % of the air supplied to the ASU was supplied by the gas turbine compressor and the other 50 % was supplied by an independent compressor. This level of integration was recommended due to reliability, availability and efficiency (European Benchmarking Task Force, 2008). O_2 and N_2 was available at 2.6 bar from the ASU. The oxygen to the gasifier was compressed to 48 bar, while a fraction of the nitrogen was used as fuel preparation gas.

After gasification the syngas contained slag, ash and impurities and had to be cooled prior to cleaning. The syngas was cooled by gas recycle quench and convective coolers. The syngas was purified through a scrubber and a COS hydrolysis, which removed particles and water-soluble components. The COS-hydrolysis resulted in a 98 % conversion of COS.

Before the gas was further treated to remove sulfur-containing components, the gas was cooled to 37.8 °C. The H_2S removal efficiency was set to 99.99 %. Next, the syngas was heated by heat recovery and by a preheater to increase the temperature to 175.2 °C before the combustion in the gas turbine. The treated syngas now consisted mainly of H_2 and CO and was combusted in the gas turbine to produce power. The stream parameters of the syngas going to the gas turbine are given by stream 7 in table 47.

The gas turbine was a GE 9371F, which is a large-scale “F-class” 50 Hz state of the art gas turbine recommended by European Benchmarking Task Force (2008). Air was extracted from the compressor section to supply the ASU with 50 % of the air input required. The gas turbine parameters are given in table 49.

Table 49: Gas turbine parameters

GE 9371F Gas turbine parameters	
Pressure ratio	16.7
Air mass flow rate in to compressor [kg/s]	639.9
Syngas fuel rate [kg/s]	63.2
Syngas temperature [°C]	175.2
Nitrogen flow rate [kg/s]	33.3
Nitrogen temperature [°C]	223.6
Inlet and outlet pressure drop [mBar]	10
LHV efficiency [%]	36.8
Specific work [kJ/kg_{air}]	395.5
Turbine inlet temperature [°C]	1309.2
Turbine outlet temperature [°C]	594.0
Power [MW]	253.1

The flue gas from the gas turbine was further cooled down in the HRSG to utilize the remaining heat for steam and power generation. The HRSG and steam turbine was a four pressure cycle, one HP, one IP, and two LP with a single reheat. The superheated IP steam was mixed with cold reheat steam before reheat. The HRSG and steam turbine parameters are given in table 50.

Table 50: HRSG and steam turbine parameters

HRSG and steam turbine parameters	
HRSG	
Steam side pressure loss in HP superheater [%]	7
Steam side pressure loss in reheaters [%]	7
Steam side pressure loss in LP superheater [%]	11
Minimum HRSG temperature difference [°C]	5
Minimum economizer approach temperature difference [°C]	5
Condenser pressure [Bar]	0.048
Steam turbine	
Steam turbine HP group blading efficiency [%]	92
Steam turbine IP group blading efficiency [%]	94
Steam turbine LP1 group blading efficiency [%]	93
Steam turbine LP2 group blading efficiency [%]	90
HP inlet pressure [Bar]	144
HP inlet temperature [°C]	555
HP steam flow rate [kg/s]	129.5
Hot reheat pressure [Bar]	50
Hot reheat temperature [°C]	545
Steam turbine power [MW]	192.6

The IGCC flow sheet is presented in figure C1 appendix C. The operational performance of the power plant is given in table 51. The power plant achieved a net electricity output of 395.8 MW with an efficiency of 47.3 % with a specific CO_2 emission of 730.5 kg/MWh_{net} for a coal flow rate of 33.3 kg/s. Table 51 clearly illustrates that the power plant was very similar to DECARBit with regards to operating performance. They were not identical, but the model serves well as a reference plant based on realistic industry-standard assumptions for component performance and intrinsic losses. The model represents a state of the art power plant which was used to compare and evaluate the performance of an IGCC power plant with CO_2 capture.

Table 51: IGCC operational performance

Operational performance		
	Simulation	DECARBit
Coal flow rate [kg/s]	33.3	32.9
Coal LVH [MJ/kg]	25.2	25.2
Net fuel input [MW_{th}]	837.3	828.0
Gas turbine output [MW]	253.1	254.4
Steam turbine output [MW]	192.6	182.4
Air expander [MW]	4.5	5.0
Gross electrical output [MW]	450.2	441.7
Total auxiliary power consumption [MW]	54.3	50.3
Net electrical output [MW]	395.8	391.5
Net electrical efficiency [%]	47.3	47.3
Specific CO_2 emissions [kg/MWh_{net}]	730.5	734.0

5.6 IGCC with CO_2 Capture by Absorption

The simulation of the IGCC power plant with CO_2 capture by absorption was performed according to DECARBit. The CO_2 was removed by physical absorption, and a total plant capture rate of 90.9 % was specified. The simulation was performed in Thermoflex. Most of the units and their operational characteristics were similar to those of IGCC without CO_2 capture. A sour water-gas shift was added, and the CO_2 was removed by absorption in the acid gas removal unit. For the shift reactor, the conversion ratio of CO was 96 %, the H_2O/CO ratio was 2.0 and the CO_2 was compressed to 110 bar for transport.

Since the focus of this report is not on absorption, only the main results are presented. The power plant performance is given in table 52 and the accounting of CO_2 is given in table 53. The power plant obtained a net electrical output of 352.8 MW with an efficiency of 36.4 %. The absorption capture rate was 94.6 %, the CO_2 purity was 100 %, and the total plant capture rate was 90.9 %. The efficiency dropped 10.9 percentage points from 47.3 % to

36.4 % when introducing CO_2 capture. The specific CO_2 emissions were reduced from 730.5 kg/MWh_{net} to 86.2 kg/MWh_{net} and the SPECCA was 3.5 MJ_{LHV}/kg_{CO2}.

Table 52: Operational performance IGCC with CO_2 capture by absorption

Operational performance		
	Simulation	DECARBit
Coal flow rate [kg/s]	38.5	37.9
Coal LHV [MJ/kg]	25.2	25.2
Net fuel input [MW_{th}]	968.4	954.1
Gas turbine output [MW]	282.9	282.9
Steam turbine output [MW]	170.2	168.5
Air expander [MW]	5.7	5.8
Gross electrical output [MW]	458.8	457.2
CO_2 separation power consumption [MW]	16.5	
CO_2 compressor power consumption [MW]	18.8	
Total ancillary power consumption [MW]	106.1	104.4
Net electrical output [MW]	352.8	352.7
Net electrical efficiency [%]	36.4	37.0
CO_2 separation capture rate [%]	94.6	
Total Plant CO_2 capture rate [%]	90.9	90.9
CO_2 purity [%]	100	98.2
Capture efficiency [%]	88.2	
Specific CO_2 emissions [kg/MWh_{net}]	86.2	85.3
SPECCA [MJ_{LHV}/kg CO_2]	3.5	3.3

Table 53: Accounting of CO_2

Accounting of CO_2	
CO_2 captured [kg/MWh_{net}]	861.3
CO_2 avoided [kg/MWh_{net}]	644.3
CO_2 emitted [kg/MWh_{net}]	86.2
Total CO_2 formed [kg/MWh_{net}]	947.5
Additional CO_2 [kg/MWh_{net}]	217.0
Additional fuel per kWh_{net} [%]	29.8

5.7 IGCC with CO_2 Capture by PSA

The plant layout of the IGCC power plant with PSA is given in figure 18 and the corresponding streams in table 54. The PSA process was added to the cycle downstream the H_2S absorber. The IGCC plant using PSA was very similar to the absorption plant prior to the

CO_2 separation process. Compared to the reference plant without CO_2 capture, the IGCC plants with capture (both absorption and PSA) had an increased coal flow rate input. This was according to DECARBit and the reason for this seems to be to maintain the gross power output from the power plant and to be able to use the same gas turbine.

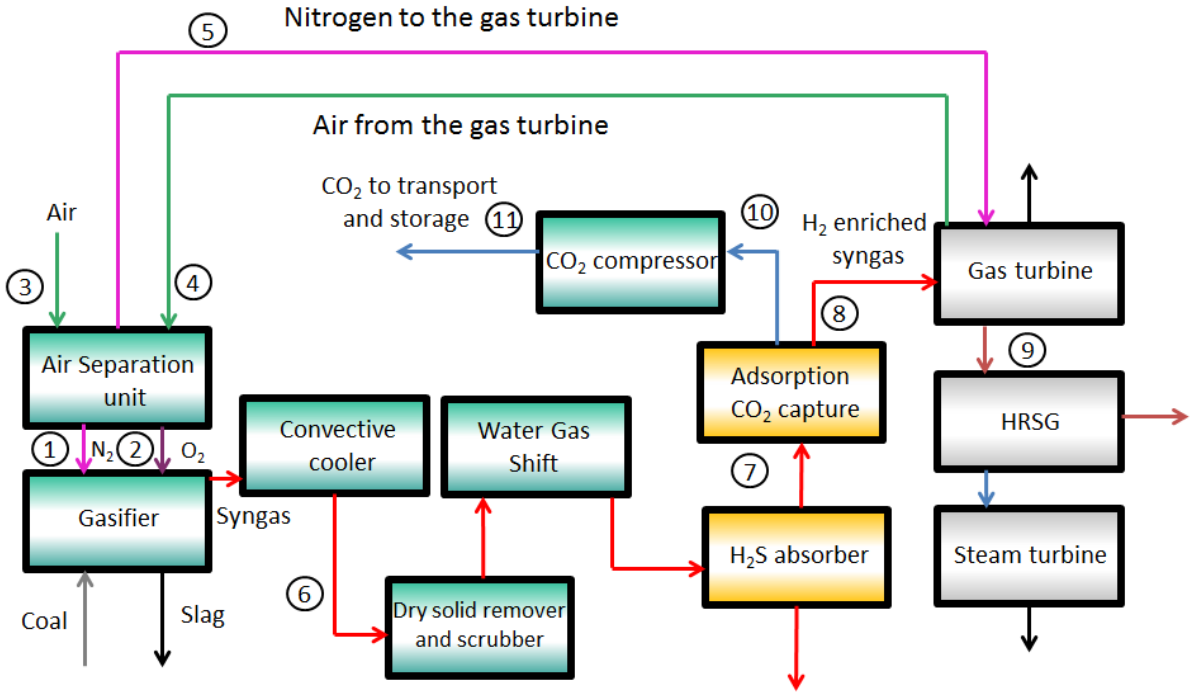

Figure 18: IGCC plant layout with CO_2 capture by PSA

Table 54: Stream table for IGCC with CO_2 capture by PSA

Stream compositions and conditions														
Stream	Mass flow	T	P	MW	Composition									
	Kg/s	°C	Bar	g/mol	N_2	H_2	CO_2	CO	O_2	Ar	H_2S	H_2O	CH_4	COS
Coal	38.47	25	1.01											
1	8.49	82.5	88.0	28.02	100.00									
2	31.24	123.9	44.9	31.98	3.50				95.00	1.50				
3	64.57	15.0	1.01	28.86	77.29		0.03		20.74	0.93		1.01		
4	64.57	423.1	16.8	28.86	77.29		0.03		20.74	0.93		1.01		
5	87.46	116.9	24.4	28.02	100.00									
6	76.34	497.1	43.1	21.31	10.01	26.21	3.07	55.72		0.41	0.16	4.33	0.08	0.01
7	107.61	34.9	38.8	20.18	6.72	53.54	37.89	1.50		0.27		0.02	0.06	
8	26.38	230.0	38.8	7.88	7.13	82.63	8.28	1.59		0.29		0.02	0.06	
9	655.58	565.4	1.05	27.51	74.99		1.42		10.41	0.77		12.42	0.00	
10	81.23	27.8	1.0	40.89	6.04	4.54	87.76	1.35		0.25		0.02	0.05	
11	81.23	28.0	110.0	40.89	6.04	4.54	87.76	1.35		0.25		0.02	0.05	

The input parameters of the gasifier were equal to that of the reference plant. The gasifier output parameters are given as stream 6 in table 54. One major difference to the reference

plant was that the syngas flow rate was increased due to the increase in coal flow rate. The cold gas efficiency was 82.4 %

The pressure and temperature of which the oxygen and nitrogen were supplied from the ASU were also similar to that of the benchmark plant. However, the flow rate of nitrogen supplied to the gas turbine was increased compared to the reference plant. This was necessary since the syngas entering the gas turbine was no longer diluted with CO due to the WGS reaction. In this context the Wobbe index is used as a guiding tool to decide whether two different fuels can use the same combustion system. By diluting the H_2-rich syngas with N_2, a Wobbe index similar to the no-capture syngas fuel could be achieved. Hence, it is likely that the same combustion system could be utilized. A high hydrogen fraction also increases the flame temperature, which causes an increase in NO_x production (Bolland, 2012). To solve this challenge, the amount of separated nitrogen supplied to the gas turbine in the simulation was increased from 33.3 kg/s to 87.5 kg/s. This was the same amount as used in IGCC plant with absorption.

The gas turbine parameters are given in table 55. Due to the increased coal input, the net fuel input increased compared to the benchmark plant. In addition the gas turbine LHV efficiency increased from 36.8 % given in table 49 to 39.5 % given in table 55. Due to a reduction in power output, the gas turbine was changed from GE 9371FB (rated 291 MW) to Siemens SGT5-4000F (rated 279 MW) allowing the gas turbine to operate closer to design point. This increased the efficiency to the same level as the gas turbine in the IGCC plant with absorption, which also achieved 39.5 %. In order to compare capture technologies, a similar gas turbine LHV efficiency is obviously beneficial.

Table 55: Gas turbine parameters

Siemens SGT5-4000F	
Pressure ratio	16.6
Air mass flow rate in to compressor [kg/s]	606.3
Syngas fuel rate [kg/s]	26.4
Syngas temperature [°C]	230.0
Nitrogen flow rate [kg/s]	87.5
Nitrogen temperature [°C]	116.9
Inlet and outlet pressure drop [mBar]	10.0
LHV efficiency [%]	39.5
Specific work [kJ/kg_{air}]	447.2
Turbine inlet temperature [°C]	1269
Turbine outlet temperature [°C]	565.4
Power [MW]	271.1

The HRSG and steam turbine parameters are given in table 56. The steam turbine output decreased from 192.6 MW, given in table 50, to 161.0 MW as seen in table 56. The reason for this was that with CO_2 capture less steam was available, primarily due less heat recovery

from the gasifier cooler, and steam extraction to be used in the CO-shift. This is further explained in section 5.8.1.

Table 56: HRSG and steam turbine parameters

HRSG and steam turbine parameters	
HRSG	
Pressure loss in HP superheater [%]	3
Pressure loss in reheaters [%]	7
Pressure loss in LP superheater [%]	11
Minimum HRSG temperature difference [°C]	5
Minimum economizer approach temperature difference [°C]	5
Condenser pressure [Bar]	0.048
Steam turbine	
Steam turbine HP group blading efficiency [%]	92
Steam turbine IP group blading efficiency [%]	94
Steam turbine LP group blading efficiency [%]	91
HP inlet pressure [Bar]	138.0
HP inlet temperature [°C]	540.0
HP steam flow rate [kg/s]	147.7
Hot reheat pressure [Bar]	47.0
Hot reheat temperature [°C]	536.9
Steam turbine power [MW]	161.0

The syngas entered the PSA column at 38.8 bar so compression of the feed stream was not necessary. The gPROMS simulations output showed a negligible pressure drop during both the feed and purge step. This meant that no auxiliary blowers or fans were in reality needed, hence the PSA process with the exception of actuation of valves, did not use power.

The adsorbed CO_2 mixture left the PSA column at 1.0 bar and was compressed to 110 bar for transport and storage. The temperature of the CO_2-mixture leaving the column varied depending on which step it was desorbed. The average temperature of the mixture was calculated to be 27.8 °C. The specified maximum compressor inlet temperature of 28 °C was therefore achieved without further cooling downstream the PSA process. The H_2-rich syngas outlet temperature of the PSA column was calculated to 41 °C, giving it a 6 °C temperature increase from its inlet temperature of 35 °C. To achieve the correct temperature before being injected into the combustion chamber the syngas was further heated to 230 °C. This was conducted by heat exchange with surplus heat from the hot syngas downstream the WGS reactor. In contrary to the IGCC plant without capture it was not necessary with an additional syngas preheater, as the syngas required less heating due to the removal of CO_2 from the stream.

The operational performance is summarized in table 57. The net electrical efficiency dropped 12.5 percentage points from 47.3 % achieved in the simulation without capture to 34.8 %. This is lower than the 36.4 % net efficiency achieved for the IGCC plant with CO_2 capture using absorption.

Table 57: Operational performance of IGCC with capture by PSA

Operational performance	
	Simulation
Coal flow rate [kg/s]	38.5
Coal LHV [MJ/kg]	25.2
Net fuel input [MW_{th}]	968.2
Gas turbine output [MW]	271.1
Steam turbine output [MW]	161.0
Air expander [MW]	5.3
Gross electrical output [MW]	437.5
PSA power consumption [MW]	0.0
CO_2 compressor power consumption [MW]	33.0
Total auxiliary power consumption [MW]	101.0
Net electrical output [MW]	336.5
Net electrical efficiency [%]	34.8
CO_2 separation capture rate [%]	86.3
Total plant CO_2 capture rate [%]	83.8
Capture efficiency [%]	78.2
CO_2 purity [%]	87.8
Specific CO_2 emissions [kg/MWh_{net}]	159.1
SPECCA [MJ_{LHV}/kg CO_2]	4.8

Table 58: Accounting of CO_2

Accounting of CO_2	
CO_2 captured [kg/MWh_{net}]	820.9
CO_2 avoided [kg/MWh_{net}]	571.4
CO_2 emitted [kg/MWh_{net}]	159.1
Total CO_2 formed [kg/MWh_{net}]	980.0
Additional CO_2 [kg/MWh_{net}]	249.5
Additional fuel per kWh_{net} [%]	36.0

5.8 Discussion of IGCC Simulations

5.8.1 Breakdown of Efficiency Losses due to CO_2 Capture

Table 62 in section 5.8.3 summarizes the performance of the three simulated power plants. As already mentioned the PSA process did not perform to the expectations and resulted in a CO_2 separation capture rate and purity of 86.3 % and 87.8 %, respectively. In comparison, absorption achieved 94.6 % CO_2 separation capture rate and 100 % purity. The net electrical efficiency with CO_2 capture by PSA was 1.7 percentage points lower than absorption and 12.5 percentage points lower than the plant without capture. This section will discuss where these efficiency losses occurred and put them in context with the performance of the CO_2 separation methods.

There were three main factors reducing the performance of the power plant when capturing CO_2:

- Auxiliary power consumption due to the CO_2 compressor
- Auxiliary power consumption due to the CO_2 separation
- Reduction of gross power output

The factors affecting the reduction in gross output was the reduction of fuel Lower Heating Value (LHV) and reduced exhaust heat due to the CO-shift reaction, adsorption of fuel in the separator and the increased use of generated steam in other parts of the plant.

Increased Auxiliary Power Consumption

The CO_2 compressor was the main auxiliary consumer in the power plant. When comparing the CO_2 compression power consumption in table 60, using PSA increased the power consumption by 75 % compared to absorption. In the power plant with the PSA process the CO_2 compressor compressed the gas stream from 1 bar to 110 bar. On the other hand, the absorption process regenerated the CO_2 using flash tanks at three different pressure levels: 40 % at 12.7 bar, 25 % at 7.5 bar and 35 % at 1.1 bar. Hence, the CO_2 compression duty was lower than for PSA.

The performance of the PSA process played a significant role for the power consumption. A high purity decreased the power consumption while a high capture rate had the opposite effect. The purity achieved in the absorption process was 100 %, so no power was wasted on compressing impurities. Although high CO_2 recovery in general is desired, it increases the CO_2 compression duty, and there is therefore a trade-off between capture rate and net plant efficiency. Since the PSA process achieved a lower capture than absorption, this actually helped to increase the net plant efficiency. For the sake of comparison, decreasing the absorption capture rate to the same level as PSA (86.3 %) would have decreased the compression duty from 18.8 to 17.1 MW and with this have increased the net plant efficiency by 0.2 percentage points.

The CO_2 separation process itself was the second highest auxiliary power consumer for the power plant using absorption. The PSA process used no power except for the actuation of valves, which was insignificant in this context. The main power consumers in the absorption

process were the pumps, which circulated the solvent. It should be noticed that in the case of absorption since the CO_2 was regenerated due to pressure reduction no steam was generated for this purpose. 4.5 MW of steam was however generated for both the capture plants in order to remove H_2S. CO_2 capture also caused additional power consumption from miscellaneous units as seen in table 60. This included increased N_2 compression duty in order to dilute the H_2-rich syngas in the gas turbine, and additional pumping of cooling water for the CO-shift reaction.

When studying the additional power consumption in table 60 it can be seen that the total consumption was actually lower when using PSA instead of absorption. This was because the absorption process was a very large power consumer. The reduced efficiency when using PSA compared to absorption was therefore due to reduced gross output.

Reduction in Gross Power Output

CO_2 capture led to a reduction in the gross power output. Although the gross output was higher for the two IGCC plants with CO_2 capture, seen in table 62, it must be taken into account that the net fuel input was significantly higher. In contrary to the reduction of efficiency due to additional auxiliary power consumption, to quantify the different factors that contributed to the reduction in gross output was not straight forward. Introduction of CO_2 capture changed the plant size with regards to net fuel input, changed unit efficiencies and introduced new components. In this section, the numbers presented were calculated with the assumption of constant gas turbine and steam cycle efficiencies. In the discussion concerning loss of steam, the differences in net fuel input needed to be accounted for in order to compare with the no-capture plant. This was solved by assuming that the capture plants could be scaled to the same size as the no-capture plant.

Adsorbed Syngas

One important aspect that separated the PSA process and the absorption process from another was the loss of syngas fuel such as H_2, CO and CH_4 due to adsorption of these components. Table D2 in appendix D identifies the reduction of fuel LHV, which was 30.1 MW, and it can be noticed that adsorption H_2, even though only 3.2 % of the produced H_2 was adsorbed, accounted for about 70 % of the total fuel LHV reduction. Due to adsorption of syngas the gas turbine net power output, based on its LHV efficiency of 39.5 %, decreased by 4.2 %, which corresponded to 11.9 MW.

The consequences of fuel loss due to adsorption could also be seen in the reduced steam turbine output as well, since the impact of the reduced fuel LHV cascaded down to give a reduced gas turbine exhaust gas flow rate. Table D2 in appendix D also shows the reduction of recovered exhaust gas heat when using PSA compared to absorption. By using the bottoming steam cycle net efficiency of 39.6 % calculations showed that the steam turbine output decreased by 4.3 %, which corresponded to 7.2 MW. Table 60 shows the total loss of gas turbine and steam turbine power output due to fuel loss, which was 19.1 MW. This caused the net plant efficiency to decrease by 2.0 percentage points.

Figure 19 shows a graphical presentation of the gross output that was reduced due to adsorption of syngas fuel. The fuel LHV was reduced by 30.1 MW. This could have been used to produce 11.9 MW from the gas turbine and 7.2 MW from the steam turbine. It is important to notice that since the ASU, gasifier and gas cleanup system already had consumed auxiliary power in order to produce the clean syngas, over 60 % of the lost fuel LHV could have been converted into net power.

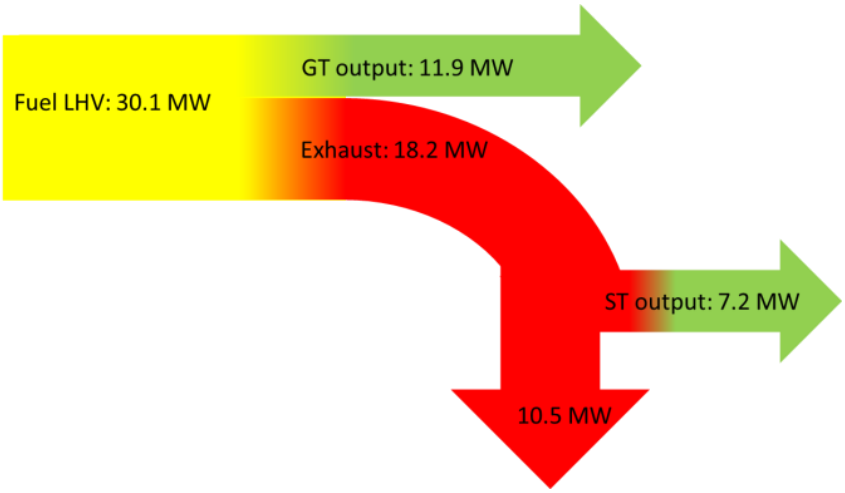

Figure 19: Breakdown of losses due to adsorption of syngas fuel

It should be noted that although adsorption of syngas fuel containing carbon such as CO and CH_4 reduced the power output, it also contributed to increase the total plant capture rate. As CO_2 is formed when CO and CH_4 is combusted in the gas turbine, the emissions are increased. Figure 20 illustrates this aspect and the equations, using the flow rate of CO_2 from the respective stream numbers, shows why the total plant capture rate was lower than the CO_2 separation rate:

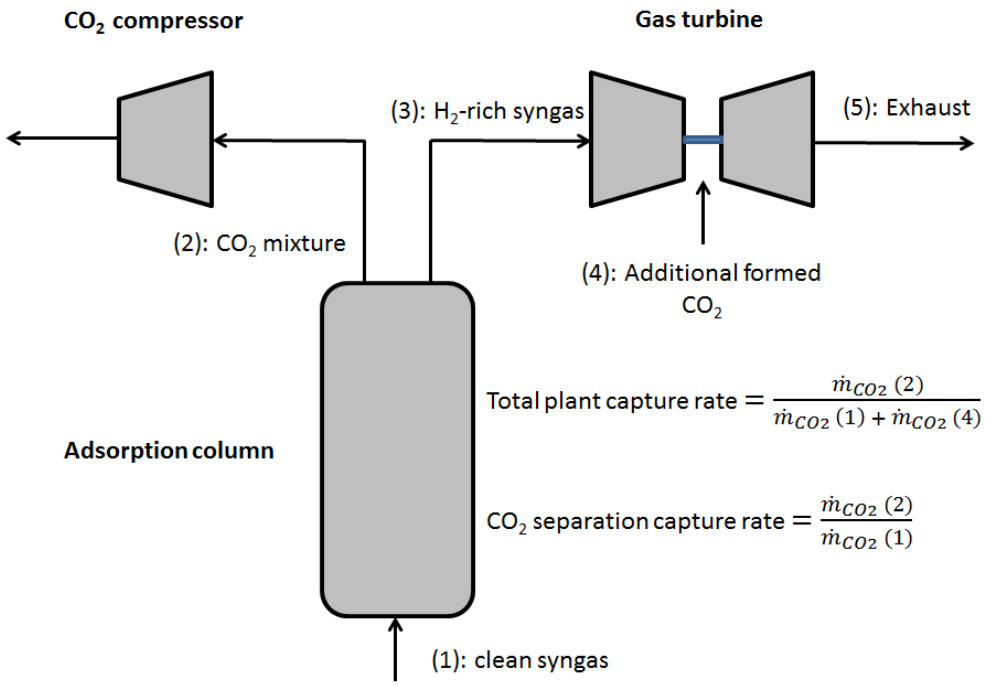

Figure 20: Increased emissions by additional formation of CO_2

For the two IGCC plants with capture, the total CO_2 formation was increased by 4.1 percentage points in the combustor for the absorption case, while due to adsorption of CO and CH_4 for PSA the increase was 3.0 percentage points.

When designing a capture process for an IGCC power plant it is therefore important to taken into account that additional CO_2 is formed in the combustor. If a total plant capture rate of 90 % is the goal, the separation capture rate needs to be higher in order to achieve this. It should be mentioned that for the IGCC plants simulated the CO conversion efficiency was 96 %. Improving this could also help achieving a higher total plant capture rate.

CO-Shift Fuel LHV Reduction

Common for both PSA and absorption is that CO_2 capture involved the use of a CO-shift reactor, which in the software Thermoflex is a part of the gas cleanup system where acid gas and CO_2 removal takes place. The introduction of CO-shift caused the fuel LHV to decrease as this is an exothermic reaction. Moreover, as steam was required for the reaction, steam loss was inevitable, although some of this could be recovered from the surplus heat produced by the CO-shift reaction. Figure D1 in appendix D shows the reduction of fuel LHV, which occurred during the gas cleanup step, where the raw syngas entered and the clean syngas left to be used as fuel in the gas turbine. For the no-capture IGCC plant this reduction was insignificant, only 0.4 %. The small reduction was due to the acid gas removal. For the two capture plants, the reduction was increased to 10.3 %. In order to identify the contribution of the CO-shift reaction the no-capture reduction was subtracted and the result became 9.9 %. It can be seen in table 60 that the gas turbine output due to the CO shift was reduced by 9.9 %, which corresponded to 32.5 MW, and caused the net plant efficiency to decrease by 3.4 %.

Steam Loss

The final contributors to reduced gross output were the loss of steam from steam integration with other units of the plant and the loss of recovered exhaust gas heat for steam production. These two factors reduced the steam turbine power output. Table 59 shows all the units in the IGCC plant where steam or water was integrated. Figure 21 shows a flow diagram of the syngas and the steam integration. The stream numbers in figure 21 corresponds to the stream numbers in table 59. As mentioned, due to the difference in net fuel input between the two capture plants and the no-capture plants, a column of values which was corrected for differences in net fuel input have been added. It can be seen that the steam generated by the raw syngas cooler was significantly decreased for the two capture plants. The reason was due to the CO-shift reactor, which required the raw syngas to enter at a higher temperature (capture: 497 °C, no capture: 351 °C). Further, it can be seen that the 164 MW of heat (142 MW corr.) was used for the CO-shift reaction. However, around half of this heat was recovered from the cooling of surplus heat from the CO-reaction. Moreover, the heat recovered in syngas cooler 2 was higher for the capture plants, due to the surplus heat from the CO-shift reaction. The syngas preheater for the no-capture plant did not demand significant amounts of heat. The sum shows that net heat recovered from steam integration for the capture plants was reduced by over 50 % compared to the no-capture plant.

The reduction in recovered exhaust heat due to adsorbed fuel has already been explained. However, a reduced exhaust gas flow rate due to the CO-shift reaction also caused a reduction in recovered exhaust heat for both of the capture plants. Table 59 therefore also shows the recovered exhaust heat for all plants. The reduction of recovered exhaust gas and the reduction of recovered heat from steam integration accounted for about 50 % each of the heat reduction for steam generation. By using the bottoming net steam cycle efficiency, the loss of net power output from the steam cycle could be calculated. The results are shown in table 60. It shows that the reduced heat from steam integration caused the steam turbine output to decrease by 28.3 MW for absorption and 29.1 MW for PSA. The lower exhaust gas flow rate reduced the output by 27.2 MW for absorption and 27.6 MW for PSA. This caused a combined net plant efficiency loss of 5.7 and 5.9 percentage points for the absorption and PSA, respectively.

Table 59: Recovered exhaust heat and steam integration

Technology	No capture	Absorption		PSA	
Steam integration: +/- corresponds to heat recovered/lost	Heat [MW]	Heat [MW]	Corr. Heat [MW]	Heat [MW]	Corr. Heat [MW]
Gasifier (1):	-1.9	-2.4	-2.1	-2.4	-2.1
Raw syngas cooler (2):	100.2	99.6	86.1	99.6	86.1
Steam to CO-shift (3):		-163.6	-141.5	-163.6	-141.5
CO-shift cooling (4):		81.0	70.0	81.0	70.0
Syngas cooler 2 (5):	18.5	47.5	41.0	45.0	39.0
Acid gas removal (6):	-3.9	-4.5	-3.9	-4.4	-3.8
Syngas preheater (7): (no-capture only):	-1.49				
Sum	**111.4**	**57.6**	**49.8**	**55.2**	**47.8**
Recovered exhaust heat	368.5	357.6	309.2	338.3	292.5
Total sum	**480.0**	**415.2**	**359.1**	**393.5**	**340.3**

The corrected heat is added to the CO_2 capture cases because of the increased net fuel input. It takes this into consideration and presents comparable values to the no-capture case.

$$corr.Heat = Heat * \frac{net\ fuel\ input_{no-capture}}{net\ fuel\ input_{capture}}$$

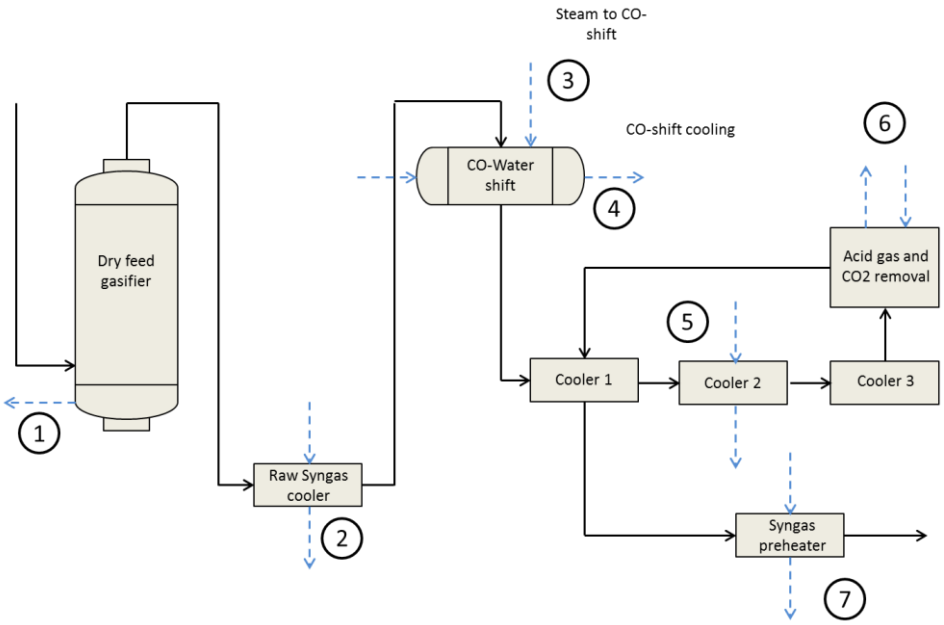

Figure 21: Steam integration with gasifier island and gas cleanup system

When summarizing the efficiency losses in table 60, it can be seen that the IGCC plants capturing CO_2 had an efficiency loss of 13.6 and 15.1 percentage points, respectively for absorption and PSA. These numbers shows in reality a too high efficiency loss when comparing to the reference plant without CO_2 capture. Removing these losses would take the capture plants' net efficiencies to 50 %, which is almost three percentage points more

than the reference plant without capture. The efficiency losses were corrected by taking into account the fact that the reference plant had a lower net efficiency for both the gas turbine and the bottoming steam cycle. Moreover, the power output from the air turbine utilizing the high pressure of the air entering the ASU, was proportionally lower for the reference plant when correcting for net fuel input. The corrected total sum therefore shows a 10.8 and 12.4 decrease in net plant efficiency. Removing these losses would take the capture plants' net efficiencies to 47.2 %, which was close to the net efficiency of the reference plant without capture.

Table 60: Accounting of losses due to CO_2 capture

Technology	Absorption		PSA	
Auxiliary power consumption:	Power consumption [MW]	Efficiency reduction [%]	Power consumption [MW]	Efficiency reduction [%]
CO_2 compression	18.8	1.9	33.0	3.4
CO_2 separation	16.5	1.7	0	0
Misc. aux consumption	8.0	0.8	5.2	0.5
Sum	**43.3**	**4.5**	**38.2**	**3.9**
Reduction gross output:	Reduced power output [MW]	Efficiency Reduction [%]	Reduced power output [MW]	Efficiency Reduction [%]
Adsorption of fuel	0	0	19.1	2.0
CO-shift fuel LHV reduction	32.5	3.4	32.5	3.4
Reduced heat from steam integration	28.3	2.9	29.1	3.0
Reduced recovered exhaust heat	27.2	2.8	27.6	2.9
Sum	**88.0**	**9.1**	**108.3**	**11.2**
Total sum	**131.2**	**13.6**	**146.5**	**15.1**
Corrected total sum	**104.7**	**10.8**	**120.1**	**12.4**

The corrected total sum is calculated by these adjustments:

The loss of gas turbine output is multiplied with the LHV efficiency ratio:

$$\frac{\eta_{GT\ no-capture}}{\eta_{GT\ capture}}$$

The loss of steam turbine output is multiplied with the bottoming steam cycle efficiency ratio:

$$\frac{\eta_{ST\ no-capture}}{\eta_{ST\ capture}}.$$

The loss of power output from the air expander is adjusted by multiplying with the ratio:

$$\frac{net\ fuel\ input_{no-capture}}{net\ fuel\ input_{capture}}$$

Figure 22 graphically presents the loss contributions from the units presented in this section and in table 60.

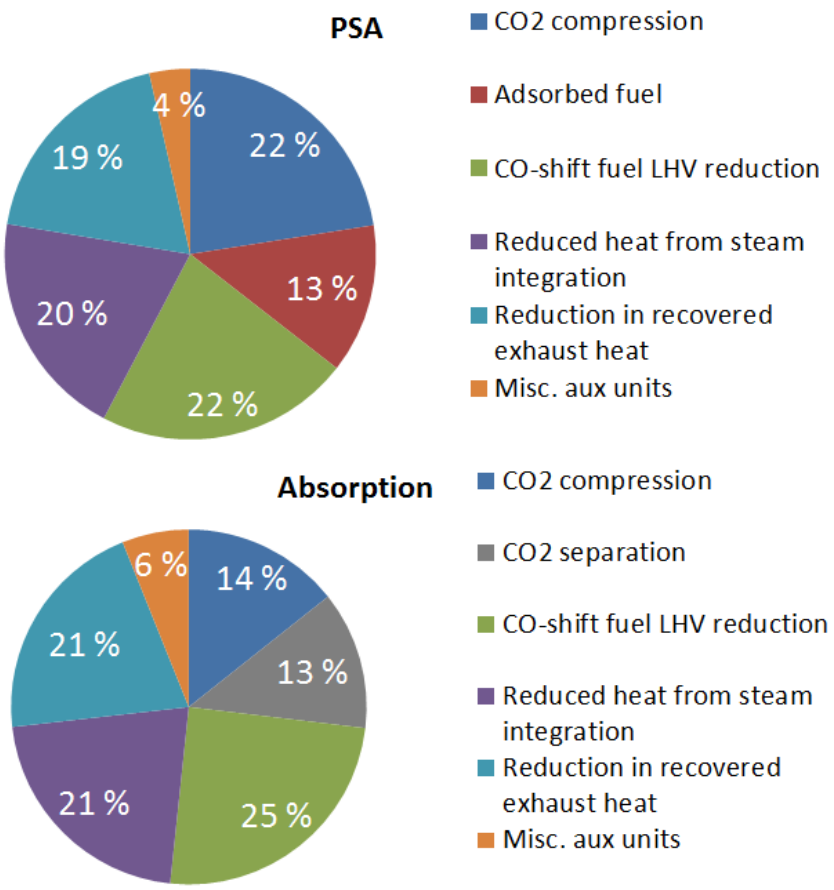

Figure 22: Losses associated with CO_2 capture

5.8.2 Size of PSA Plant

For an explanation on how the dimensioning was done, see section 5.3.1.3.

The pressure drop was set to 0.1 bar and the molar flow rate for all the cases was 5.3 kmol/s. This was based on the results from the power plant. The results, which show the number of trains and size of columns, are given in table 44.

It can be seen from the results in table 61, compared to table 44, that the size of the PSA plant was significantly smaller for pre-combustion than for post-combustion. The syngas flow rate was about five times lower than the flow rate of flue gas in post-combustion. In addition, a feed pressure of 38.8 contributed to decrease the column diameter. The results show that it could be possible to use only one train consisting of seven columns to operate the process. This indicates that the size of the PSA plant is in fact feasible to build, and should not be used as an argument against decarbonisation by PSA.

Table 61: Size and number of columns

	Column length 10 m					
Particle size	3 mm particle			5 mm particle		
Number of trains	1	2	3	1	2	3
Number of columns	7	14	21	7	14	21
Column diameter [m]	7.7	5.4	4.4	6.7	4.7	3.9
	Column length 15 m					
Particle size	3 mm particle			5 mm particle		
Number of trains	1	2	3	1	2	3
Number of columns	7	14	21	7	14	21
Column diameter [m]	8.6	6.1	4.9	7.4	5.3	4.3

5.8.3 Power Plant Comparison

As mentioned in the previous section table 62 summarizes the performance of the three IGCC power plants. Table 63 summarizes the accounting of CO_2. The power plant using absorption achieved higher efficiency, higher capture rate and purity, and significantly lower emissions than the power plant using PSA. The difference in emissions was caused by the difference in CO_2 capture rate in the two plants. However, the main advantage of the IGCC plant using absorption was the CO_2 product purity, as it delivered a 100 % pure stream of CO_2. This was the main reason to why the plant achieved higher efficiency, as adsorption of syngas fuel caused an efficiency reduction of 2.0 percentage points to the plant using PSA. Moreover, given the low purity of the PSA process, it was uncertain whether transport and storage of the CO_2-mixture was feasible.

Regarding auxiliary power consumption table 60 shows that the consumption related to separation and compression of CO_2 was actually higher for absorption than for PSA. This would also be the case if the absorption capture rate was reduced to the same level as achieved by PSA. This aspect is the main strongpoint of the PSA process. However, In order to prefer PSA as a capture technology, a process with a lower adsorption rate of impurities, H_2 and CO in particular, would have to be designed. This would increase the CO_2 purity and decrease the CO concentration to acceptable levels in the transport stream. In addition the gross power output would increase, hence increasing the net plant efficiency.

Calculations indicated that if the CO_2 capture rate in the PSA process could be increased to the same level as absorption (94.6 %), the adsorption rate of impurities would have to be decreased to around 15 % of the current level in order to increase the net plant efficiency to the same level as the IGCC plant using absorption. This would also enable an acceptable level of impurities in the transport stream. To put that number in context, a reduction to 15 % would correspond to a CO_2 purity of 98 %. This means that if absorption and PSA had the same separation capture rate, the plant using PSA would with 98 % purity match the plant using absorption, which had with 100 % purity, in terms of net plant efficiency. This is explained by the fact that absorption had higher auxiliary power consumption PSA, allowing

the PSA to adsorb small amounts of syngas fuel. However, a purity level of 98 % is still far ahead of what was achieved in the simulation of this PSA cycle.

Table 62: Summary IGCC simulations

Operational performance			
	No capture	PSA	Absorption
Coal flow rate [kg/s]	33.3	38.5	38.5
Coal LHV [MJ/kg]	25.2	25.2	25.2
Net fuel input [MW_{th}]	837.3	968.2	968.4
Gas turbine output [MW]	253.1	271.1	282.9
Steam turbine output [MW]	192.6	161.0	170.2
Air expander [MW]	4.5	5.3	5.7
Gross electrical output [MW]	450.2	437.5	458.8
CO_2 separation power consumption [MW]		0.0	16.5
CO_2 compressor power consumption [MW]		33.0	18.8
Total auxiliary power consumption [MW]	54.3	101.0	106.1
Net electrical output [MW]	395.8	336.5	352.8
Net electrical efficiency [%]	47.3	34.8	36.4
CO_2 separation capture rate [%]		86.3	94.6
Total plant CO_2 capture rate [%]		83.8	90.9
CO_2 capture efficiency [%]		78.2	88.2
CO_2 purity [%]		87.8	100
Specific CO_2 emissions [kg/MWh_{net}]	730.5	159.1	86.2
SPECCA [MJ/kg_{CO2}]		4.8	3.5

Table 63: Summary CO_2 accounting

Accounting of CO_2		
	PSA	Absorption
CO_2 captured [kg/MWh_{net}]	820.9	861.3
CO_2 avoided [kg/MWh_{net}]	571.4	644.3
CO_2 emitted [kg/MWh_{net}]	159.1	86.2
Total CO_2 formed [kg/MWh_{net}]	980.0	947.5
Additional CO_2 [kg/MWh_{net}]	249.5	217.0
Additional fuel per kWh_{net} [%]	36.0	29.8

5.8.4 CO_2 as Fuel Preparation Gas

As the performance of the PSA process with regards to purity was not satisfactory, methods to increase this have been investigated. This section discusses the possibilities of using CO_2 as a fuel preparation gas instead of N_2. As mentioned in section 4.2.2 the high N_2 feed fraction reduced the purity and recovery of CO_2. Although N_2 is the most common fuel preparation gas, using CO_2 as a fuel preparation gas is possible and actually preferred in chemical plants where N_2 is unwanted. If CO_2 is used the flow rate should be twice the rate of N_2 (European Benchmarking Task Force, 2008). One method of using CO_2 is by recirculating a fraction of the adsorbed CO_2-mixture (Botero, et al., 2013) as seen in figure 23. Liquid CO_2 is separated after compression, and mixed with water and coal. This mixture is then pumped to the slurry feed gasifier. Although this topic has been researched on slurry feed gasifiers, Siemens does offer a dry feed gasifier, similar to the gasifier used in the IGCC simulations, which can handle both CO_2 and N_2 as fuel preparation gas (Siemens, 2012). An uncertainty with this method is that Botero et al. (2013) did not consider impurities in the recirculated CO_2-mixture. The effect of impurities in the fuel preparation gas is therefore not known, and should be studied further.

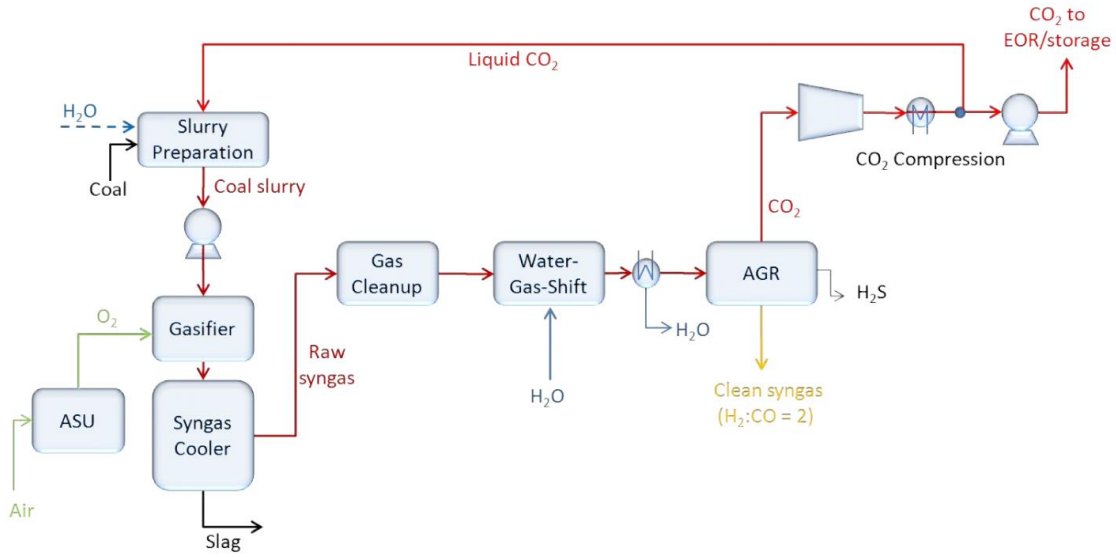

Figure 23: CO_2 as fuel preparation gas (Botero, 2014)

Calculations investigating the effect of the PSA performance when using CO_2 as fuel preparation gas have been conducted. CO_2 replaced N_2 at twice the mass flow rate, while the other input streams to the dry feed gasifier were kept constant. Results showed that the syngas feed composition would have been significantly changed as seen in table 64.

Table 64: Syngas feed composition with CO_2 as fuel preparation gas

Fuel preparation gas	H_2	CO_2	N_2	CO	Ar	H_2O	CH_4	COS	H_2S
CO_2	52.72	44.44	1.02	1.47	0.27	0.02	0.06	0.00	0.00
N_2	53.54	37.89	6.72	1.50	0.27	0.02	0.06	0.00	0.00

The new feed composition was simulated in gPROMS, which resulted in the CO_2-mixture composition given in table 65.

Table 65: Composition of CO_2-rich gas mixture [mol%]

H_2	CO_2	N_2	CO	Ar	H_2O	CH_4	COS	H_2S
4.74	92.72	0.91	1.31	0.24	0.02	0.05	0.00	0.00

With the new feed composition the purity of CO_2 increased to 92.7 %, while the recovery increased to 89.4 %. The N_2 fraction was below the maximum recommended DYNAMIS value of 4 %. However, the fraction of H_2 was still slightly above the 4 % limit. Moreover, the CO fraction was still 6.6 times the limit of 2000 ppm. This shows that the level of impurities was still not satisfactory. Moreover, these results were not connected to the IGCC power plant in Thermoflex, as CO_2 recirculation would have required extensive modification of the existing plant. This topic and other modification to the PSA cycle to improve the purity should be further investigated.

6 Conclusion

The two-stage Pressure Swing Adsorption (PSA) process in the post-combustion case achieved a purity of 96.4 % for a specified recovery of 90.0 %. The specific power consumption was 1.3 MJ/kg_{CO2}. Integrating the PSA process in the PCC power plant resulted in a net power plant efficiency of 28.7 %, a reduction of 16.6 percentage points from the reference plant. If the power plant efficiency was to match the absorption case, either the purity or recovery had to be lowered to below 90 %. The flue gas compressor, PSA process and the CO_2 export compressor were the main contributors to the reduction in efficiency. The absorption case, with 90 % capture rate and 100 % purity, achieved in contrast a net plant efficiency of 33.4 %. The absorption case was superior in all aspects of the power plant. The net power output, the plant efficiency and the CO_2 capture efficiency were higher, while the specific CO_2 emissions and additional fuel per kWh_{net} were lower.

One major factor in favor of absorption is the size of the PSA plant. In order to accommodate all the flue gas from the power plant, 120-160 columns of diameter 5-12 m and length 10-15 m where required. This shows that the footprint of the PSA plant is huge, and indicates high investment costs. Another factor is the fact that the PSA simulations were performed without water affecting the performance. In reality, the water would decrease the power plant efficiency even further. When everything is taken into account, the results indicate that PSA as a technology for decarbonisation as an alternative to absorption is not realistic for PCC power plants.

The PSA process in the pre-combustion case achieved a purity of 87.8 % and a separation capture rate of 86.3 %, giving a total plant capture rate of 83.8 %. This was not high enough to satisfy the performance targets of 90 % recovery and 95.5 % purity. The concentration of impurities in the CO_2-mixture was in general too high. This was especially true for CO, which had a concentration 6.7 times the proposed limit. Due to the high impurity level, it is uncertain whether or not transport and storage is at all feasible. To ensure feasibility the PSA process needs to achieve a higher purity.

Integrating the PSA process in the IGCC power plant resulted in a net plant efficiency of 34.8 %, which was 1.7 percentage points below the benchmark plant using absorption and 12.5 percentage points below the reference plant without capture. The purity of the adsorbed CO_2-mixture was the main reason to why the plant with PSA had lower performance than the plant with absorption. Due to adsorption of syngas fuel, the net output from the gas turbine and steam turbines decreased and reduced the net plant efficiency by 2.0 percentage points. A factor in favor of PSA was that the auxiliary power consumption related to CO_2 capture was less than when using absorption. Moreover, the size and numbers of PSA columns required for full scale CO_2 capture were, in contrary to post-combustion, at a feasible level. The results showed that PSA as a capture technology for IGCC power plants could not perform quite as well as with absorption. However, based on the auxiliary power consumption and the size of the PSA plant, PSA as a capture technology could have a potential if the purity could be increased.

7 Further Work

As concluded, the PSA processes were not able to compete with the absorption technology. Future work should attempt to improve the performance by simulating new cycle configurations in combination with different adsorbents for both pre- and post-combustion. The post-combustion process can achieve sufficiently high recovery and purity, but measures to reduce the power consumption is the key element to study. For pre-combustion, measures to increase both the CO_2 purity and recovery should be investigated. Adding a rinse step will increase the purity, while using CO_2 as a fuel preparation gas will increase both recovery and purity.

The mathematical model can also be improved. For post-combustion it would be beneficial to obtain fitting parameters for the Langmuir isotherm and transport data for O_2, Ar and SO_2 so that they could be modeled accurately as separate components. The adsorption properties of water should be researched in an attempt to include water in the model as well. The same goes for pre-combustion; the main components carbon monoxide and argon should be modeled as separate components. Sips isotherm parameters and either the k_{LDF} parameters or transport parameters for each component are needed. There are also small traces of other components such as CH_4, COS, H_2S and H_2O that could be included in the models. As increasing the number of components makes the models more unstable, methods to make them more robust should be investigated to make this possible.

The capital cost and operational cost of a full scale system should be calculated and compared to the cost of absorption. Although the literature suggests that PSA may be cheaper than absorption, the actual cost for each plant needs to be estimated and taken into account to fully assess which technology is preferred. Lower cost may compensate for a slightly lower performance in some cases.

Finally, the simulations should be performed in full scale with actual flow rates from the power plant to be fully capable of evaluating all aspects of the PSA process.

8 Works Cited

Agarwal, A., 2010. *Advanced Strategies for Optimal Design and Operation of Pressure Swing Adsorption Processes,* Pittsburgh, PA: Carnegie Mellon University.

Alibaba, 2014. *Alibaba.com.* [Online]
Available at: http://www.alibaba.com/product-detail/Zeolite-Pellet-3A-4A-5A-13X_1124749706.html?s=p
[Accessed 24 Mai 2014].

Andrei, M. et al., n.d. *Enhanced Oil Recovery with CO2 Capture and Sequestration,* s.l.: Eni exploration & production division.

Azevedo, D. C. S. & Rodrigues, A. E., 1999. Bilinear Driving Force Approximation in the Modeling of a Simulated Moving Bed Using Bidisperse Adsorbents. *Ind. Eng. Chem.,* Issue 38, pp. 3519-3529.

Bandari, M. R., Behjat, Y. & Shahhosseini, S., 2012. CFD Investigation of Hydrodynamic and Heat Transfer Phenomena around Trilobe Particles in Hydrocracking Reactor. *International Journal of Chemical Reactor Engineering,* Volume 10.

Bolland, O., 2012. *Power Generation: CO2 Capture and Storage.* s.l.:s.n.

Botero, C., 2014. *The Phase Inversion-based Coal-CO2 Slurry (PHICCOS) Feeding System: Design, Coupled Multiscale Analysis, and Technoeconomic Assessment,* s.l.: s.n.

Botero, C., Field, R. P., Herzog, H. J. & Ghoniem, A. F., 2013. Coal-CO2 Slurry Feed for Pressurized Gasifiers: Slurry Preparation System Characterization and Economics. *Energy Procedia,* Issue 37, pp. 2212-2223.

Brúder, P., 2012. *Solvent Developement and Testing for Post-combustion Carbon Dioxide Capture,* s.l.: s.n.

Carbochem, 2014. *Carbochem.* [Online]
Available at: http://carbochem.com/activated-carbon/activated-carbon-101/
[Accessed 24 may 2014].

Casas, N., Schell, J., Joss, L. & Mazzotti, M., 2012. A Parametric Study of a PSA Process for Pre-Combustion CO2 Capture. *Separation and Purification Technology,* Issue 104, pp. 183-192.

Casas, N., Schell, J., Pini, R. & Mazzotti, M., 2012. Fixed Bed Adsorption of CO2/H2 Mixtures on Activated Carbon: Experiments and Modeling. *Adsorption,* Issue 18, pp. 143-161.

Choi, S., Drese, J. H. & Jones, C. W., 2009. Adsorbent Materials for Carbon Dioxide Capture from Large Anthropogenic Point Sources. *ChemSusChem,* Issue 9, pp. 796-854.

Choi, W.-K.et al., 2003. Optimal Operation of the Pressure Swing Adsorption (PSA) Process for CO2 Recovery. *Chemical Engineering,* Issue 20, pp. 617-623.

CO2now.org, 2014. *CO2now.org.* [Online]
Available at: http://co2now.org/images/stories/data/co2-atmospheric-mlo-monthly-scripps.pdf
[Accessed 21 Mai 2014].

D'Alessandro, D. M., Smit, B. & Long, J. R., 2010. Carbon Dioxide Capture: Prospects for New Materials. *Angewandte Chemie International Edition,* Issue 35, pp. 6058-6082.

de Visser, E. et al., 2008. Dynamis CO2 quality recommendations. *International journal of greenhouse gas control 2,* pp. 478-484.

European Benchmarking Task Force, 2008. *DECARBit: Enabling advanced pre-combustion capture techniques and plants: European best practise guidelines for assessment of CO2 capture technologies,* s.l.: s.n.

Foo, K. & Hameed, B., 2010. Insights into the Modeling of Adsorption Isotherm Systems. *Chemical Engineering Journal,* Issue 156, pp. 2-10.

Froment, G. F., Bischoff, K. B. & De Wilde, J., 2011. *Chemical Reactor Analysis and Design.* 3rd ed. s.l.:John Wiley & sons, Inc.

Global CCS Institute, 2013. *Global CCS Institute.* [Online]
Available at: http://www.globalccsinstitute.com/projects/browse
[Accessed 16 December 2013].

Hedin, N., Chen, L., Laaksonen & Aatto, 2010. Sorbents for CO2 capture from flue gas - aspects from materials and theoretical chemistry. *Nanoscale,* Issue 2, pp. 1819-1841.

Imtiaz, F., 2002. *Adsorption of Alcohol Vapours on Yttria Stabilized Zirconia Catalysts,* Islamabad: s.n.

Jakobsen, H. A., 2011. *Fixed Bed Reactors,* s.l.: Department of Chemical Engineering, NTNU.

Karger, J., Ruthven, D. M. & Theodorou, D. N., 2012. *Diffusion in Nanoporous Materials.* s.l.:John Wiley & Sons.

Khajuria, H., 2011. *Model-Based Design, Operation and Control of Pressure Swing Adsorption Systems,* s.l.: s.n.

Kikkindes, E. S., Yang, R. T. & Cho, S. H., 1993. Concentration and Recovery of CO2 from Flue Gas by Pressure Swing Adsorption. *Ind. Eng. Chem. Res.,* Issue 11, pp. 2714-2720.

Ko, D., Siriwardane, R. & Biegler, L. T., 2005. Optimization of Pressure Swing Adsorption and Fractionated Vacuum Pressure Swing Adsorption Processes for CO2 Capture. *Ind. Eng. Chem. Res.,* Issue 21, pp. 8084-8094.

Laughlin, L., 2009. *Equilibrium Doesn't Equal Equality,* s.l.: s.n.

Li, G. et al., 2008. Capture of CO2 from high humidity flue gas by vacuum swing adsorption with zeolite 13X. *Adsorption,* Issue 14, pp. 415-422.

Limited, I. G. C., 2014. *Indo German Carbons Limited.* [Online]
Available at: http://www.igcl.com/php/activated_carbon.php
[Accessed 24 may 2014].

Liu, Z. et al., 2011. Multi-bed Vacuum Pressure Swing Adsorption for carbon dioxide capture from flue gas. *Separation and Purification Technology,* Issue 81, pp. 307-317.

Lopes, F. V. et al., 2009. Enhancing Capacity of Activated Carbons for Hydrogen Purification. *Ind. Eng. Chem. Res.,* Issue 48, p. 3978–3990.

Lopes, F. V. S. et al., 2009. Adsorption of H2, CO2, CH4, CO, N2 and H2O in Activated Carbon and Zeolite for Hydrogen Production. *Separation Science and Technology,* Issue 44, pp. 1045-1073.

Marathe, R. P., 2006. *Adsorption and Diffusion of Gases in ETS-4,* s.l.: s.n.

Miller, B. G., 2010. *Clean Coal Engineering Technology.* s.l.:Butterworth-Heinemann.

Na, B.-K.et al., 2001. CO2 Recovery from Flue Gas by PSA Process using Activated Carbon. *Korean J. Chem. Eng.,* Issue 2, pp. 220-227.

Na, B.-K., Lee, H. L., Koo, k.-K. & Song , H. K., 2002. Effect of Rinse and Recycle Methods on the Pressure Swing Adsorption Process To Recover CO2 from Power Plant Flue Gas Using Activated Carbon. *Ind. Eng. Chem. Res.,* Issue 41, pp. 5498-5503.

Nitta, T., Shigetomi, T., Kuro-Oka, M. & Katayama, T., 1984. An Adsorption Isotherm of Multi-Site Occupancy Model for Homogeneous Surface. *Journal of Chemical Engineering of Japan,* 17(1), pp. 39-44.

Park, J.-H., Beum, H.-T., Kim, J.-N. & Cho, S.-H., 2002. Numerical Analysis on the Power Consumption of the PSA Process for Recovering CO2 from Flue Gas. *Ind. Eng. Chem. Res.,* Issue 16, pp. 4122-4131.

Park, Y. et al., 2014. Adsorption Isotherms of CO2, CO, N2, CH4, Ar and H2 on Activated Carbon and Zeolite LiX up to 1.0 MPa. *Adsorption,* Issue 20, pp. 631-641.

Pooling, B. E., Prausnitz, J. M. & O'Connell, J. P., 2000. *The Properties of Gases and Liquids.* 5th ed. s.l.:McGraw-Hill.

Ribeiro, A. M. et al., 2008. A Parametric Study of Layered Bed PSA for Hydrogen Purification. *Chemical Engineering Science,* Issue 63, pp. 5258-5273.

Rodrigues, A. E., 2014. *Personal Communication.* s.l.:arodrig@fe.up.pt.

Rodrigues, A. E., LeVan, M. D. & Tondeur, D., 1988. *Adsorption: Science and Technology.* s.l.:Kluwer Academic Publishers.

Ruthven, D. M., Farooq, S. & Knaebel, K. S., 1994. *Pressure Swing Adsorption.* s.l.:VCH Publishers Inc..

Samanta, A. et al., 2011. Post-Combustion CO2 capture Using Solid Sorbents: A Review. *Ind. Eng. Chem. Res.,* Issue 51, pp. 1438-1463.

Schell, J., Casas, N., Marx, D. & Mazzotti, M., 2013. Precombustion CO2 Capture by Pressure Swing Adsorption (PSA): Comparison of Laboratory PSA Experiments and Simulations.

Schell, J., Casas, N., Pini, R. & Mazzotti, M., 2012. Pure and Binary Adsorption of CO2, H2, and N2 on Activated Carbon. *Adsorption,* Issue 18, pp. 49-65.

Siemens, 2012. *Siemens Fuel Gasification Technology.* [Online]
Available at: http://www.energy.siemens.com/hq/pool/hq/power-generation/fuel-gasifier/fuel-gasification-technology-for-integrated-gasification_brochure.pdf
[Accessed May 2014].

Solsvik, J. & Hugo A., J., 2011. Modeling of multicomponent mass diffusion in porous spherical pellets: Application to steam methane reforming and methanol synthesis. *Chemical Engineering Science,* 66(9), p. 1986–2000.

Suzuki, M., 1990. *Adsorption Engineering.* s.l.:Kodansha LTD and Elsevier Science Publishers.

Takamura, Y. et al., 2001. Evaluation of Dual-Bed Pressure Swing Adsorption for CO2 Recovery from Boiler Exhaust Gas. *Saparation and Purification Technology,* Issue 3, pp. 519-528.

Working Group III of IPCC, 2005. *IPCC Special Report Carbon Dioxide Capture and Storage: Summary for policy makers,* s.l.: s.n.

Yang, R. T., 1986. *Gas Separation By Adsorption Processes.* s.l.:Butterworth Publishers.

9 Appendix

9.1 Appendix A: PSA Simulation Results

Table A1: Preliminary simulation results pre-combustion model

Run	Q_{feed}	Q_{purge}	FP [s]	Feed [s]	EQ [s]	B [s]	Pu [s]	0 [s]	t tot [s]	Rec tot [%]	Purity [%]	Prod [$kg_{CO2/kgads}h$]
Casas, et al.	38.98	1.72	2	40	4	50	24	33	240	90.0	95.3	20.5
1	38.98	1.72	4	40	4	50	26	32	280	90.20	85.13	18.68
2	38.98	1.72	4	45	4	60	26	37	315	84.97	86.23	17.28
3	38.98	1.72	4	45	4	64	22	37	315	83.77	86.34	16.98
4	38.98	1.72	4	45	4	55	31	37	315	86.22	86.05	17.60
5	38.98	1.72	4	40	4	45	31	32	280	91.37	84.92	19.01
6	38.98	1.72	4	40	4	45	31	32	280	88.93	85.46	18.36
7	38.98	1.72	15	40	15	45	20	10	280	84.00	87.80	17.35
8	38.98	1.72	19	40	19	45	16	2	280	81.65	88.03	16.80
9	38.98	1.72	12	40	12	45	23	16	280	85.75	87.54	17.75
10	38.98	1.72	22	50	22	50	28	6	350	72.89	87.77	14.67
11	38.98	1.72	16	35	16	40	14	3	245	87.91	87.54	18.54
12	38.98	1.72	15	32	15	35	14	2	224	89.52	86.04	19.31
13	38.98	1.72	15	34	15	38	15	4	238	89.40	87.14	19.01
14	38.98	1.72	14	34	14	38	16	6	238	89.91	86.99	19.14
15	38.98	1.72	14	34	14	36	18	6	238	90.74	86.94	19.36
16	38.98	1.72	14	33	14	33	19	5	231	91.44	86.39	19.69
17	38.98	1.72	16	33	16	35	15	1	231	89.85	86.82	19.26
18	38.98	1.72	14	35	14	42	14	7	245	88.12	87.34	18.58
19	38.98	1.72	16	35	16	39	15	3	245	88.43	87.53	18.67
20	38.98	1.72	16	35	16	38	16	3	245	88.91	87.52	18.84
21	38.98	1.72	16	35	16	36	18	3	245	89.78	87.47	19.01
22	38.98	1.72	16	35	16	34	20	3	245	90.55	87.42	19.22
23	38.98	1.72	16	35	16	32	22	3	245	91.25	87.34	19.41
24	38.98	1.72	16	35	16	30	24	3	245	91.86	87.26	19.58
25	38.98	1.72	16	35	16	28	26	3	245	92.39	87.16	19.74
26	38.98	1.89	16	35	16	28	26	3	245	92.85	87.03	19.88
27	38.98	1.55	16	35	16	28	26	3	245	91.89	87.28	19.58
28	38.98	1.38	16	35	16	28	26	3	245	91.33	87.39	19.42
29	38.98	1.20	16	35	16	28	26	3	245	90.69	87.48	19.24
30	38.98	1.03	16	35	16	28	26	3	245	89.97	87.56	19.05
31	38.98	0.86	16	35	16	28	26	3	245	89.13	87.61	18.80
32	31.18	0.86	16	35	16	28	26	3	245	92.45	86.93	19.04
Final result	42.88	0.86	16	35	16	28	26	3	245	86.28	87.76	19.17

9.2 Appendix B: PCC Simulation Flow Sheets

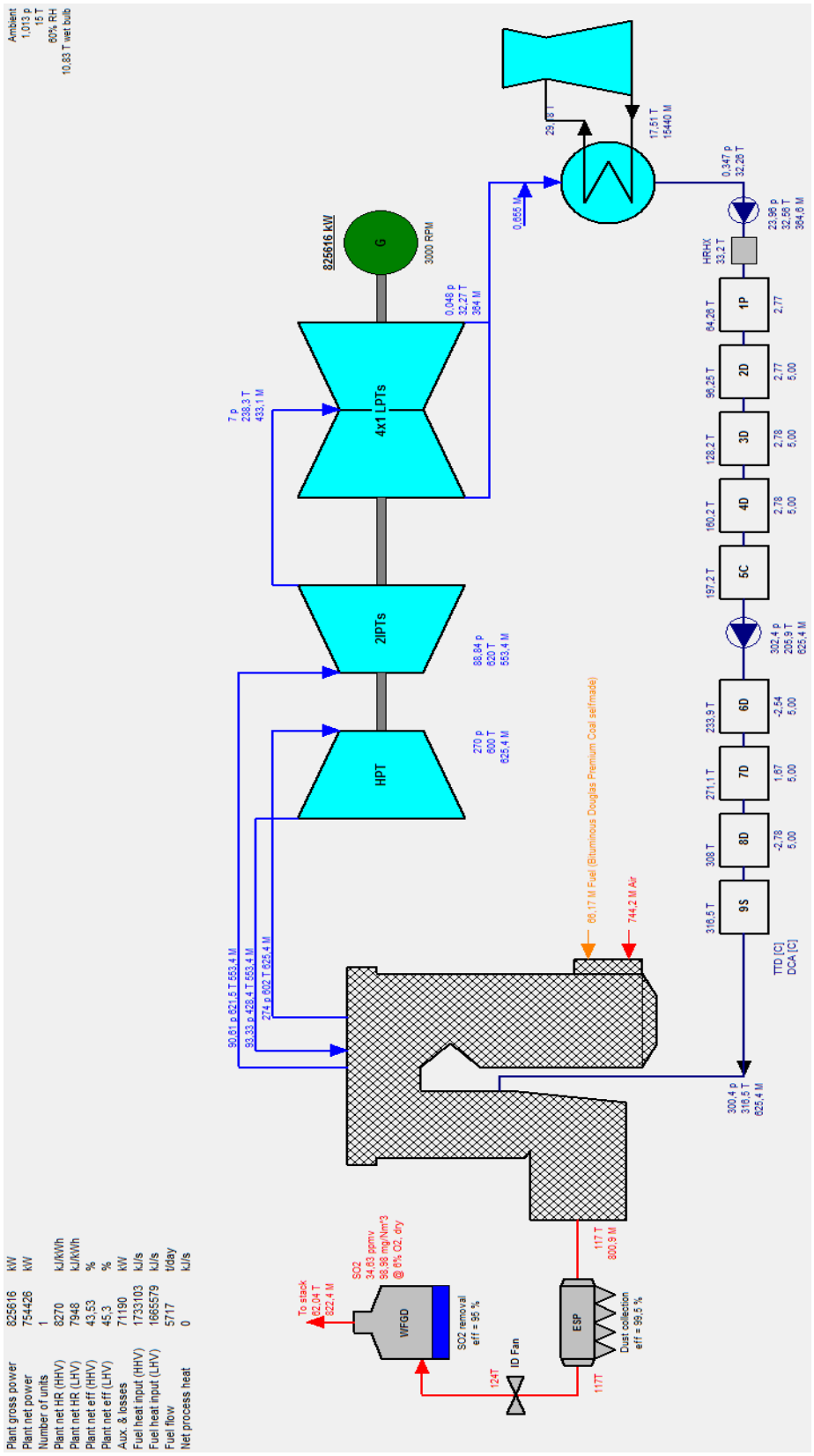

Figure B1: PCC without CO_2 capture

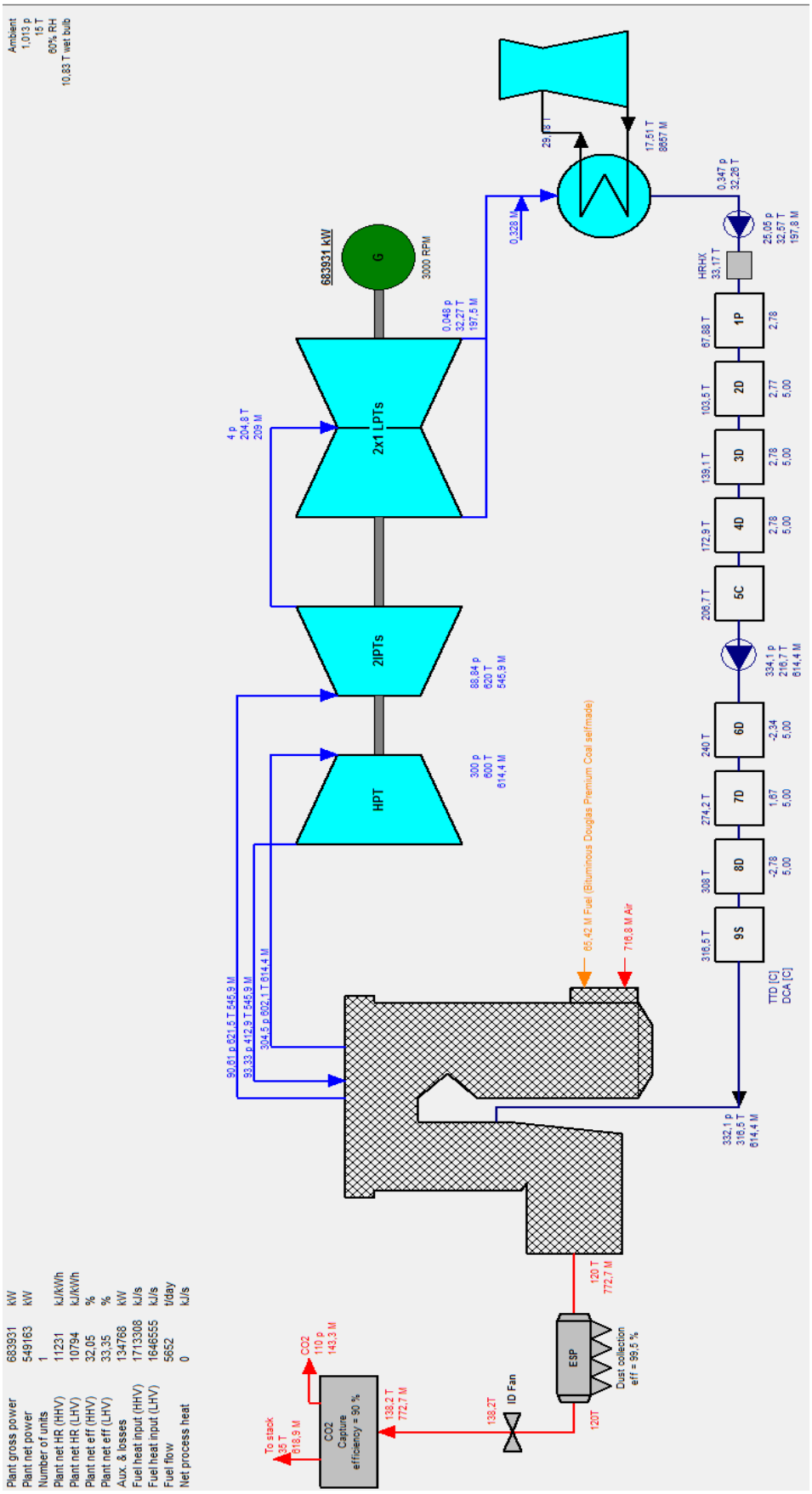

Figure B2: PCC with CO_2 capture by absorption

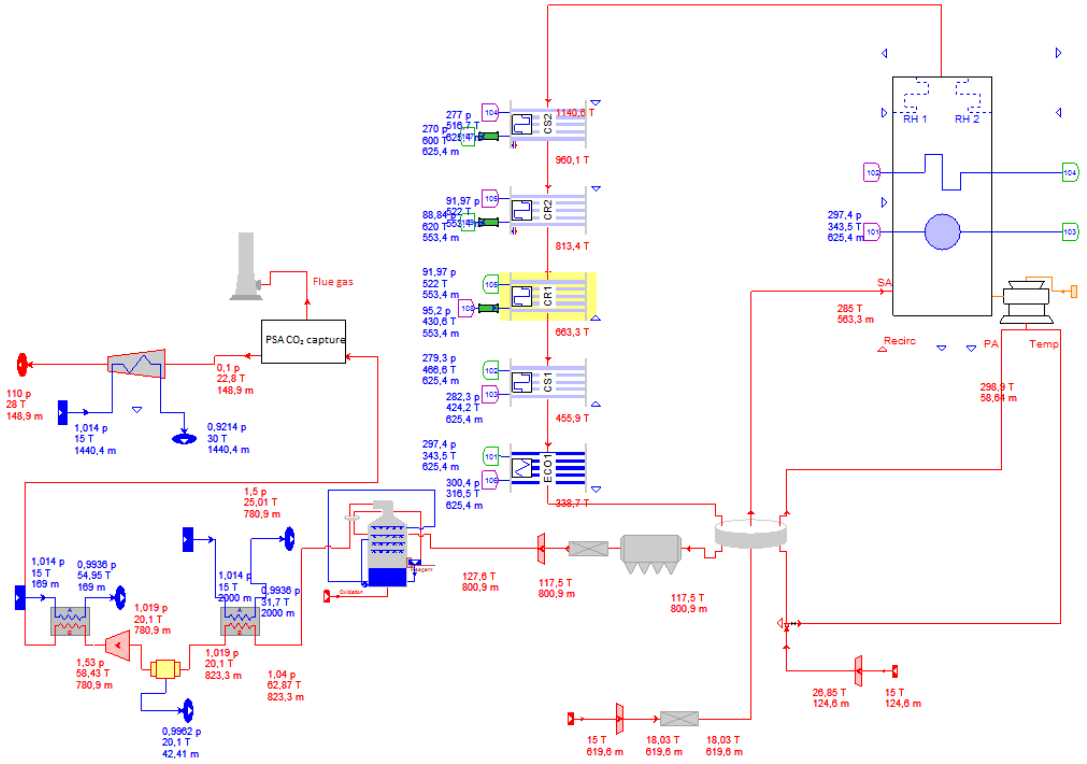

Figure B3: PCC with CO_2 capture by PSA – boiler and CO_2 capture

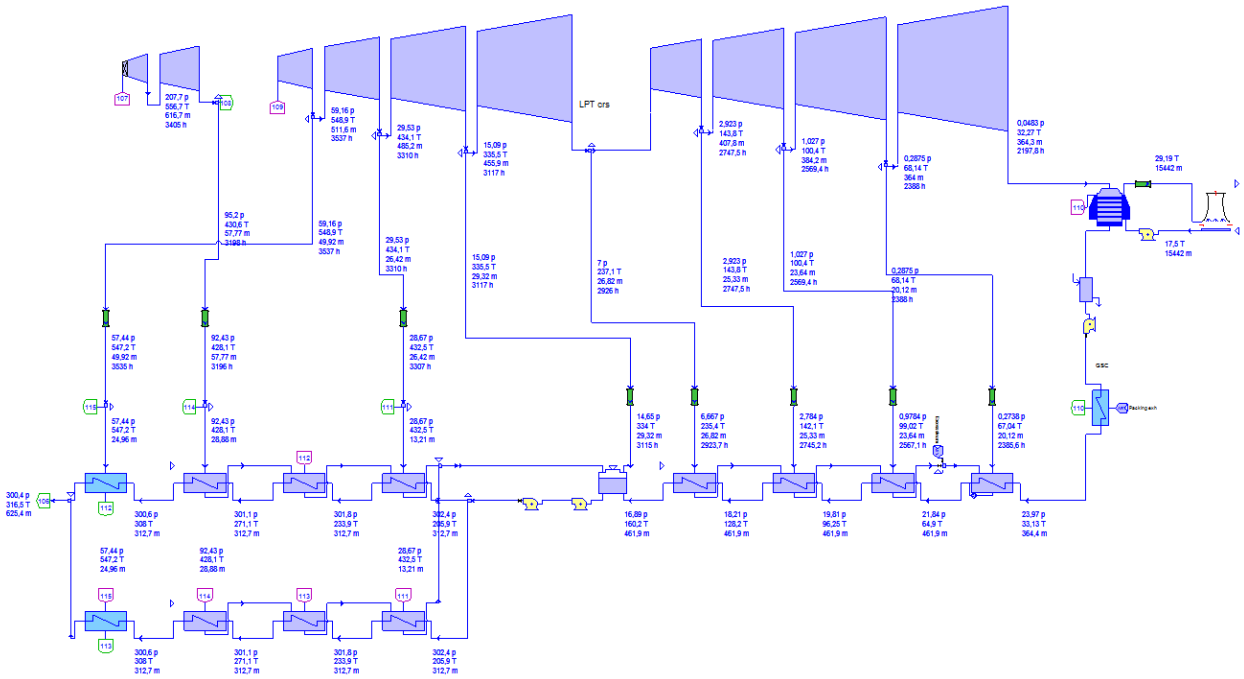

Figure B4: PCC with CO_2 capture by PSA - steam cycle

9.3 Appendix C: IGCC Simulation Flow Sheets

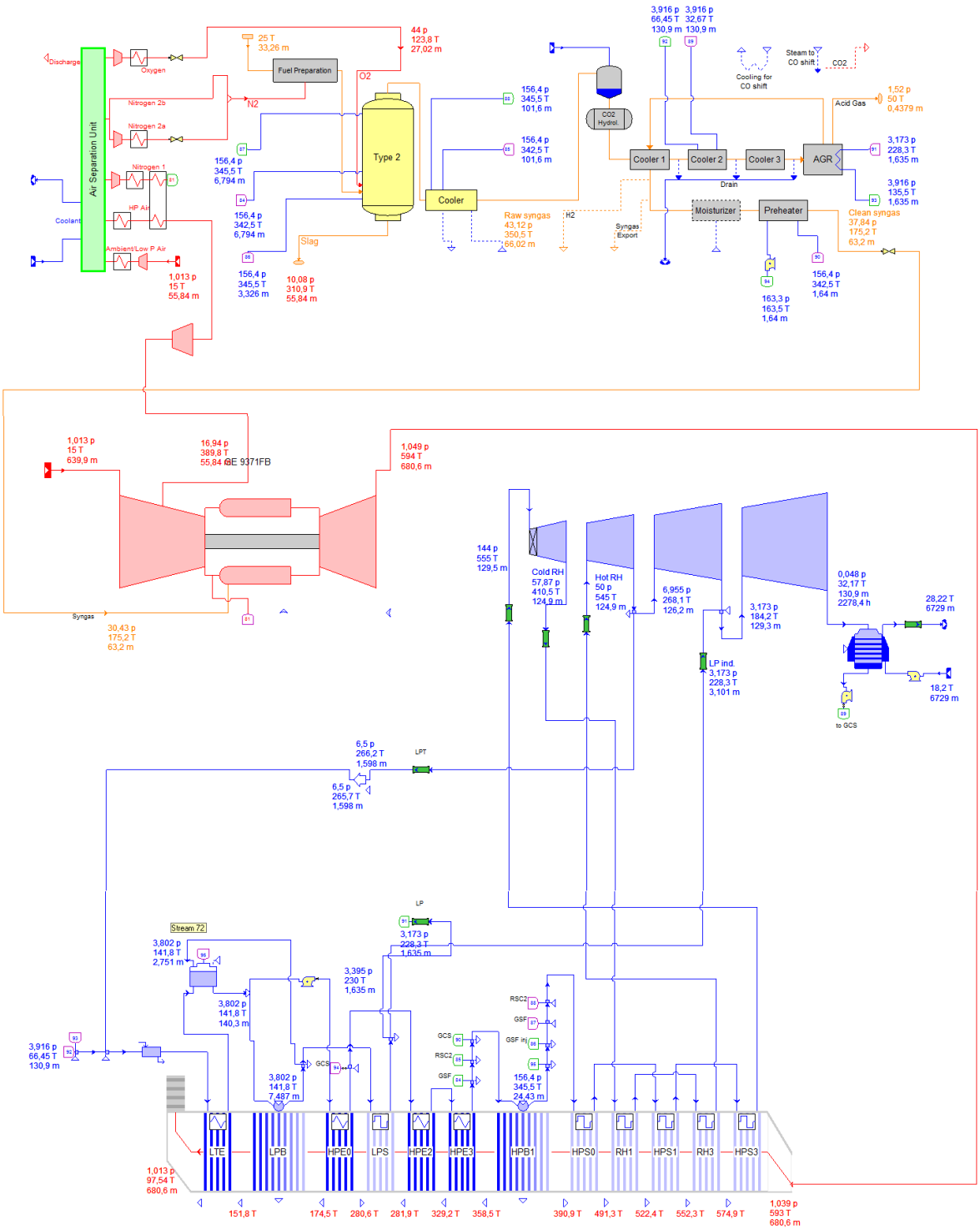

Figure C1: IGCC without CO_2 capture

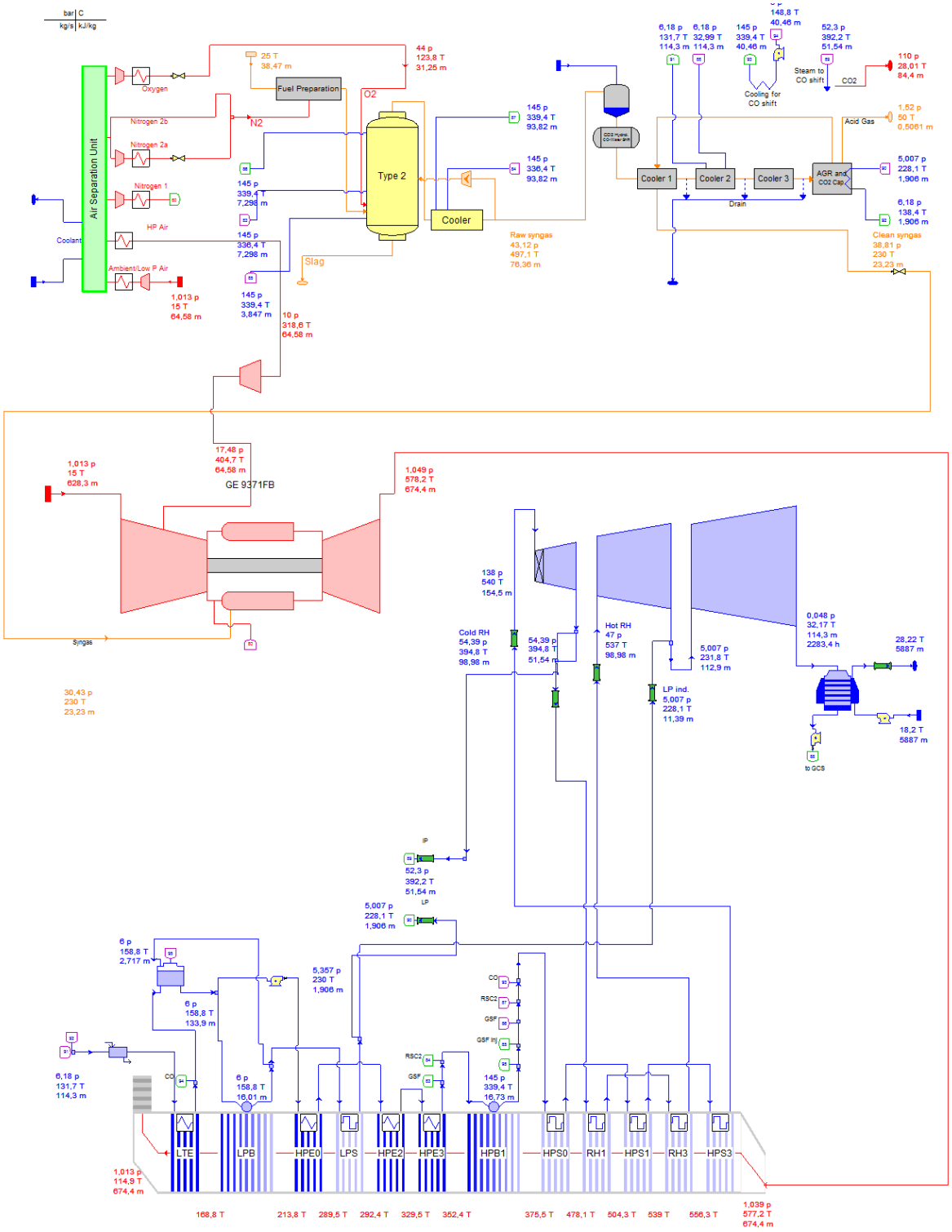

Figure C2: IGCC with CO_2 capture by absorption

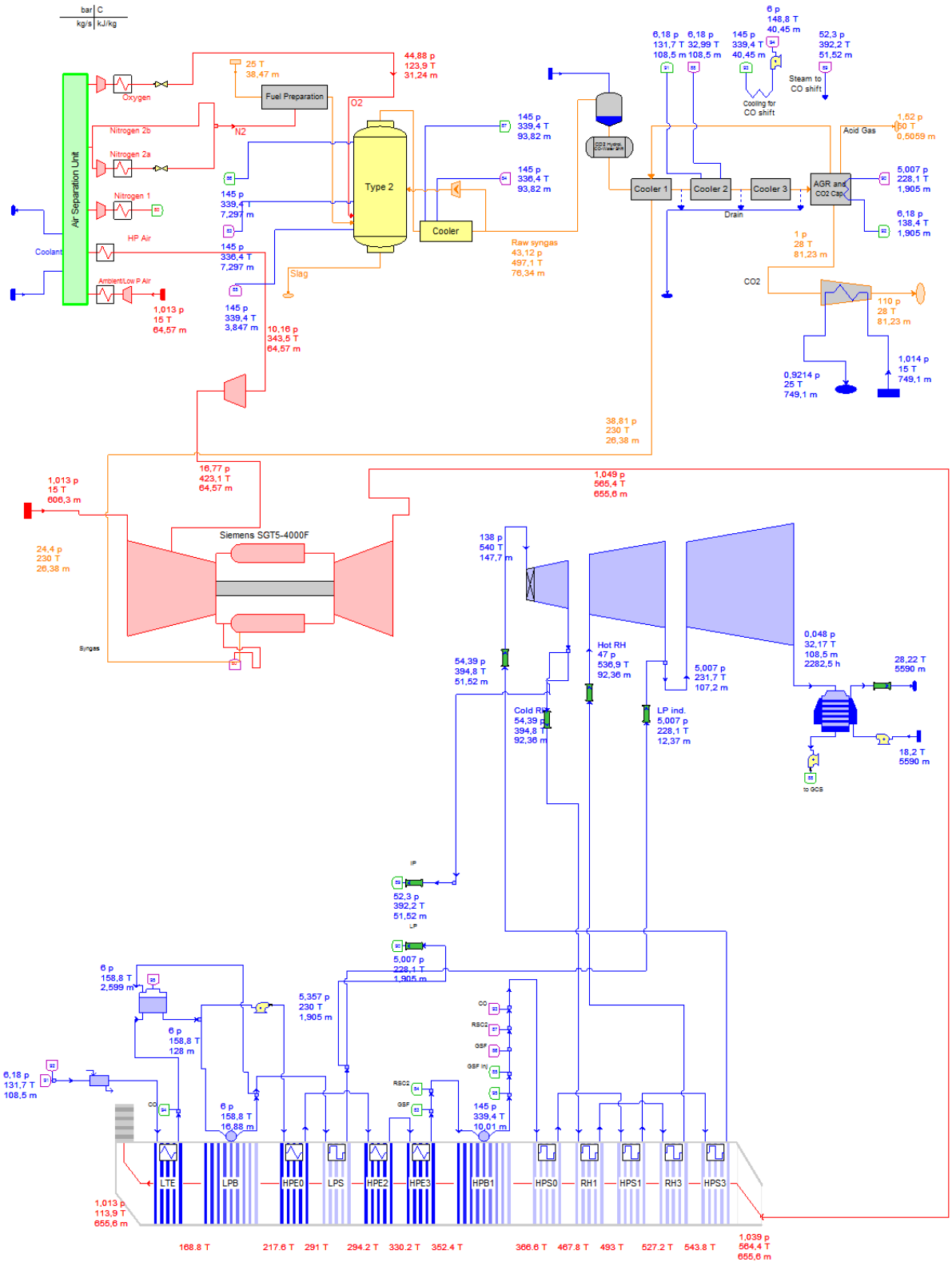

Figure C3: IGCC with CO_2 capture by PSA

9.4 Appendix D: Losses Associated with CO_2 Capture Pre-Combustion

Table D1: Fuel LHV loss due to CO-shift reaction

Technology	No capture	Absorption	PSA
Raw syngas LHV [MW]:	690.2	798.3	798.1
Clean syngas LHV [MW]:	687.4	716.0	716.0
Reduction [MW]:	2.8	82.3	82.1
Reduction [%]:	0.4 %	10.3	10.3
Relative reduction [%]:		9.9	9.9
Reduced gas turbine output [%]:		9.9	9.9
Contribution to total net plant efficiency reduction [%]:		**3.4**	**3.4**

Table D2: Impact of fuel LHV reduction for gas turbine

Technology	PSA	
	[MW]	[%]
Fuel LHV reduction by component:		
H_2	21.8	3.0
CO	7.5	1.1
CH_4	0.8	0.1
Total fuel LHV reduction:	30.1	4.2
Reduced Gas Turbine output:	11.9	4.2
Reduction in recovered exhaust heat:	18.2	5.1
Reduced steam turbine output:	7.2	4.3
Contribution to total net plant reduction:	**19.1**	**2.0**